UNIVERSIDADE DE LISBOA
FACULDADE DE CIÊNCIAS
DEPARTAMENTO DE QUÍMICA E BIOQUÍMICA

# New sensors based on chiral and achiral coordination polymers

Bárbara Luís de Oliveira

**Mestrado em Química**
Especialização em Química

Dissertação orientada por:
Doutora Ana Isabel Ferreira Franco Vicente
Doutor Paulo Nuno Martinho

2018

# Acknowledgments

First, I would like to thank my supervisors. A special acknowledgment to Ana Isabel Vicente, I would like to thank you for all the advice and support and for being always on my side. I owe you so much, thank you for all the guidance and for always having my back, I am forever grateful for everything. To Paulo Martinho I would like to thank for all the amazing opportunities and also for the guidance, you are extraordinary, and I could not be more thankful for having the privilege of working with you and learning from you, thank you for making me grow professionally and personally. Thank you both for this amazing year of new experiences and tremendous amount of learning, I could have not asked for more. I only hope we can work together again soon.

To Professor Maria José Calhorda, thank you for having me in your group and for all the opportunities.

To Sara Realista I would like to make a special acknowledgement for always being so supportive, eager to help and for always being in the best mood. You are brilliant, and I wish you nothing but the best in the world. Thank you so much.

To Marta Saraiva, thank you for always being so nice to me and for the help during this year.

To all my colleagues: Marcos, thank you for being so fun and easy going, you are the best!; Frederico Martins, thank you for all the deep talks and serious debates, it was so fun having you around.; Janaina, my roommate in Tenerife, what a great experience, thank you for the great spirit; Mohamed, thank you for always being ready to help. I would also like to thank sweet Olga and Rafaela for always being so kind. To Ana Elisa Ferreira, you are definitely one of the best people I have met this year, thank you for being the best secretary neighbour ever.

Last but not least, I would like to thank my family and friends, specially César Reis for all the love, comprehension and companionship. I love you and I am so grateful that we got the opportunity of experiencing this year together.

# Resumo

A área dos materiais funcionais tem sido alvo de muita atenção por parte da comunidade científica nos últimos anos. Esta área abrange os campos da física, química supramolecular, química orgânica e inorgânica e química de coordenação. Estes materiais são estruturas (unidimensionais, bidimensionais ou tridimensionais) que têm de reunir mais do que uma propriedade e, como tal, a combinação de todas estas áreas da química, e da ciência em geral, é necessária, se não essencial.

O trabalho desenvolvido ao longo deste projeto tem como objetivo primário a síntese de novos materiais funcionais que possam ser aplicados como dispositivos, mais concretamente, como sensores. Uma das características que se procurou para este tipo de material foi a transição de spin. Esta é uma propriedade inerente aos metais de transição com configuração eletrónica entre $d^4$ e $d^7$, sendo estes compostos sensíveis à aplicação de estímulos externos, como temperatura, pressão ou exposição à luz. A transição pode também ser provocada pela interação com outras espécies, no caso de serem estruturas que permitam o enclausuramento de moléculas hospedeiras. No caso de iões metálicos com configuração $d^6$, caso do Fe(II), a transição de spin é muitas vezes acompanhada de uma alteração da cor do composto. Isto deve-se ao facto de o centro metálico passar de um estado de spin-baixo, em que todos os eletrões se encontram emparelhados (diamagnético), para um estado de spin-alto, em que quatro dos eletrões se encontram desemparelhados (paramagnético). O estudo do comportamento magnético é efetuado utilizando um dispositivo supercondutor de interferência quântica (*superconducting quantum interference device- SQUID*) que consegue medir a resposta do composto quando exposto a um campo magnético. Esta medida pode ser traduzida em suscetibilidade magnética ($\chi_M$) e é característica para cada distribuição eletrónica dependendo do número de eletrões desemparelhados no estado de spin-alto e de spin-baixo. No caso do Fe(II) ($d^6$) o valor de $\chi_M T$ é de 3 $cm^3mol^{-1}K$ para o spin-alto e de 0 $cm^3mol^{-1}K$ para o spin-baixo. No caso de Fe(III) ($d^5$) os valores são de 0.37 $cm^3mol^{-1}K$ no estado de spin-baixo e de 4.34 $cm^3mol^{-1}K$ no estado de spin-alto.

A luminescência é também uma propriedade que se pretendeu promover nos polímeros sintetizados. Uma vez que o perfil de emissão de um composto também se pode alterar com a temperatura, a conjugação deste comportamento com a transição de spin e a mudança de cor contribuiria para a obtenção de um material multifuncional com possível aplicação em sensores. Na procura de ligandos que pudessem promover a luminescência do material, foram escolhidos ligandos derivados de unidades naftaleno e perileno. Uma vez que estas unidades são também conhecidas pelas suas capacidades condutoras, a condutividade foi mais uma das propriedades exploradas para um dos ligandos.

A primeira estratégia adotada foi a síntese de ligandos baseados em unidades de benzeno substituídos com grupos piridina nas posições *para*. Por serem lineares e possuírem dois sítios de coordenação, estes ligandos visam a síntese de polímeros de coordenação de Fe(II) tridimensionais, usando para este efeito um segundo ligando quadrangular plano (tetracianometalato). Estas estruturas denominam-se clatratos de Hofmann e, por serem unidades tridimensionais, possuem cavidades que permitem o enclausuramento de moléculas hospedeiras. A inserção destes compostos poderá afetar as propriedades magnéticas das entidades porosas. Muitos compostos intermediários foram obtidos na tentativa de síntese de vários ligandos seguindo esta estratégia. No entanto, apenas um foi possível isolar e caracterizar por espectroscopia de RMN, infravermelho e de luminescência no estado sólido. Através deste composto e de outro, sintetizado por uma colega, foram obtidos dois clatratos de Hofmann e foram avaliados os seus perfis magnéticos bem como as propriedades luminescentes de um deles. Em relação ao perfil magnético, nenhuma das estruturas apresentava transição de spin, em que uma era spin-alto e a outra spin-baixo. Ao contrário do observado para o respetivo ligando, que apresentou um comportamento bastante emissivo, verificou-se que a estrutura tridimensional não era emissiva. Ambos os polímeros 3D foram submetidos a testes de inserção de diversas moléculas hospedeiras por difusão de vapor e conseguiu-se promover uma transição de spin gradual-rápida próxima da temperatura

ambiente num dos clatratos com a piridina. Foi também testada a capacidade de inserção de compostos quirais por parte de umas das estruturas polímericas 3D. Deste modo, foi testada a inserção, em solução, de quatro aminoácidos: L- fenilalanina, D- fenilalanina, L-alanina e D-alanina. Verificou-se que o perfil magnético foi alterado para todos os sistemas, apesar de em nenhum dos casos ter havido uma promoção da transição de spin. Para os dois primeiros, L- fenilalanina e D- fenilalanina, o composto manteve um comportamento de spin-alto enquanto que para os dois últimos, L-alanina e D-alanina, o composto apresentou valores de suscetibilidade magnética característicos para compostos de Fe(III) no estado de spin-alto. Diversas tentativas de obtenção de um cristal único foram também efetuadas, nomeadamente através da síntese das estruturas por difusão lenta em tubos-H com pequenas quantidades de reagente. Dado que a síntese efetuada por este método é extremamente lenta, a obtenção de cristais não é imediata.

Paralelamente, uma segunda estratégia sintética foi adotada em que foram sintetizados ligandos visando a formação de polímeros unidimensionais. Os ligandos desta segunda categoria são assimétricos e não lineares e a sua constituição divide-se em três partes essenciais: um grupo triazole (coordenante ao metal), uma diimida aromática como grupo central e uma zona alifática constituída por cadeias carbonadas. Desta forma foram sintetizados e caracterizados, (por espectroscopia de RMN, infravermelho e luminescência), oito novos ligandos que se dividem em dois grupos: quatro deles formando uma unidade de naftaleno-diimida e os restantes formando um fragmento de perileno-diimida. Destes oito ligandos, apenas os quatro primeiros (naftaleno-diimidas) foram usados na síntese de polímeros unidimensionais por precipitação., Para os ligandos baseados em unidades de perileno-diimidas foi realizada a síntese de dímeros ou oligómeros através da difusão lenta em tubos de ensaio devido à sua baixa solubilidade. Para a obtenção destes oligómeros foi usado um sal de NCS (NaNCS) que se coordena ao ferro impedindo o crescimento do polímero e facilitando a obtenção de pequenas unidades representativas da estrutura. Para os polímeros de coordenação 1D obtidos por precipitação foram estudadas as suas propriedades magnéticas, concluindo-se que apenas um deles apresentava transição de spin, ainda que incompleta, caracterizada como gradual abrupta. Os restantes polímeros apresentaram um perfil magnético característico de spin-alto e para um deles os valores de susceptibilidade magnética apresentaram valores característicos de spin-alto para Fe(III). Para o polímero que apresentou transição de spin, foram também estudadas as suas propriedades condutoras e verificou-se que se comporta como um semi-condutor. As suas propriedades de luminescência foram também estudadas e observou-se que o polímero 1D é extremamente emissivo e que o seu perfil de emissão se altera com a temperatura. Estas três características combinadas fazem deste polímero um excelente candidato para ser aplicado como um material funcional. Os restantes quatro ligandos (perileno-diimida) não foram usados na síntese por precipitação devido à sua elevada insolubilidade em solventes orgânicos. No entanto, através da sua solubilização parcial em clorofórmio, estes ligandos mostraram ser extremamente luminescentes em solução quando expostos a luz a 366 nm. Estudos futuros serão necessários para confirmar este comportamento luminescente bem como se esta propriedade se verifica também no estado sólido. Devido à emissão de luminescência, estes ligandos poderão, no futuro, ter aplicação como dispositivos orgânicos de emissão de luz (*organic light-emitting devices -OLEDs*).

**Palavras-chave:**

Polímeros de coordenação 1D, ferro(II), diimidas, diamidas, hóspede, clatratos de Hofmann 3D.

# Abstract

Functional materials have attracted great attention of the scientific community in the last few years. This area of study comprises the fields of physics, supramolecular chemistry and also organic, inorganic and coordination chemistry. These structures have a combination of different properties and the merge of all these areas is necessary, if not essential.

The research work here presented aimed to develop new functional materials with different properties, so they could have applications as sensor devices, and, for this, we focused our efforts in combining spin crossover (SCO) with other properties such as luminescence and/or conductivity. SCO compounds respond to external changes, such as temperature, pressure or light. They can also respond to host-guest interactions, especially in three dimensional (3D) structures.

The first strategy adopted was to synthesise *para*-substituted bipyridine ligands in order to obtain 3D Hofmann clathrates. Another approach used was the synthesis of ligands constituted by a triazole unit, a naphthalene diimide intermediate fragment and an aliphatic region for the assembly of 1D coordination polymers.

The magnetic behaviour of all synthesised polymers was obtained by SQUID magnetometry. One of the 1D polymers showed a fast-gradual SCO while the rest showed a behaviour characteristic of mainly HS. In the case of the 3D Hofmann clathrates one of them showed the metal centres were mainly in the HS state and the other one showed profile of a LS state compound. For the insertion tests it was observed that one of the 3D polymers altered its magnetic behaviour in the presence of a guest molecule.

The conductivity properties of the 1D polymer with SCO and luminescent properties showed a semiconductor behaviour.



**Keywords:**

1D coordination polymers, iron(II), diimides, guest molecules, 3D Hofmann clathrates.

# Symbols and Abreviations

| | |
|---|---|
| **1D** | one-dimensional |
| **2D** | two-dimensional |
| **3D** | three-dimensional |
| **$\mu_{eff}$** | effective magnetic moment |
| **$\mu_{exp}$** | expected magnetic moment |
| **$\eta$** | yield |
| **$\chi_M$** | molar magnetic susceptibility |
| **A** | anion |
| **AIBN** | azobisisobutyronitrile |
| **APT** | attached proton test |
| **COSY** | correlation spectroscopy |
| **DMF** | *N*,*N*-dimethylformamide |
| **EPR** | electron paramagnetic resonance |
| **EtOH** | ethanol |
| **FTIR** | Fourier transform infrared spectroscopy |
| **HMBC** | heteronuclear multiple bond correlation |
| **HS** | high-spin |
| **HSQC** | heteronuclear single-quantum correlation |
| **ISC** | inter-system crossing |
| **LMCT** | ligand-metal charge transfer |
| **LS** | low-spin |
| **$M(CN)_4$** | tetracyanometallate |
| **Med** | medium |
| **MeOH** | methanol |
| **MLCT** | metal-ligand charge transfer |
| **MOFs** | metal-organic frameworks |
| **NBS** | *N*-bromosuccinimide |
| **NMR** | nuclear magnetic resonance |
| **OLEDs** | organic light-emitting device |
| **R-trz** | **s**ubstituted 1,2,4-triazole |
| **S** | singlet state |
| **SCO** | spin crossover |
| **SQUID** | superconducting quantum interference device |
| **Str** | strong |
| **T** | triplet state |
| **TGA** | thermogravimetric analysis |
| **TLC** | thin-layer chromatography |
| **TMS** | tetramethylsilane |
| **Wk** | weak |

# List of Contents

# List of Figures

# List of Schemes

# List of Tables

# 1 Introduction

## 1.1 Functional Materials

The development of new materials is an ongoing task in the chemistry world and probably one of the most essential chemistry areas when it comes to technologic progress. Therefore, the search for multifunctional materials with unique characteristics is a great opportunity to thrive.[1,2]

Supramolecular chemistry is a subject directly involved in the development of these materials. Thus, there has been an effort to modify some already known compounds and change their properties. Metal-organic frameworks (MOFs) are a great example. These structures have been studied for decades and are still among the most important three-dimensional assemblies used in processes such as catalysis, separation, gas adsorption and drug delivery systems **(figure 1.1)**. [3,4]

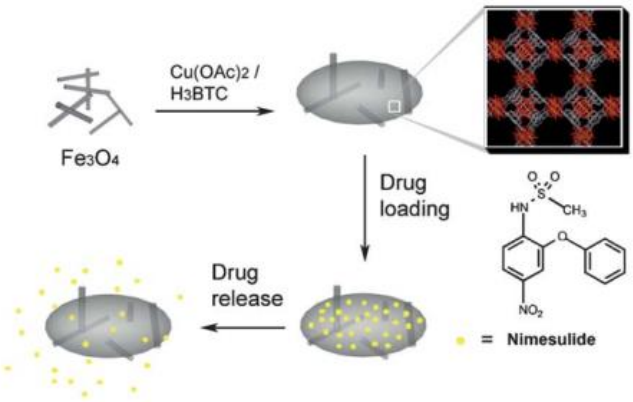


Figure 1.1. Schematic example of a magnetic MOF being used as a drug delivery system.[4]

Other exciting systems are the coordination polymers, that can fit in the MOF category. These structures can have one of the three dimensions (1D, 2D, 3D) and are assembled with transition metals that can have interesting magnetic properties, such as spin crossover (SCO). When combined with other features, such as luminescence, chirality and pore size, extraordinary multifunctional materials can be created.[5,6] In **figure 1.2** is represented an example of a coordination polymer hosting ethanol (EtOH) molecules inside the pores. This 3D structure results on the interpenetration of 2D networks and the host guest interaction promotes the SCO behaviour of the polymer.[7]

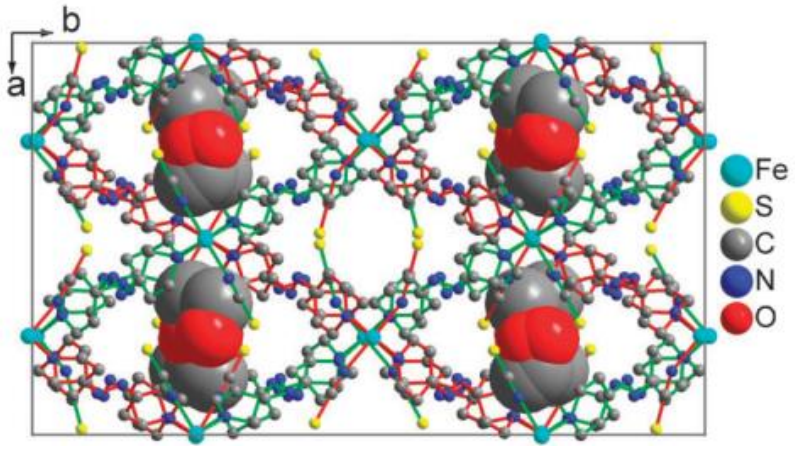


Figure 1.2. Schematic representation of a coordination polymer hosting EtOH molecules inside the pores. [5]

## 1.2 Spin Crossover

Crystal field theory is one model that explains the splitting of the orbitals in metal complexes. The splitting pattern is determined by the type of ligands and by their arrangement. Therefore, the energy values of the d orbitals vary according to the geometry of the metal centre in the complexes. In the octahedral geometry the five d orbitals split in two levels of degenerated orbitals: the $e_g$ and the $t_{2g}$ **(figure 1.3)**. [8]

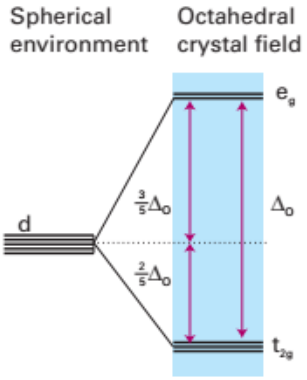


Figure 1.3. *d* orbital energy distribution in an octahedral geometry metal centre. [8]

Transition metals with electronic configuration between $3d^4$ and $3d^7$ can display two different spin states according to the electronic distribution. This is influenced by the strength of the ligands field: low spin (LS) if the electron pairing energy is larger than the ligand field splitting resulting in a spin multiplicity with the lowest possible value; high spin (HS) when spin multiplicity is the highest possible. **(figure 1.4)**. [8–10]

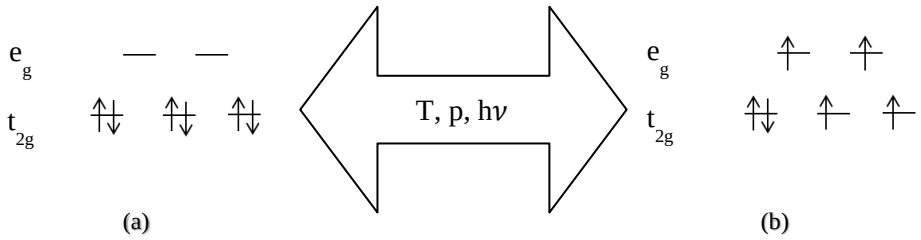


Figure 1.4. Electronic distribution for an octahedral $3d^6$ metal ion; (a) LS distribution; (b) HS distribution (T= temperature, p= pressure, hν= energy).

However, the transition between spin states can occur and is termed spin crossover (SCO). For this transition to occur is necessary to destabilise the spin state in which the complex stabilises (HS or LS) and this can be done by external changes in the complex environment. Being such an interesting phenomenon, SCO has been the centre of the attention for many years to those who study molecular magnetism.[10–13] SCO can be induced by external stimuli such as temperature, light, pressure and guest molecules insertion, involving simultaneously changes in colour, dielectric constant or electrical resistance. Therefore, there was an increase in the development of these new switchable materials with properties that can be somehow controlled and a considerable amount of work has been published since the first SCO compounds started to appear.[14][15] All these exchangeable properties affect the structure geometry and the bond distance. The combination of all these characteristics make these entities

interesting candidates in the detection of different organic and inorganic compounds, working as sensors or, for example, applied in memory devices, depending on the SCO profile. [11,16,17]

The most commonly used techniques to evaluate the magnetic behaviour of these SCO compounds are Superconducting Quantum Interference Device (SQUID) magnetometry and Mössbauer spectroscopy. The information obtained using SQUID is based on measures of the magnetic susceptibility throughout a temperature range, that is, the magnetic response of the metal centres when exposed to an external magnetic field. This response is related to the type of transition of the metal centres and is the key to study the possible applications of these materials. As described in **figure 1.5** the transitions can be complete, (a) to (d), that is, all metal centres change their spin state, or incomplete, (e), meaning that there is a mixture between spin states of the metal centres. There are several types of complete spin transitions, such as, gradual, abrupt, abrupt with hysteresis and step wise.[10]

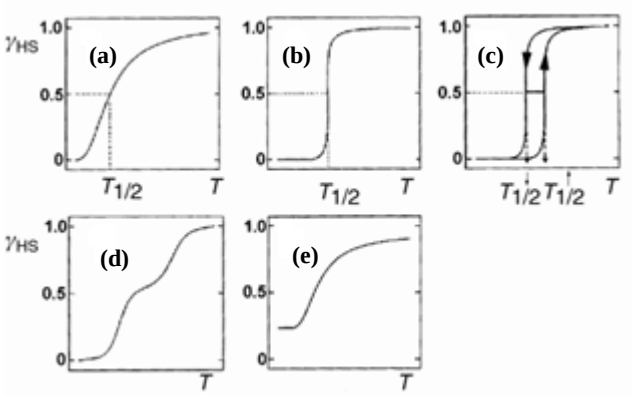


Figure 1.5. Magnetic profiles for SCO materials. Transitions: (a) gradual; (b) abrupt; (c) abrupt with hysteresis; (d) step wise; (e) incomplete [10]

## 1.3 Iron(II) SCO Compounds

Iron(II) is one of the most commonly studied metals in SCO compounds since the materials obtained with this metal frequently show spin transition. [10,18,19] Besides, iron(II) has $3d^6$ electron configuration, which means the metal centre has a diamagnetic LS state or a paramagnetic HS state as shown in **figure 1.4**. The transition between these very distinct magnetic states is associated with a change in the complex colour. [15,20–22]

SCO coordination polymers containing $d^4$-$d^7$ metal centres on octahedral environment have also been highly explored. When considering coordination polymers, we must take into account that these can be assembled in the three dimensions, depending, for example, on the number of coordination sites in the ligand **(figure 1.6)**. [23–25] The final polymeric structure is also influenced by the synthesis method since that affects the way the structure crystallises and, sometimes, different motifs in a structure with the same ligand can be obtained. [26,27]

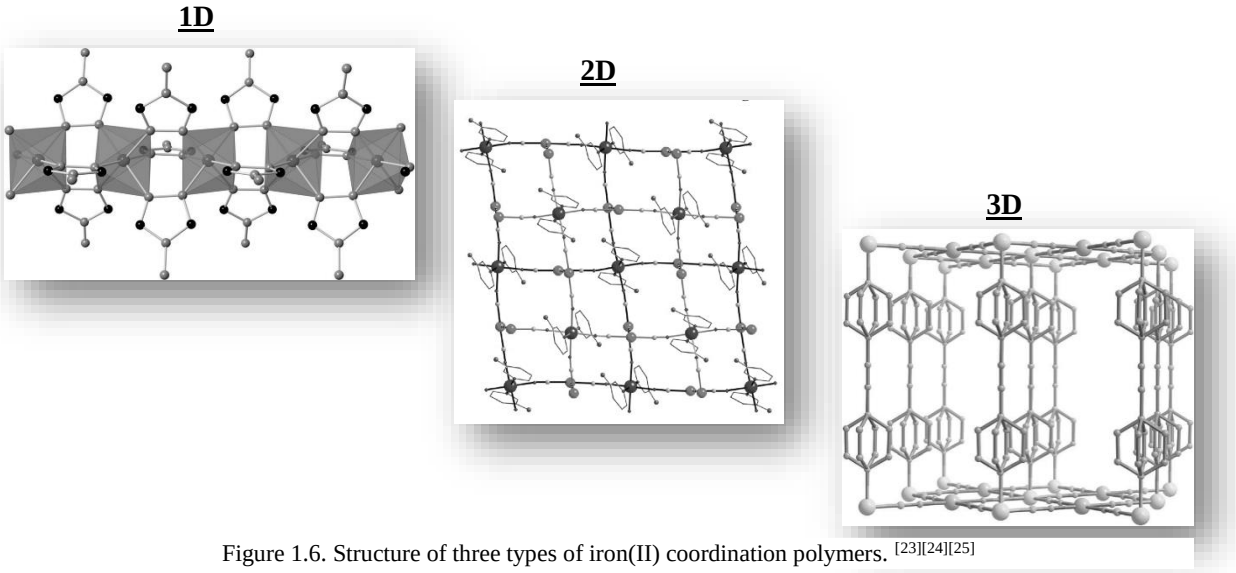


Figure 1.6. Structure of three types of iron(II) coordination polymers. [23][24][25]

The optical and magnetic properties, intrinsic to the SCO compounds, promote a synergetic effect when combined with other singular characteristics, such as luminescence emission. This is very interesting when applied in sensors or memory devices in various fields of science and technology **(figure 1.7)** [28,29] Thus, the importance of the development of new ligands that bring together a sequence of promising characteristics to the formation of structures with interesting magnetic and luminescence properties is clear.[30,31]

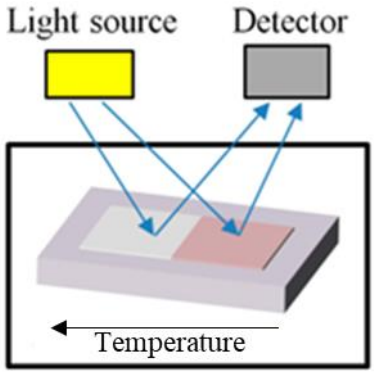


Figure 1.7. Schematic representation of a SCO compound used as a sensor. [31]

## 1.3.1 Ligands with Particular Properties

Diimides are well studied entities known for being ligands that have luminescence and conductivity properties. They are also very interesting for their donor/acceptor properties which reflects in their capacity for establishing π-π- interactions. All of these characteristics allied with SCO create the perfect conditions for obtaining extremely versatile materials with multiple applications such as, for example, transistors. These units are usefull in the assembly of coordination polymers in any of the three dimensions, depending on the R group used **(figure 1.8)**. [32,33]

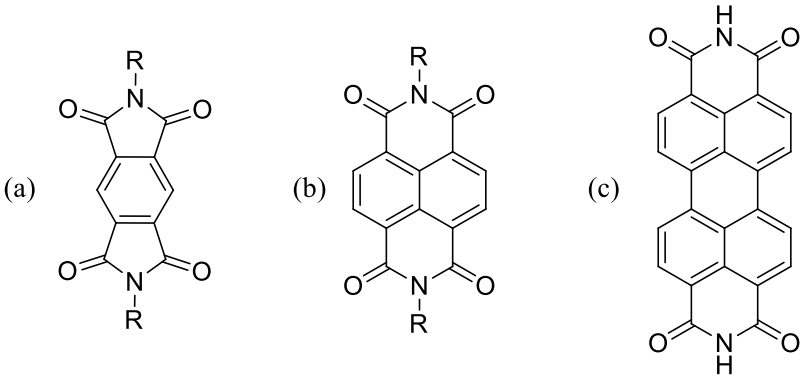


Figure 1.8. General structure of three diimides families: (a) pyromellitic diimides; (b) naphtalene diimides; (c) perylene diimides.[33]

Other units to be used in the assembly of coordination polymers derive from benzene. These simple units are also known for establishing π-π interactions and for promoting luminescence properties in the structures. The derivatised benzene units benefit from these properties and add new ones if, for example, the ring is derivatised with chiral compounds or functional groups that can promote different interactions. This benzene derivatives have been much used in the past in the assembly of coordination polymers **(figure 1.9)**.[34]

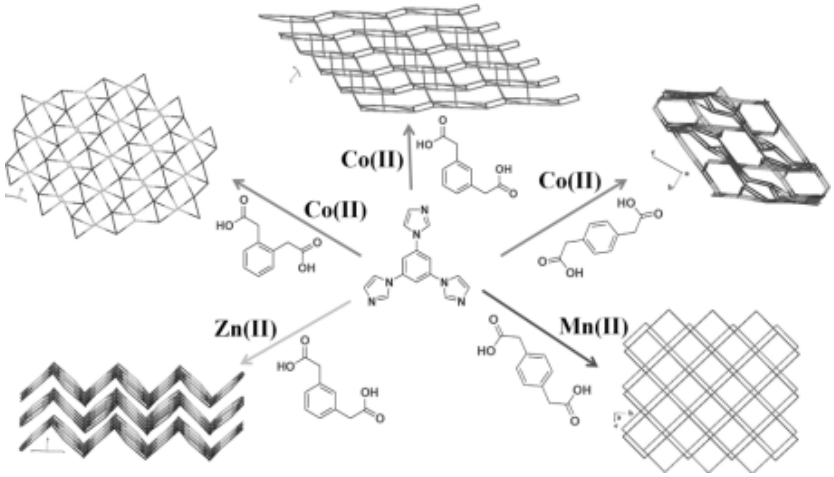


Figure 1.9. Schematic representation of benzene derivatives used as ligands in the assembly of coordination polymers. [34]

## 1.3.2 1D Coordination Polymers

Coordination polymers are structures in which the repeat unit includes a coordination of a ligand to a transition metal. Nitrogen atoms are a good example of electron donors and are the most used in these cases.

In the case of 1D coordination polymers the structures obtained are amorphous or poorly organised chains and the ligands used to assemble these can have one or two coordination sites. Triazole based ligands, for instance, are very used in the synthesis of 1D polymers, granting unique properties to these compounds, including SCO.[24,35,36]

Out of all the nitrogen based ligands , 1,2,4-triazole derivatives are specially adequate for the assembly of 1D polymeric structures **(figure 1.10)**.[37] Iron(II) coordination polymers that incorporate these ligands- $[Fe(R\text{-}trz)_3][A]_2$- are often suitable to be applied in electronic devices (switches, memory and data storage, etc) due to the proclivity for forming gels, to be deposited as films, liquid crystals and obtaining nanoparticles. These ligands also contribute to the formation of highly cooperative systems.[38,39]

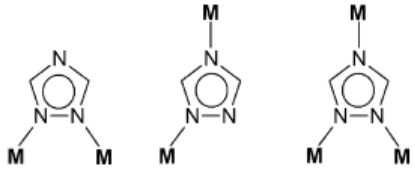


Figure 1.10. Coordination possibilities of 1,2,4-triazole ligands to the metal centres. [39]

As opposed to the 3D and 2D coordination polymers, the 1D structures do not form pores or host guest molecules between layers but, this does not mean that they do not establish intermolecular interactions. In fact, they have the capacity, sometimes, to create two dimensional structures as a result of the intertwist of several 1D chains. This may provide a way of crystallising these chains since they lack organisation.

The group of Bauer *et al.* developed a strategy to counteract this crystallisation problems and to optimise the spin transition profile of a coordination polymer. As can be seen in **figure 1.11** the magnetic profile of the monomer, the dimer and the polymer differ completely from each other due to the different interactions established with the surrounding species. These differences in the behaviour also reflect in the crystallisation process and sometimes it is easier to obtain the crystal of the monomer or the dimer instead of the polymer. Nevertheless, it can be helpful to understand the spatial arrangement of the atoms in the polymer, the nature of the interaction between the ligand and the metal centre and the bonds lengths. [40]

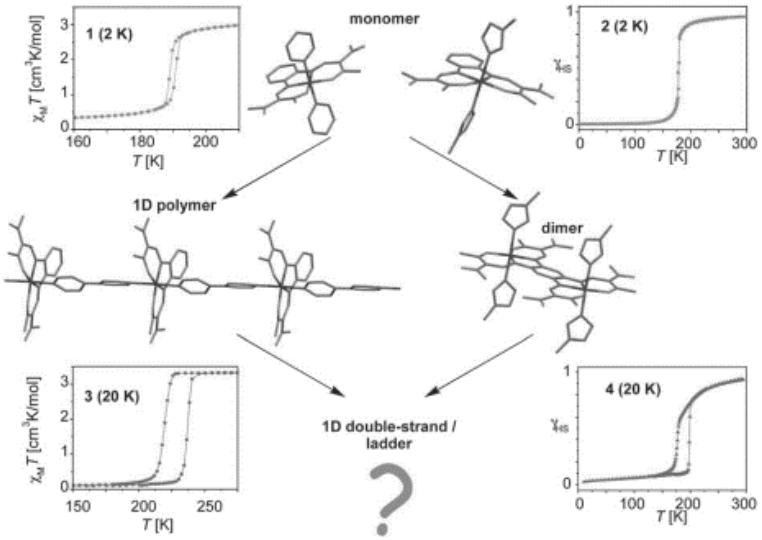


Figure 1.11. Representation of the magnetic profiles of a monomer a dimer and an oligomer of the same 1D coordination polymer. [40]

As was pointed out previously, the SCO properties allied with other useful characteristics such as luminescence emission, give to these polymers an interesting twist and these 1D coordination polymers are great structures to study these synergetic effects in, for they can be easily deposited as thin films.

## 1.3.3 3D Hofmann Type Coordination Polymers

Hofmann clathrates, a class of MOFs and their analogues, are among the most known and well-studied for practical applications as SCO compounds.[41,42]

These solids have more flexibility and ways of modifying porosity than other inorganic porous compounds, allowing desorption and adsorption of guest molecules and, consequently, leading to the perturbation of various physical and chemical properties of the framework affecting also its SCO behaviour. [43,44]

These polymeric structures are usually assembled with the coordination of an iron(II) metal centre to a double coordination sited ligand creating a 2D network. After this, iron(II) coordinates to a second compound, a tetracyanometalate $M(CN)_4$, that acts as a second coordination compound **(figure 1.12)**. These square planar tetracyanometalate complexes have the rigidity required to promote the strong cooperativity between the SCO active centres and are indispensable in the creation of the intermediate plans that allow the material to be three-dimensional.[45,46]

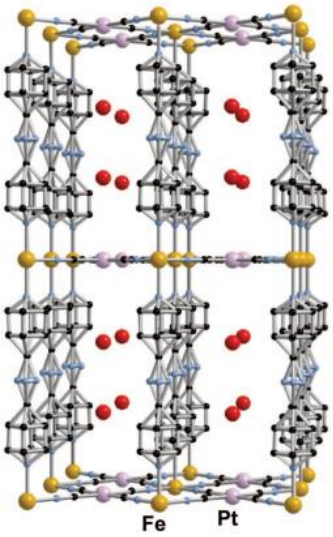


Figure 1.12. Structure of a three-dimensional Hofmann type coordination polymer. ($Pt(CN)_4$): red- oxygen; black- carbon; blue- nitrogen. [46]

As pointed out earlier, the type of ligand used to assemble these polymers is determining to obtain the desired structure. José A. Real *et al.* dedicated a vast part of their investigation to the study and optimisation of the synthesis of two and three-dimensional Hofmann-type coordination polymers with SCO. The ligands used by this group to obtain this type of materials are based in *para*-substituted pyridine compounds **(figure 1.13)**. [46]

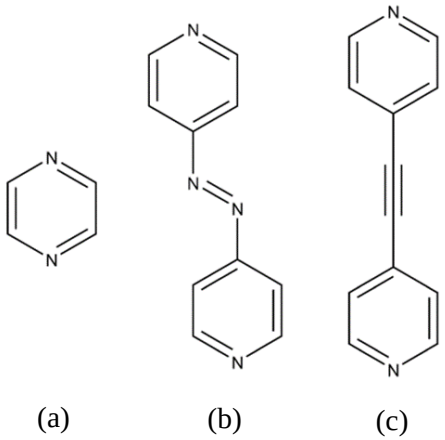


Figure 1.13. Structures of reported bipyridine compounds used in 3D polymers: (a) pyrazine, (b) azopyridine and (c) bis(4-pyridyl)acetylene. [25]

This feature has proven to be almost essential to succeed in obtaining the desired materials since the ligand linearity contributes to the self-assembly of the structure and in that way the ligands ideally function as pillars and usually result in very cooperative systems **(figure 1.14)**. [47–49]

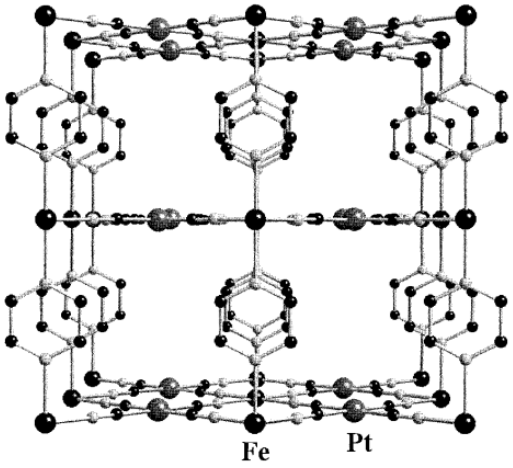


Figure 1.14. Representation of a 3D Hofmann type coordination polymer using pyrazine. [49]

### *1.3.3.1 Guest Molecules Insertion*

Being three dimensional, these structures have cavities inside which can establish interactions or form hydrogen bonds with guest molecules. These interactions are even sometimes responsible for altering the SCO behaviour. For this reason, the study of the insertion of various guest molecules is extremely important to evaluate their influence in the magnetic profile since it can diverge so much from guest to guest. Besides changing the magnetic behaviour, guest molecules insertion can have an extremely important role in obtaining a crystal of the structure. This is essential to know, using single crystal X-ray, the spatial organisation of the atoms in the structure and cavities as well as the bonds length. These guests can work either as templates (they do not necessarily stay inside the pores) or

become a part of the structure holding it more tightly together through interactions with the ligands.[50–53] In **figure 1.15** is represented an example of the transformations caused in the magnetic behaviour in an iron(II) MOF by the insertion of different guest molecules (methanol and 1-propanol).[54]

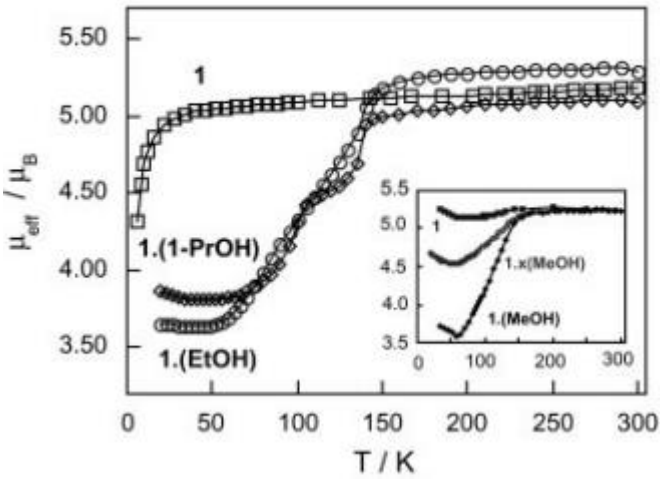


Figure 1.15. Magnetic profile of a three-dimensional structure after guest molecules insertion. [54]

## 1.4 Luminescence

Luminescence is a phenomenon defined by the emission of an electron of an excited species and characterised by the path of the energy decay when this happens. That is, a species is excited from the ground state $S_0$ to the excited state $S_1$ by energy absorption and then it decays into the ground state, again, emitting light (fluorescence). **figure 1.16** Phosphorescence occurs when the species goes from the excited singlet state to an excited triplet state ($T_1$, lower energy) by intersystem crossing (ISC) and only then relaxes to the $S_0$. Because this ISC involves a forbidden transition, the energy decay in phosphorescence takes more time.[55,56]

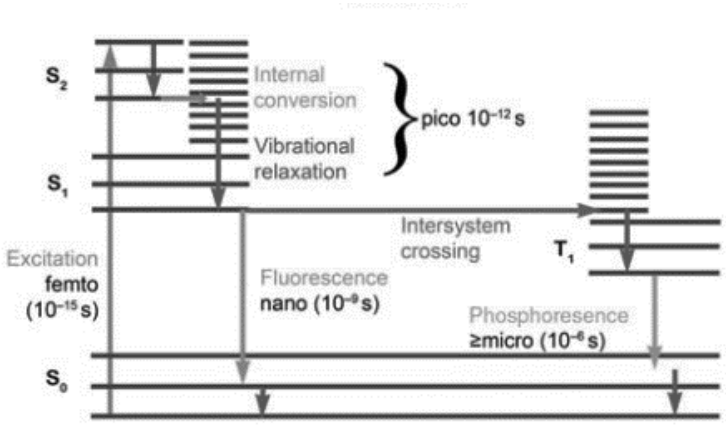


Figure 1.16. Jablonski scheme for the luminescence phenomenon. [56]

The emission spectrum of some species changes with the temperature. It can change the intensity of the emission band or even shift the wavenumber of maximum emission but, either way, we can compare the modifications in the spectrum at different temperatures. This makes it easier to associate a SCO with luminescence and verify whether there is a direct connection between both properties.

Wang et al. published their work in the study of this effect by measuring the luminescence of an iron(II) 1D coordination polymer at the same range of temperature as used for the magnetic measurements **(figure1.17)**. [57]

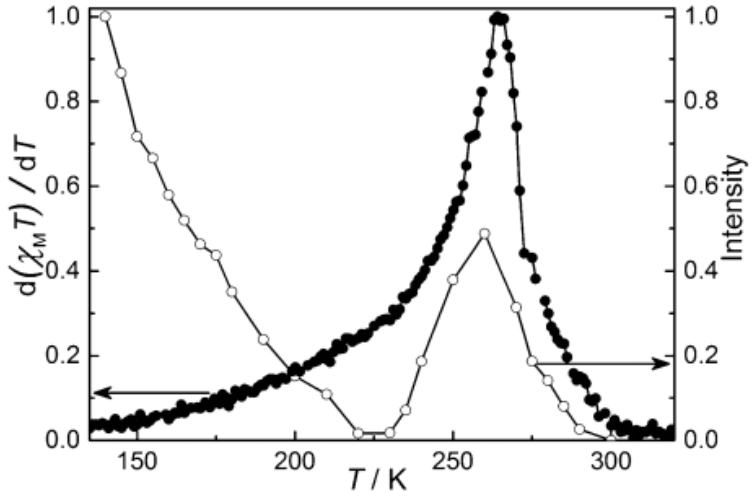


Figure 1.17. Plot of the normalised differential magnetic susceptibility and the normalised maximum intensities of emission throughout the temperature range. [44]

## 1.5 Objectives

The aim of this dissertation is to develop some 1D and a 3D coordination polymers based on iron(II) and to study the different type of structures that can be assembled. Another purpose is to highlight the very distinct properties that are obtained for these polymers according to the ligands used and to promote interactions with other molecules (solvents, guests) for the 3D polymers. The study of the luminescence properties is also an aim of this work and the synergetic effect between the luminescence and SCO is an important topic that will be discussed.

The two ligands used to synthesise the Hofmann type coordination polymers are already known ligands and are represented in **figure 1.18**.[58] One of them was synthesised in the scope of this project (**L1**) and, so far, it had not been used in the assemble of structures of this type. The other (**L2**) was given by a laboratory colleague

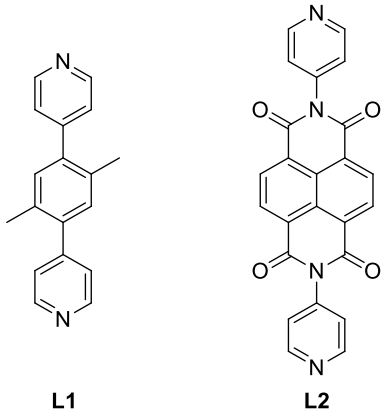


Figure 1.18. Ligands used in the synthesis of 3D Hofmann type coordination polymers.

New R-trz based ligands (**L3-L6**) synthesised for the synthesis of the 1D coordination polymers are represented in **figure 1.19**.

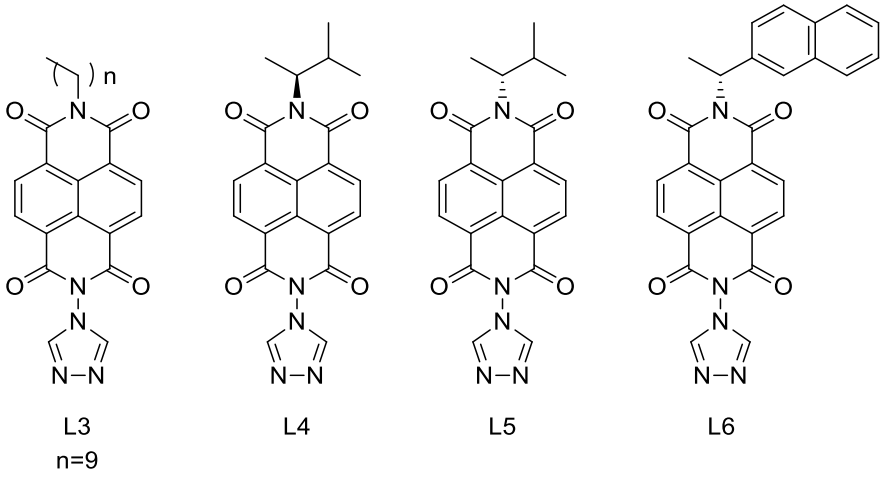


Figure 1.19. Ligands used in the synthesis of 1D coordination polymers.

Four, also new, analogues of these naphthalene diimide ligands (**L7-L10**) were synthesised using a perylene diimide unit instead **(figure 1.20)**. The synthesis of coordination polymers with these ligands failed due to the insolubility of the bulky ligands.

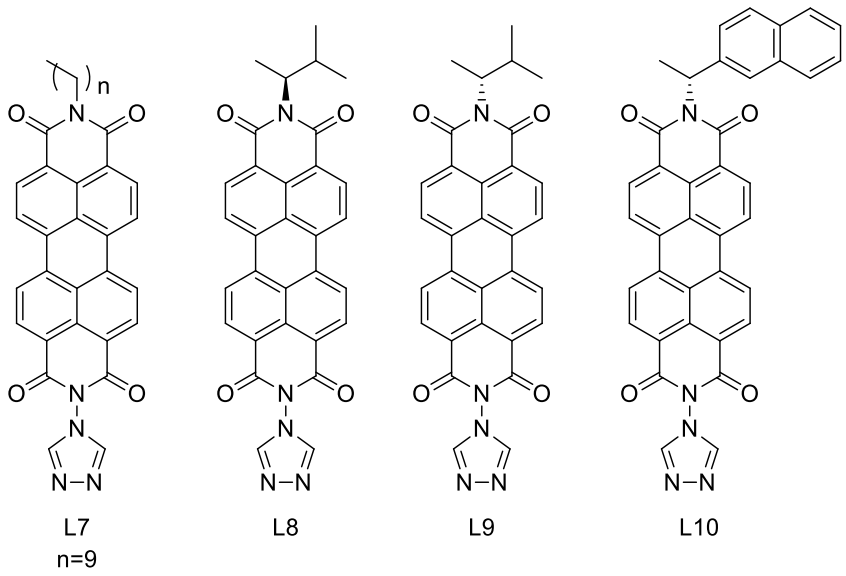


Figure 1.20. Synthesised ligands based on perylene diimide units.

The ligands were characterised by the regular characterisation techniques (NMR spectroscopy and FTIR spectroscopy), elemental analysis and, by SQUID magnetometry, was evaluated the magnetic behaviour of the coordination polymers. The magnetic profiles of the 3D structures (**P1** and **P2**) with and without inserted guest molecules was also studied. Luminescence studies were carried out for polymers **P1** and **P3** as well as the conductivity properties of **P3**.

The general structure for both Hofmann type and 1D polymers is represented below **(figure 1.21)**.

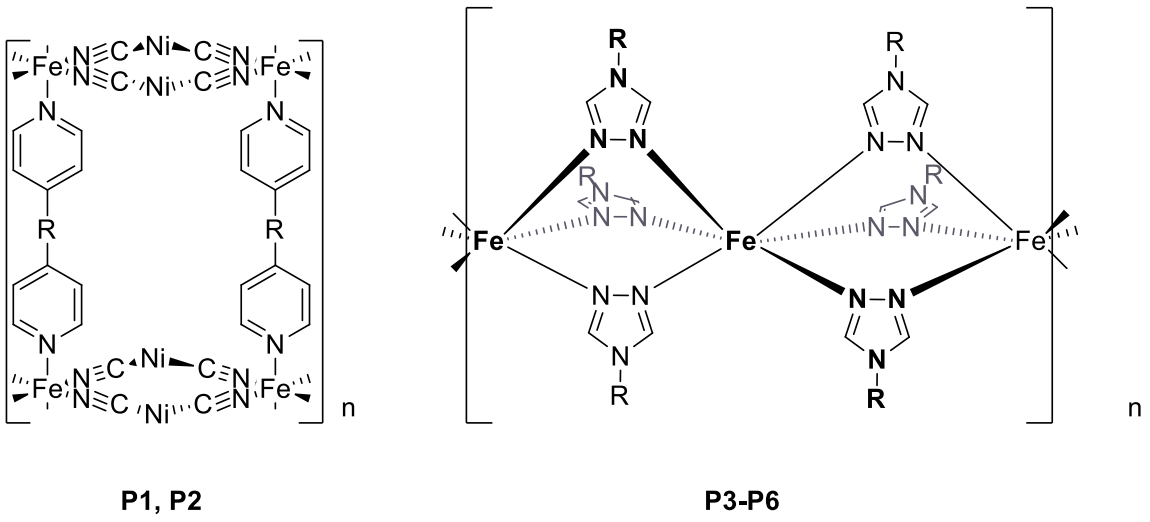


Figure 1.21. General structure for the synthesised Hofmann type 3D polymers (left) and 1D polymers (right).

# 2 3D Hofmann Type Iron(II) Coordination Polymers

Herein is presented the synthesis of two 3D coordination polymers. For the assembly of these structures two different ligands were used, **L1** and **L2**, represented in **figure 2.1**. The assembly of 3D Hofmann clathrates allows the creation of cavities that can possibly host other entities. Thus, we performed studies that addressed the insertion of guest molecules in the structures and subsequent evaluation of their effect in the magnetic profile.

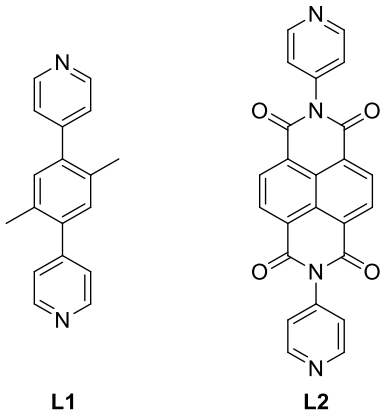


Figure 2.1. Ligands used in the assembly of the 3D coordination polymers.

## 2.1 Ligands Synthesis

The initial idea for this part of the project was to obtain linear bipyridine ligands with chiral amide groups in the benzene unit due to its versatility of being, simultaneously, a hydrogen donor and acceptor. This functionality will allow the ligand to establish hydrogen bonds with the guest molecule and for this we envisage this 3D structures as good candidates to act as racemic sensors. On the journey to synthesise these ligands, different strategies were attempted **(scheme 2.1)**.

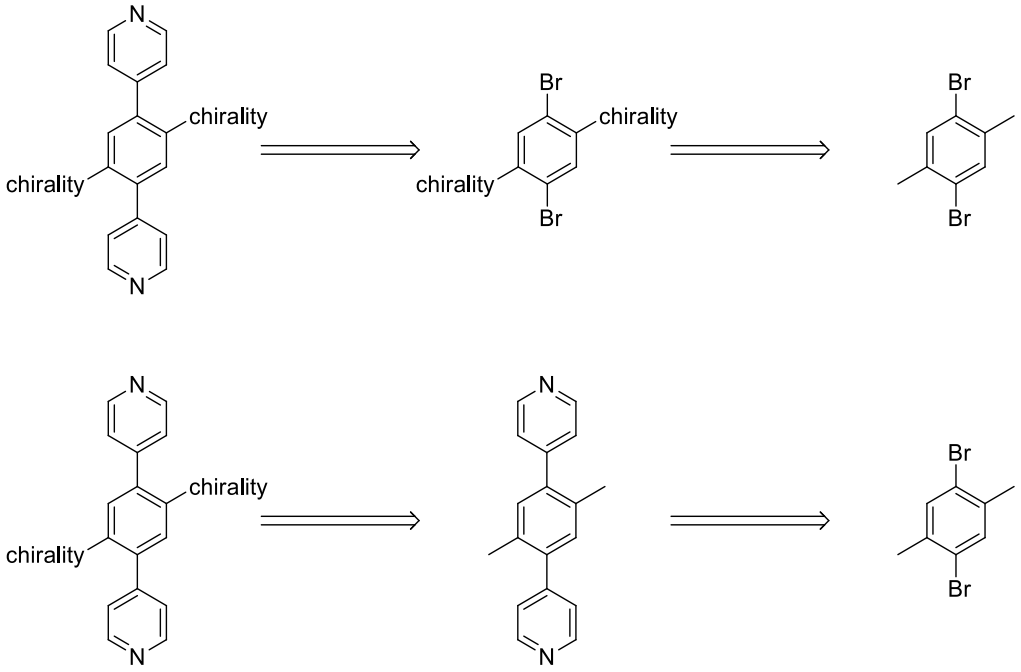


Scheme 2.1. Retrosynthetic pathways pursued to obtain the envisioned ligands.

Starting from 1,4-dibromo-2,5-dimethylbenzene, compound **1** was synthesised by a Whol-Ziegler reaction **(Scheme A1)** and it is represented in **Scheme 2.2**

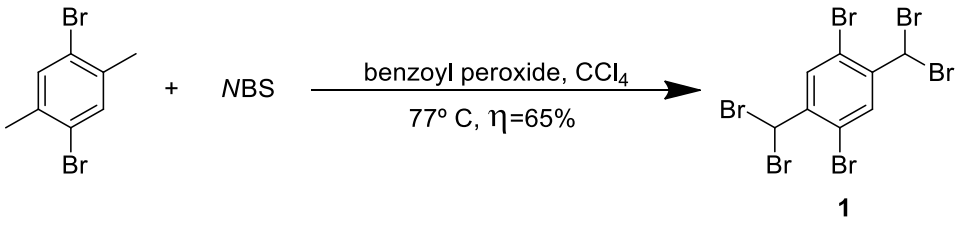


Scheme 2.2. Synthesis of compound **1**.

After, the methyl bromines functionalities were oxidised with $AgNO_3$ into carbonyl groups to give the aldehyde **2 (scheme 2.3)**.

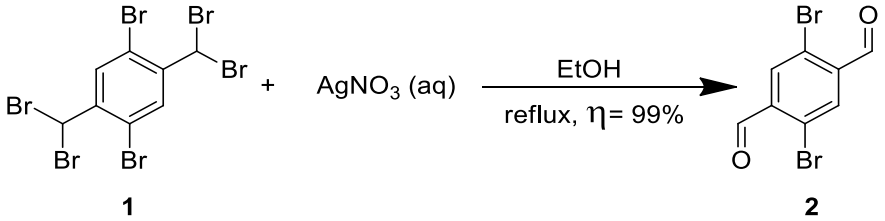


Scheme 2.3. Synthesis of compound **2**.

The subsequent reaction aimed to form the envisioned amide from compound **2** via a one-pot reaction, but it was observed by thin layer chromatography (TLC) that no product was formed **(Scheme 2.4)**. Other attempts were performed in order to obtain the chiral aromatic amide, such as the formation of an acyl chloride following the chloride substitution for an amine, but once again no product formation was observed.

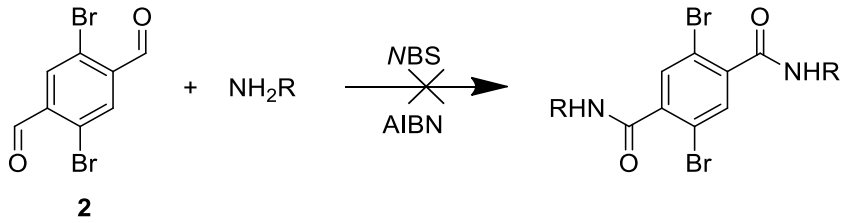


Scheme 2.4. Synthetic attempt to obtain an amide.

Since the formation of a benzene ring with a chiral amide group inserted was unsuccessful, an alternative strategy would be to synthesise benzene units with chiral amines. The plan now was to insert a chiral amine by a nucleophilic substitution of the bromine atom. Starting from 1,4-dibromo-2,5-dimethylbenzene, compound **3** was synthesised by a Whol-Ziegler reaction, in similarity to compound **2 (scheme 2.5)**.

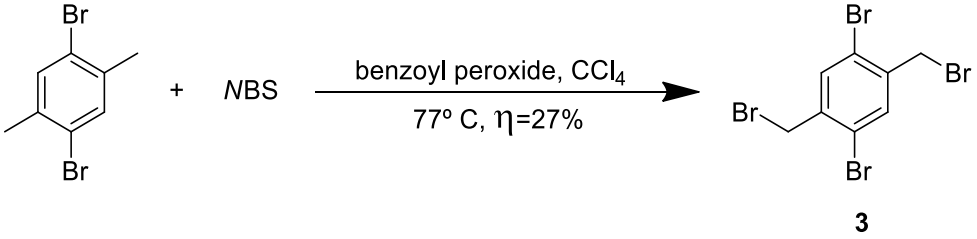


Scheme 2.5. Synthesis of compound **3**.

This bromination was followed by the nucleophilic substitution of the aliphatic bromine by the chiral amine giving, respectively, the chiral compounds **4** and **5 (scheme 2.6)**.

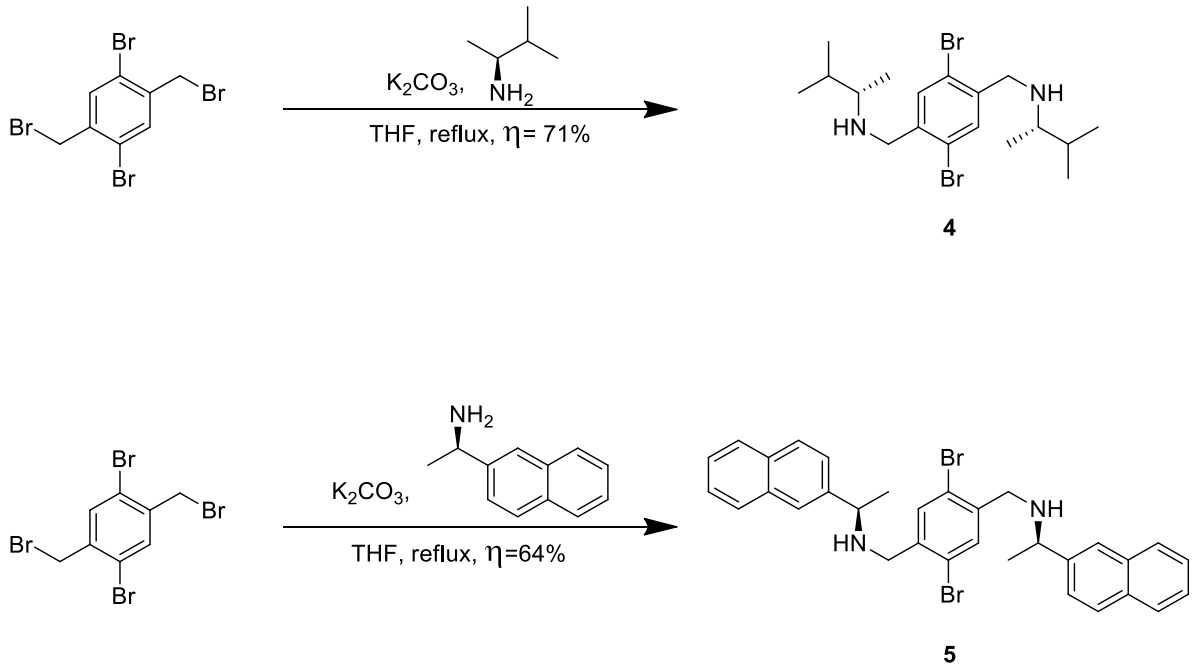


Scheme 2.6. Synthesis of compounds **4** and **5**.

Having succeeded in adding the amine in the aromatic ring, the next reaction step was to insert the pyridine units by a Suzuki coupling reaction, **(scheme A2)**, but unfortunately it was confirmed by TLC that no desired product had been formed. Therefore, a new strategy was adopted **(scheme 2.7)**.

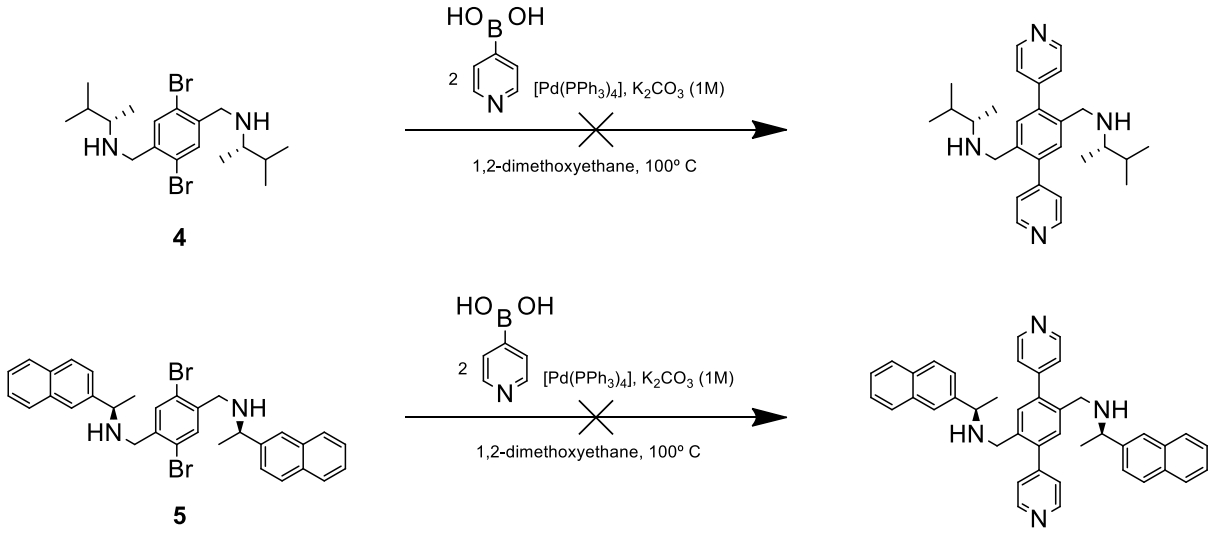


Scheme 2.7. Synthetic attempts to obtain chiral amine ligands.

The new strategy adopted was to first insert the pyridine groups in the 1,4-dibromo-2,5-dimethylbenzene **(scheme 2.8)** and derivatise it afterwards with the chiral amines. This way, it could be easier to isolate the anticipated product since the introduction of amine groups in early steps enhances the polarity of the product, increasing the difficulty of the purification.

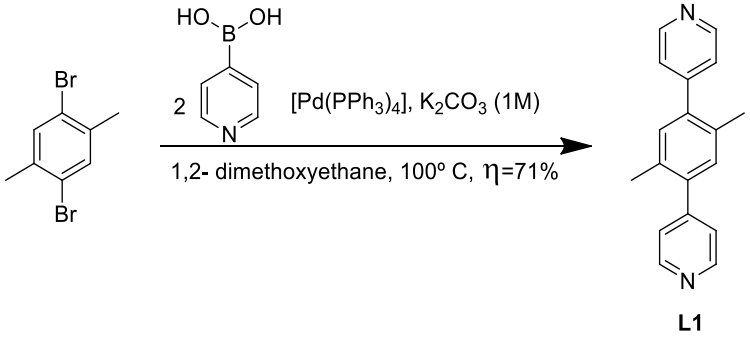


Scheme 2.8. Synthesis of **L1** by a Suzuki reaction.

Having obtained the desired bipyridine product, there was an attempt to insert one bromide in each methyl group to, subsequently, substitute them with the amines previously synthesised, but no reaction occurred **(scheme 2.9)**. This could be due to the chemical hindrance during the catalytic cycle, **scheme A2**, more precisely upon the coordination of the bipyridine pillar to the palladium.

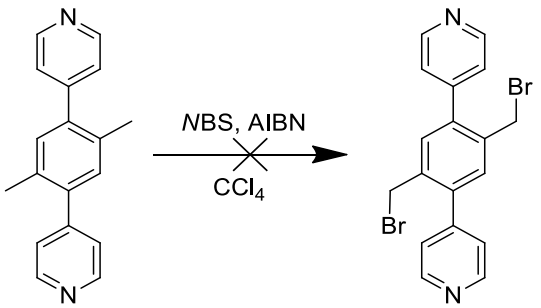


Scheme 2.9. Synthetic attempt of the bromination of the methyl groups in the ligand.

## 2.2 Ligands Characterisation

The ligand **L1** was characterised by Nuclear Magnetic Resonance (NMR) spectroscopy and Fourier Transformed Infrared (FTIR) spectroscopy and their luminescent properties were evaluated.

**L1**, as pointed out earlier, is an already known ligand that has been used in the assembly of general MOFs but not in the formation of Hofmann type coordination polymers.[58] Nevertheless, the ligand was characterised by $^{1}$H NMR spectroscopy, as shown in **figure 2.2**. It is visible the two doublets from the spin interaction of the pyridine protons and, also, the singlet correspondent to the proton of the benzene groups. At higher filed the singlet from the protons of the methyl groups is observed.

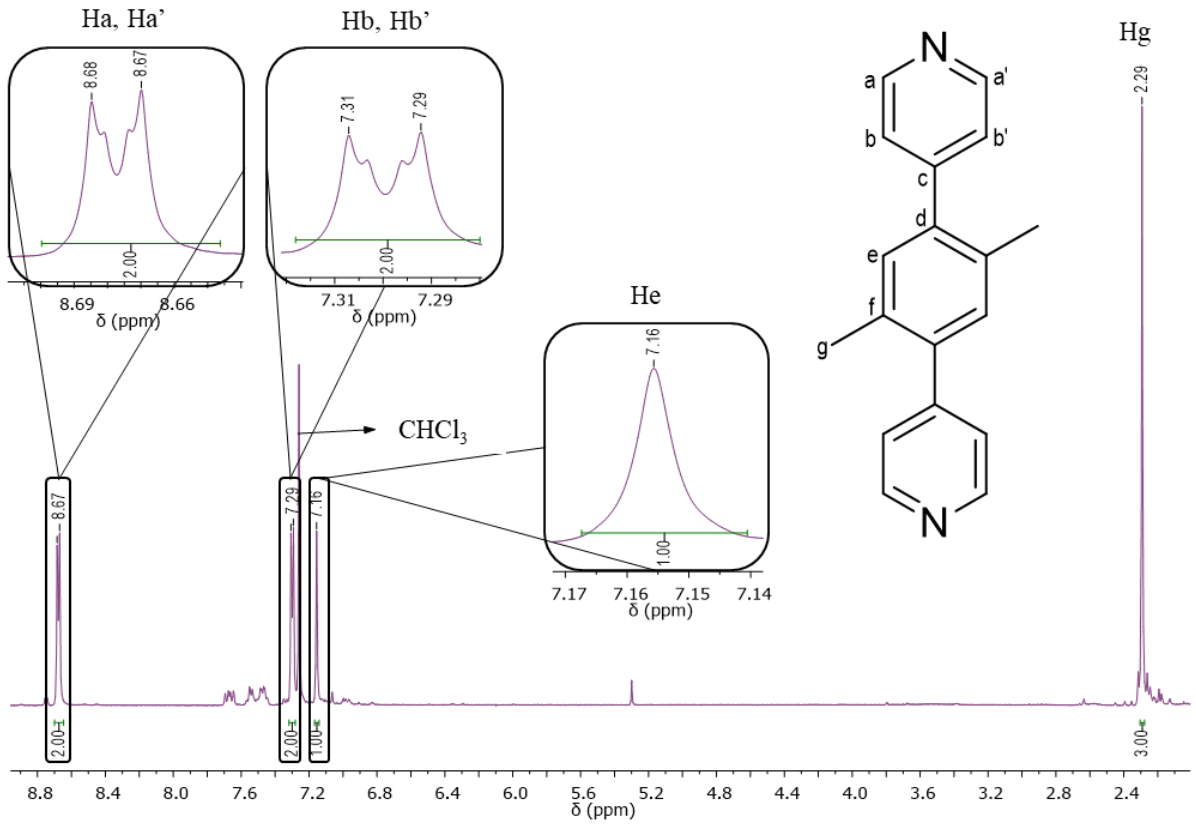


Figure 2.2. $^{1}$H NMR spectrum of L1 in $CDCl_3$.

In the FTIR spectrum can be seen the characteristic bands from the aromatics C-H bending (690-900 $cm^{-1}$), the conjugated C=C stretching bands (1500-1600 $cm^{-1}$) and the stretching band characteristic of the C-N bond in the pyridine unit (1000-1250 $cm^{-1}$) **(figure A1)**.

The synthesis and characterisation of **L2** is not reported here since it was performed by a laboratory colleague and the ligand was used as received. The FTIR data of **L2** can be found in **figure A2** in the appendix section, and the $^{1}$H NMR spectrum of **L2** in **figure A3**.

## 2.2.1 Luminescence Studies

Preliminary luminescence studies of the ligands in the solid state were carried out in collaboration with the University of Zaragoza and performed by Doctor Vanesa Fernandez. The emission of the samples was measured in the solid state at room temperature and at 77 K.

**L1** luminescence was evaluated and the results showed that the sample was very emissive. At room temperature only one emission profile was observed when exciting from 350 nm to 500 nm **(figure A4)**.

When lowering the temperature to 77 K, three different emission profiles were observed. The first one when exciting from 275 nm to 325 nm, the second when exciting from 375 nm to 475 nm and the third when exciting at 500 nm **(figure A5)**.

In the future, in order to fully characterise the luminescent behaviour of a species, it is crucial to determine the quantum yield and the luminescence lifetime. The first one gives us the ratio of the number of emitted photons to the number of absorbed photons and the luminescence lifetime determines the amount of time a species stays in the excited $S_1$ state.[59]

## 2.3 3D Polymers Syntheses

Due to a restriction, the synthesis of the Hofmann type coordination polymer proceeded using only **L1** and **L2**.

The syntheses of 3D coordination polymers are usually performed by one of two techniques: precipitation or slow diffusion. In this subchapter the polymers were prepared by precipitation. To a solution containing both the pillar ligand and the iron(II) salt ($Fe(ClO_4)_2$), was added dropwise a solution containing the $K_2[Ni(CN)_4]$ and immediately a yellow precipitate started to form. This method allows the formation of larger quantities of the product, but the powder obtained is not usually very crystalline. The slow diffusion method, usually performed in test tubes or H-shaped tubes (as presented further ahead in this work) allows the reaction to happen very slowly, increasing the chances of obtaining a crystalline product.

The Hofmann type coordination polymers are characterised, as described before, by containing a $M(CN)_x$ (x=2 or x=4) as a second coordination unit. To obtain this specific 3D structure was used $K_2[Ni(CN)_4]$. **(scheme 2.10)**. The representative yields showed for the coordination polymers synthesis were calculated considering the molecular mass of structure with no solvent or other guest molecules, even though the salts used were not anhydrous.

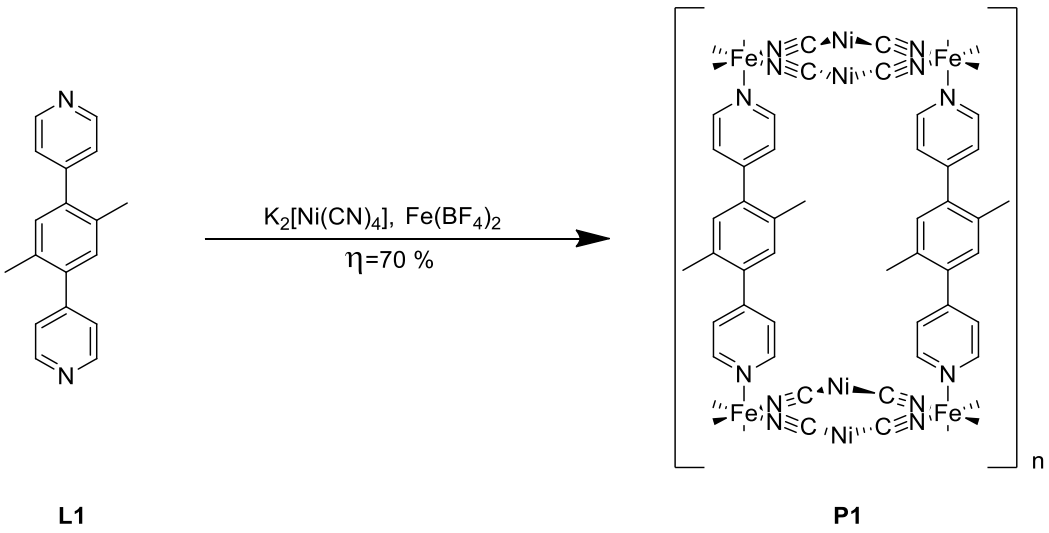


Scheme 2.10. Synthesis of 3D polymer **P1**.

Coordination polymer **P2** was synthesised using the exact same strategy as for **P1 (scheme 2.11)**.

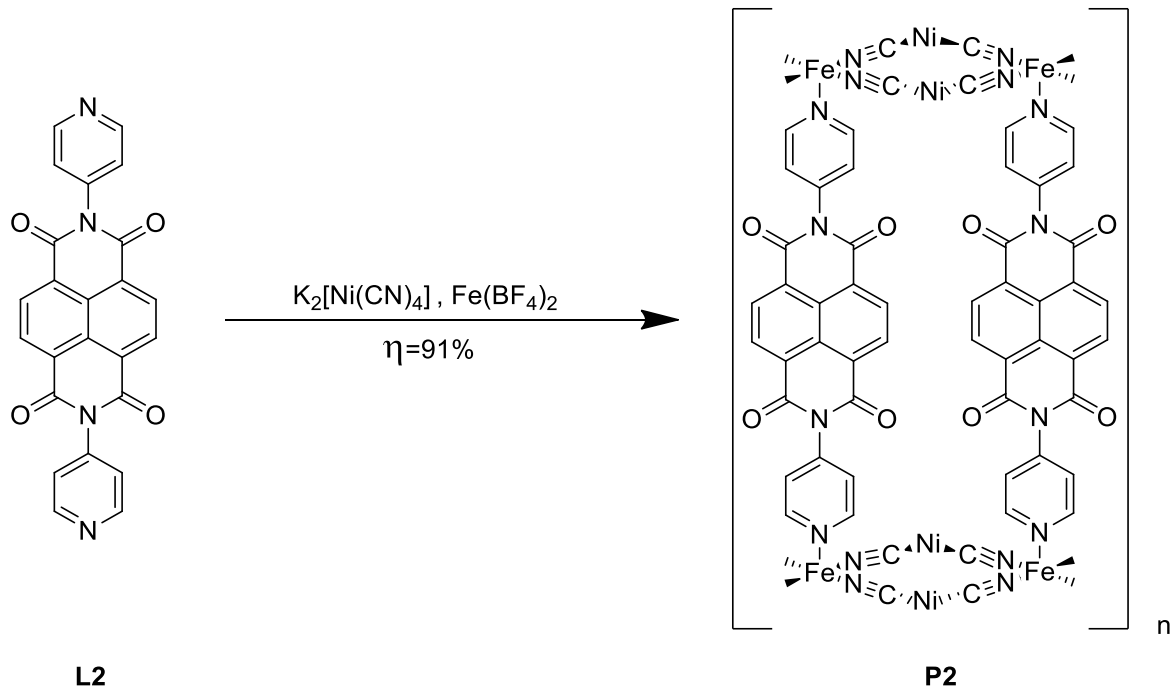


Scheme 2.11. Synthesis of 3D polymer **P2**.

In **figure 2.3** are represented the powders obtained for the Hofmann structures of **P1** and **P2**.


Figure 2.3. Solid powders of **P1** and **P2** obtained by precipitation.

## 2.3.1 Crystallisation Procedures

In order to fully understand the structure of these 3D polymers, it is very important to obtain a single crystal. Once these entities are formed they are highly insoluble, so it is hard to recrystalise them. Therefore, the best strategy for obtaining a single crystal is during the reaction.

In the assembly of **P1** a slow diffusion method was tested in H-shaped tubes **(figure 2.4)**.

Figure 2.4. H-shaped tubes used in the synthesis by slow diffusion.

This method was developed with the help of Professor José António Real from the Institute of Molecular Science (ICMol) in Valencia within the scope of a short-term scientific mission (STSM).

With this procedure guest molecules can be included in the pores of the structures as well. This could help the structure to organise or even work as a template in the assembly. In fact, this technique is very versatile and, in this work, more than one type of H-shaped tubes was used. The simplest ones had two tubes linked together and in this case the ligand and the iron(II) salt were put in one of the tubes while the tetracyanometallate compound was put in the other tube. After this, the remaining volume was made up with one or more solvents. Other systems were used as well, with three and four tubes linked together. In these cases the ligand and the iron(II) can be put together or separated (which promotes an even slower reaction) and guest molecules can be inserted in the system as well. The molecular guests used for this synthetic method were benzene, anthracene and toluene.

Since the reaction, using this method, is very slow, it can take some months to obtain a suitable crystal. With this method crystals were obtained and sent for analysis but the results have not been received to date.

## 2.4 3D Polymers Characterisation

Despite the poor crystallinity related to the precipitation synthetic method, X-ray powder diffraction was performed for both **P1** and **P2.** The first (**P1**) displayed, a diffraction pattern of an amorphous sample **(figure A6)**. **P2**, on the other hand, revealed to be more crystalline than antecipated **(figure 2.5)**.

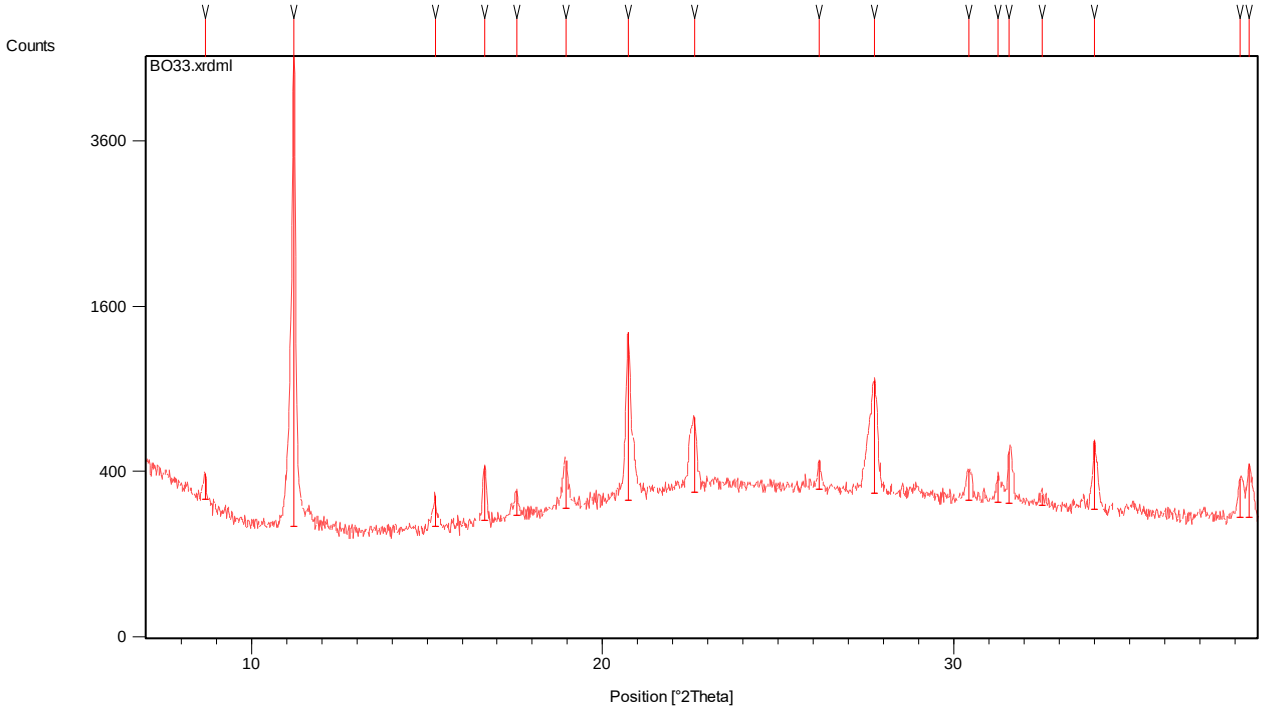


Figure 2.5. X-ray diffraction pattern of **P2**.

Elemental analysis was also used to characterise **P1**. The results for **P2** have not been received yet.

FTIR spectroscopy allowed to confirm the presence of the new bands associated to the formation of the expected Hofmann structure. The most important bands correspondent to the ligand are: aromatic C-H stretching (3100-300 $cm^{-1}$) and bending (900-690 $cm^{-1}$); in ring C=C stretching (1600-1500 $cm^{-1}$); alkyl C-H stretching (2950 $cm^{-1}$) and the amine C-N stretching (1250-1000 $cm^{-1}$) The most important bands for **P1** are marked in **figure 2.6**. As it can be seen, the band related to the CN stretching in the cyano groups is one of the most important bands to verify the assembly of the structure since it is very strong and sharp. The bands related to the iron(II) salt used are also very important and this is confirmed by the presence of the band associated with the stretching of the bonds B-F (in $BF_4^-$) at 1197/1014 $cm^{-1}$ and a deformation of the same bond at 524 $cm^{-1}$. These characteristic bands, in addition the bands related to the ligand, were also observed for **P2 (figure A7)** and the most important are nominated below in **table 2.1**.

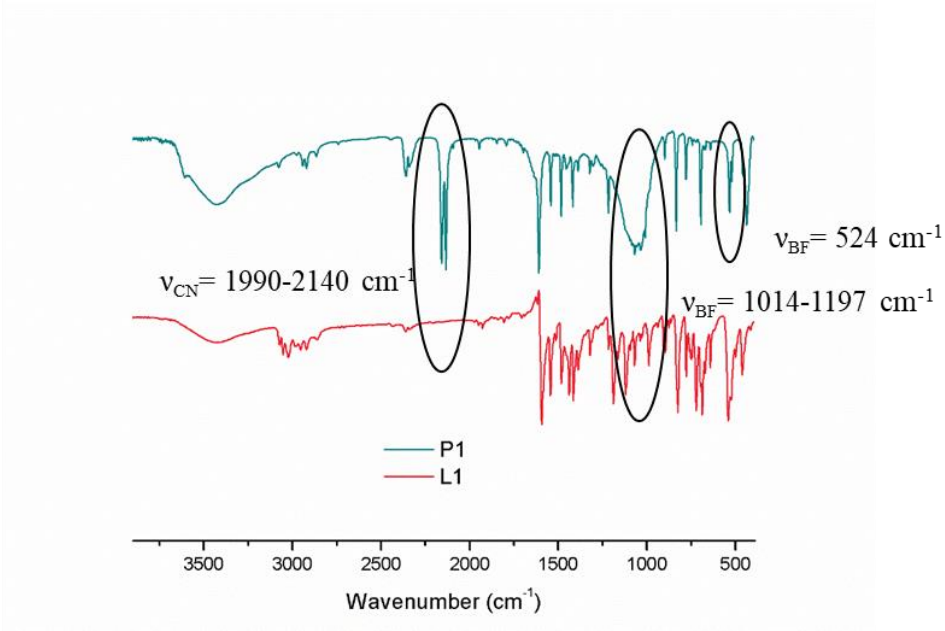


Figure 2.6. Overlapped FTIR spectra of **P1** (green) and **L1** (pink).

Table 2.1. Wavenumber values for the absorption bands observed in the FTIR spectrum of **P2**.

| ν | **Stretching** | **Bending** |
|---|---|---|
| C-H (aromatics) | **3100-3000 cm$^{-1}$ (str)** | **690-900 cm$^{-1}$ (str)** |
| C=C (conjugated) | **1600-1500 cm$^{-1}$ (med-wk)** | - |
| C=O | **1760-1665 cm$^{-1}$ (str)**<br>**1680-1630 cm$^{-1}$ (str)** | - |
| C-C (in ring) | **1500-1400 cm$^{-1}$ (wk)**<br>**1600-1585 cm$^{-1}$ (med)** | - |
| Diimides (C-N) | **1725-1728 cm$^{-1}$ (med)** | - |
| C-H (amines) | **1250-1000 cm$^{-1}$ (med)** | - |
| $BF_4$ | **1079 cm$^{-1}$**<br>**773 cm$^{-1}$** | |
| CN | **2111 cm$^{-1}$** | |

## 2.4.1 Luminescence Studies

Even though **L1** showed a very strong emissive profile, **P1** was not emissive. This could be due to a quenching effect upon the ligand coordination to the metal.

## 2.4.2 Magnetic Measurements

The magnetic measurements, performed in collaboration with Professor Liliana Ferreira from FCUL, were carried out to establish the magnetic behaviour of the coordination polymers and to, ultimately, verify if the samples displayed SCO, very useful for application as sensor. To interpret the results, the expected value for the magnetic moment ($\mu_{exp}$) of iron(II) for both spin states has to be considered. Considering only the contribution of the spin value, the magnetic moment can be calculated using the **expression 2.1** (where n= number of unpaired electrons). In the LS state, iron(II) has no unpaired electrons and in the HS state it has four unpaired electrons. Below are shown the values of the ($\mu_{exp}$) for iron(II) for both spin states **(table 2.2)**.

Table 2.2. Expected values of the magnetic moment for iron(II) for both the LS and HS states.

| **Fe(II)** | ***LS*** | ***HS*** |
|---|---|---|
| **$\mu_{exp}$ ($\mu$B)** | 0 | 4.90 |

From the $\mu_{exp}$ it is possible to calculate the value of $\chi_M T$, where $\chi_M$ is the molar magnetic susceptibility, using the **expression 2.2**. This value corresponds to the response of the compound to the magnetic field that is exposed to.

(2.1) $$\mu_{exp} = \sqrt{n(n+2)}$$

(2.2) $$\chi_M T = \left(\frac{\mu_{exp}}{2.838}\right)^2$$

The values of $\chi_M T$ for iron(II) are presented in **table 2.3**.

Table 2.3. Expected values of the $\chi_M T$ for iron(II) in both the LS and HS states.

| **Fe(II)** | ***LS*** | ***HS*** |
|---|---|---|
| **$\chi_M T$ ($cm^3 mol^{-1} K$)** | 0 | 3 |

The magnetic profile for **P1** was determined in a temperature range from 2 to 300 K and showed that the iron centres were mainly in the high spin state. **(figure 2.7)** The $\chi_M T$ value stabilised in 2.6 $cm^3 mol^{-1} K$.

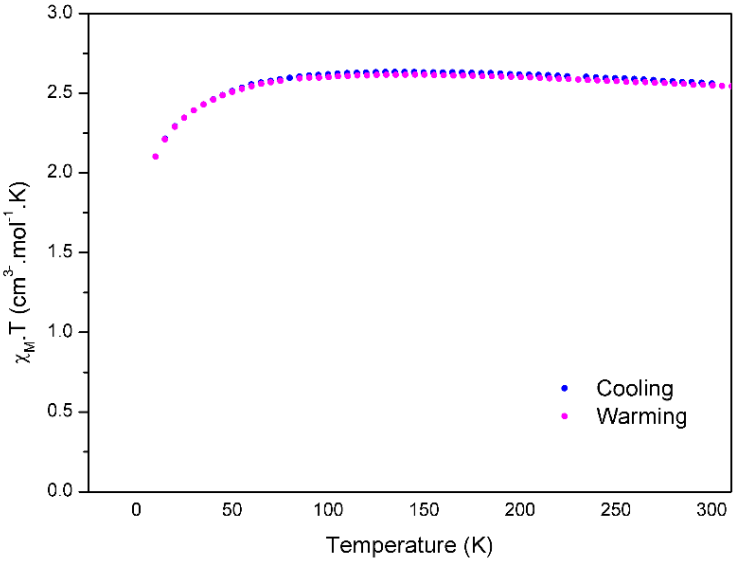


Figure 2.7. Magnetic profile of **P1**.

The magnetic behaviour of **P2** was also studied in the same range of temperatures and the results demonstrated that most of the iron centres were in the LS state **(figure 2.8).** The $\chi_M T$ value stabilised close to 0 $cm^3mol^{-1}K$.

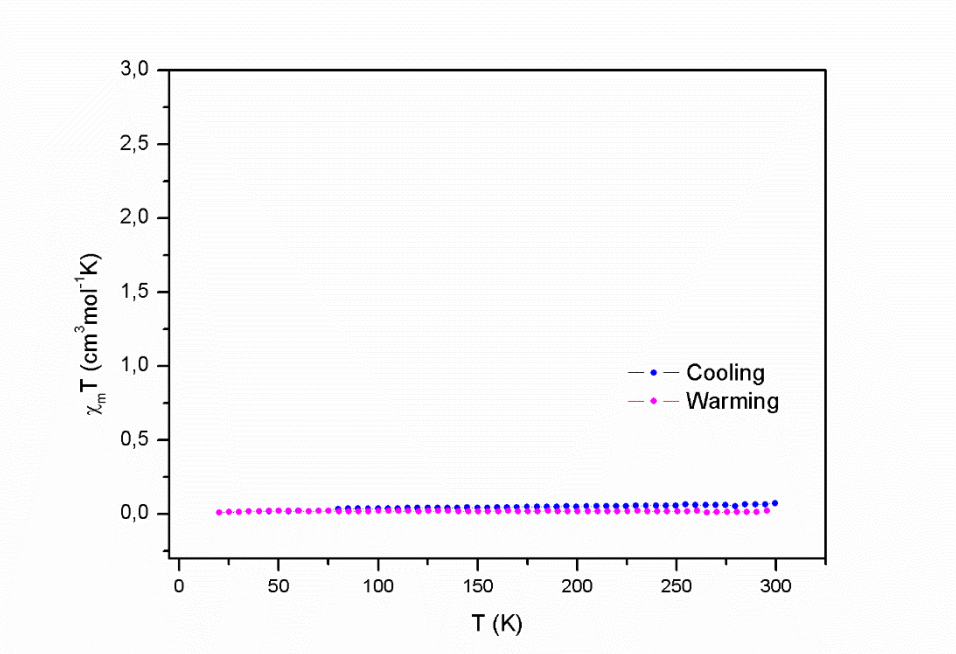


Figure 2.8. Magnetic profile of **P2**.

These results encouraged the study of the insertion of guest molecules with the objective of promoting a SCO behaviour of the compounds. The influence of these guests in the magnetic profile of these polymers is discussed below. The two ligands, **L1** and **L2**, used to assemble **P1** and **P2**, respectively, have different middle units which could explain the very different magnetic behaviours of the two polymers. **L1** has a benzene middle ring that can establish π-π interactions and methyl groups that can interact with π systems via weak C-H···π interactions. On the other hand, **L2**, has a naphthalene

middle ring that can promote more π-π stacking interactions then a benzene ring. This could result in a more stabilised system with a more organised structure promoting the LS state of the metal.

## 2.4.3 Guest Molecule Insertion

The guest molecules insertion test consists in introducing a vial with a solid sample of the 3D polymer inside a bigger and closed vial with the guest molecule (in the liquid phase) we wish to insert in the structure. The vapour pressure created inside the closed vial promotes the motion of the guest molecule that goes from liquid to gas phase and could be inserted inside the pores of the host structure. **(figure 2.9)**

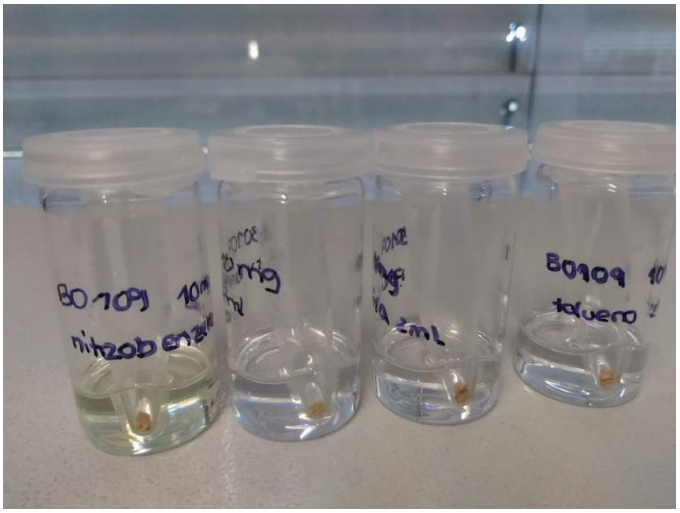


Figure 2.9. Test vials used in the guest molecule insertion.

Then, the magnetic profiles are evaluated, and the results analysed. Sometimes, aside from the magnetic profile, the guest molecules insertion generates a change in the colour of the solid as consequence of the interactions of the guest inside the host cavities. That does not necessarily mean that the magnetic profile is changed. For polymer **P1** the molecules selected for performing this test were toluene, styrene, nitrobenzene and pyridine **(figure 2.10)**.

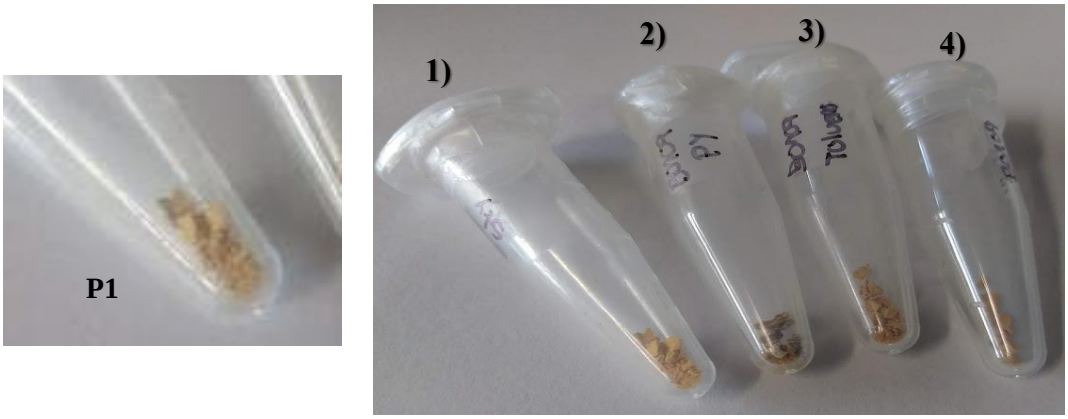


Figure 2.10. Solids of **P1** before and after insertion of guest molecules: 1) styrene; 2) pyridine; 3) toluene; 4) nitrobenzene

The magnetic profiles obtained after the insertion of these guest molecules changed slightly for all of them. The insertion of toluene, nitrobenzene and styrene did not promote SCO in the compound but the value of $\chi_M T$ increased up to a maximum of 3.4 $cm^3mol^{-1}K$ (toluene) and the profile presented for either one of the three cases is much less stabilised than **P1** alone **(figure 2.11)**. Nevertheless, we can conclude that most of the iron centres are still in the HS state.

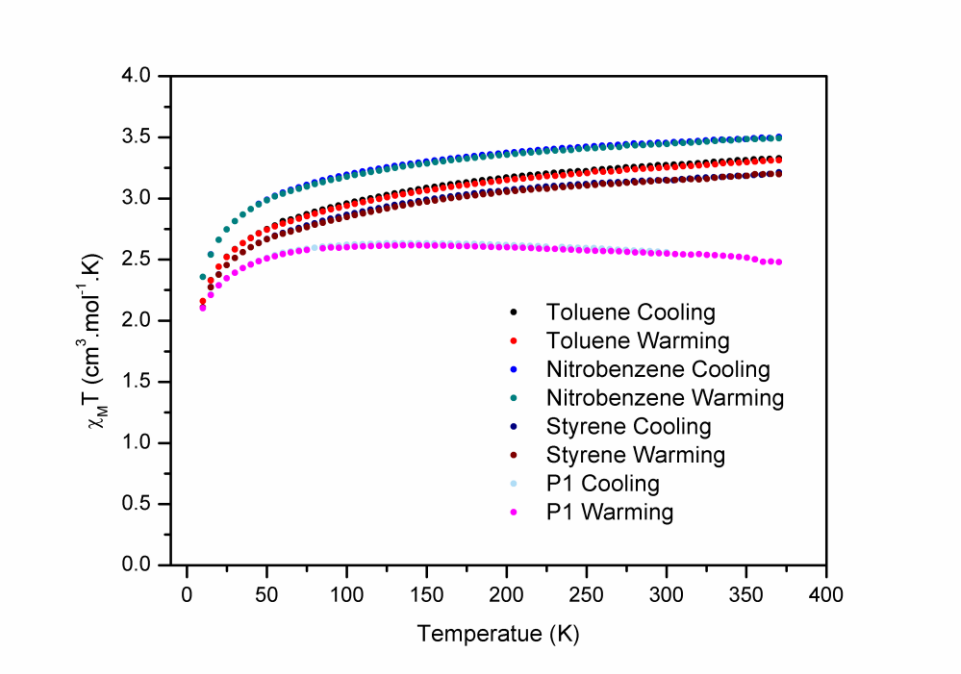


Figure 2.11. Magnetic profile of P1 after the insertion of toluene, nitrobenzene and styrene.

However, the magnetic profile of **P1** changed drastically after the insertion of pyridine **(figure 2.12)**. As it can be observed below, the insertion of this molecule promoted a SCO behaviour that can be characterised as being fast-gradual with a value of $T_{1/2}$=175 K.

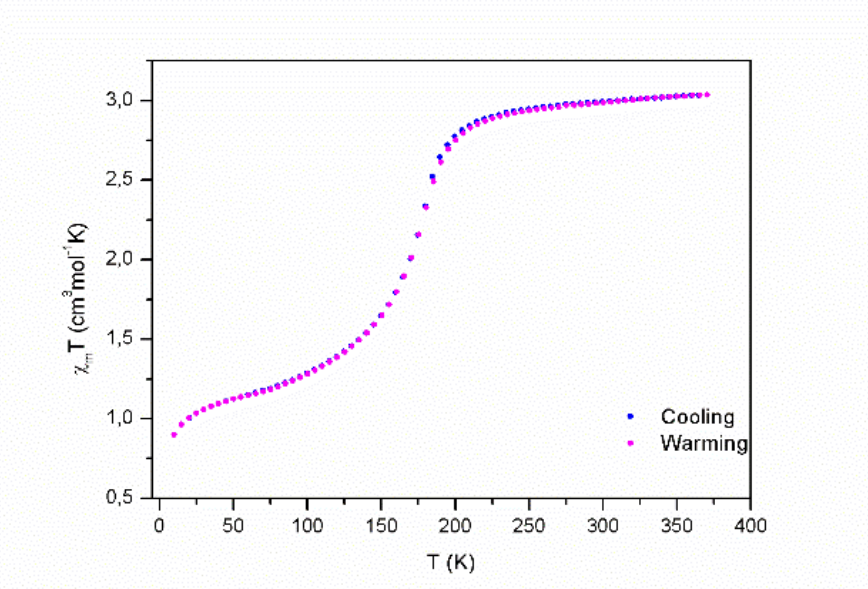


Figure 2.12. Magnetic profile of **P1** after the insertion test with pyridine.

The fact that the pyridine was the only guest molecule that promoted a SCO behaviour of the polymer raises questions. This is because pyridine, as opposed to the other guest molecules used, is the only one with a coordination site to coordinate to the iron(II) suggesting a possible ligand exchange in the 3D structure. 2D Hofmann structures using pyridine as a ligand have been reported in the past and the magnetic profile demonstrated the fast-gradual SCO behaviour with an hysteresis of approximately 10 K **(figure 2.13)**.[48] To be certain if there was indeed a ligand exchange further studies have to be performed. If the pyridine molecule is indeed inside the cavities of the structure, by thermogravimetric analysis (TGA) we could, possibly, observe the mass loss corresponding to the pyridine Another possibility with be to use Raman spectroscopy in other to determine the vibrational modes of the sample and, with the help of theoretical calculations, compare it with vibrational modes characteristic of the coordination of pyridine to the iron(II).

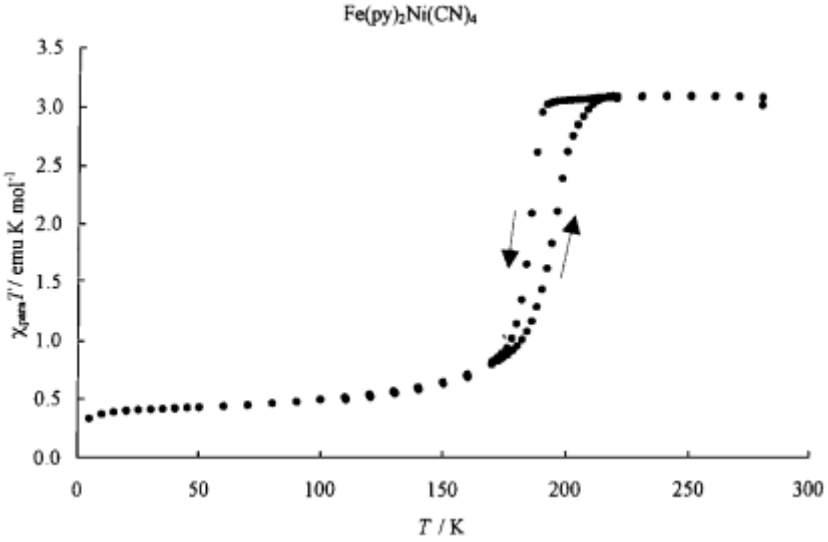


Figure 2.13. Magnetic profile of a reported 2D Hofmann structure with pyridine as ligand. [48]

In order to test the **P1** ability to separate enantiomeric mixtures another type of guest insertion test was performed. In this case were selected D-alanine, L-alanine, D-phenylalanine and L-phenylalanine **(figure 2.14)**. The insertion of these guest molecules could not be done by vapour pressure diffusion since they are solid, so the test was performed by dissolving the guest molecules in water or MeOH and then adding a powder sample of **P1** to the solution. The suspension was kept stirring for three days and after that the solid was filtered.

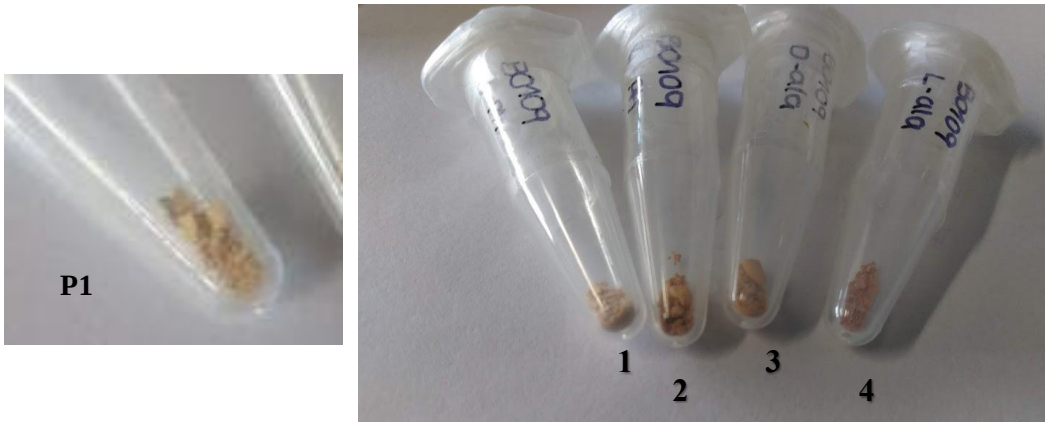


Figure 2.14. Solids of **P1** before and after insertion of guest molecules: 1) D-phenylalanine; 2) L-phenylalanine; 3) D-alanine; 4) L-alanine.

In all four cases the magnetic profile obtained after the insertion test altered and the values of $\chi_M T$ increased remaining in the HS state.

For the samples containing D-phenylalanine and L-phenylalanine the magnetic profile did not show a SCO behaviour. The $\chi_M T$ values stabilised around 3.4 $cm^3mol^{-1}K$ indicative that the iron(II) centres are in the HS state. **(figure 2.15)**.

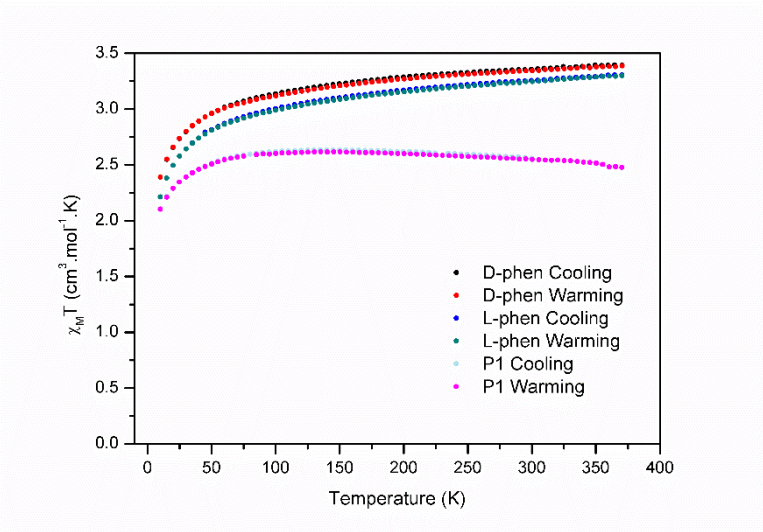


Figure 2.15. Magnetic profile of **P1** after insertion of D-Phenylalanine and L-phenylalanine.

In the case of D-alanine and L-alanine the $\chi_M T$ raised up to a maximum value of 4.5 $cm^3mol^{-1}K$ (L-alanine) **(figure 2.16)**. This value is much higher than the expected value for iron(II) (3 $cm^3mol^{-1}K$) and is much closer to the value expected for iron(III) (4.34 $cm^3mol^{-1}K$).

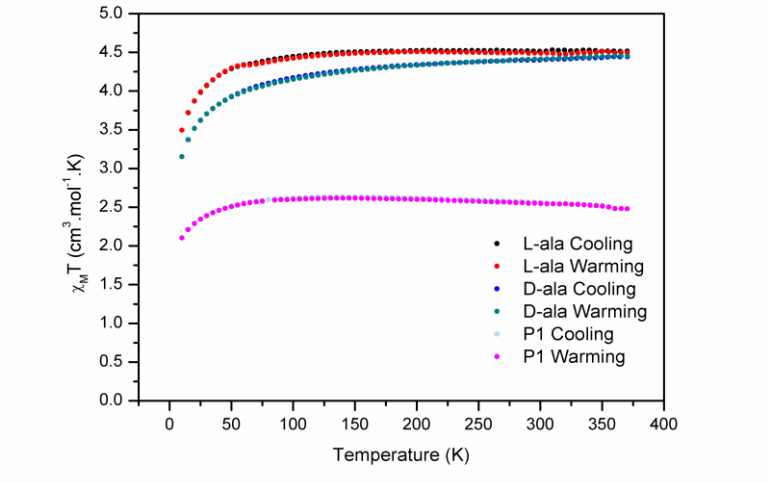


Figure 2.16. Magnetic profile of **P1** after insertion of L-alanine and D-alanine.

The expected values for both $\mu_{exp}$ and $\chi_M T$ for iron(III) are presented in **table 2.4**. This behaviour could indicate that the compound was oxidised.

Table 2.4. Expected values of the $\chi_M T$ for iron(III) in both the LS and HS states

| **Iron(III)** | ***LS*** | ***HS*** |
|---|---|---|
| **$\mu_{exp}$ ($\mu$B)** | 1.73 | 5.92 |
| **$\chi_M T$ ($cm^3mol^{-1}K$)** | 0.37 | 4.34 |

In the future will be performed circular dichroism studies to confirm insertion of these amino acids in the structure and to verify if there is indeed the capacity of separating enantiomeric mixtures. This study will, in the future, allow to compare the properties of these achiral structures with new chiral ones and debate about the influence of the chirality.

The insertion of guest molecules test was also performed for polymer **P2**. In similarity to what happened with **P1** it was also observed a change in the colour of the powders. To perform the insertion test with polymer **P2** were selected 2-propanol, nitrobenzene, toluene and pyridine as guest molecules **(figure 2.17)**.

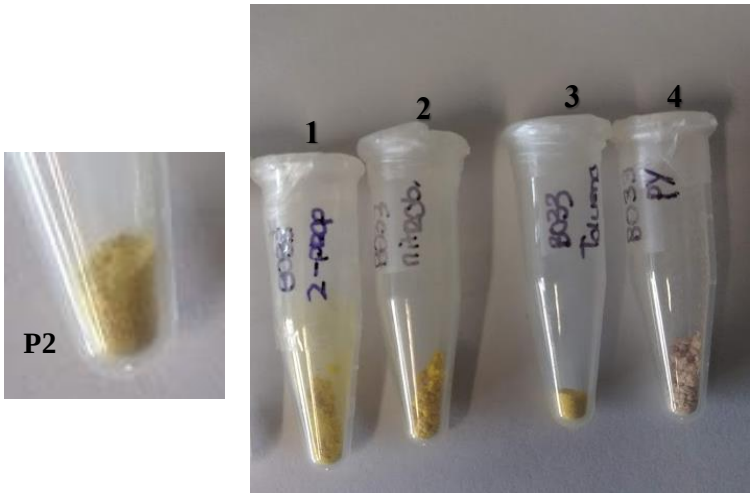


Figure 2.17. Solids of **P2** before and after insertion of guest molecules: 1) 2-propanol; 2) nitrobenzene; 3) toluene; 4) pyridine.

The insertion of 2-propanol, nitrobenzene and toluene did not change the magnetic profile of **P2 (figure A8)**. As shown below, the value of $\chi_M T$ stabilised in 0 $cm^3mol^{-1}K$ is indicative that the iron centres were still in the LS state as the initial structure with no guest molecule.

As for the pyridine sample, the magnetic profile slightly changed. As shown in **figure 2.18** the value of $\chi_M T$ goes from 0.75 $cm^3mol^{-1}K$ up to a maximum value of 1.5 $cm^3mol^{-1}K$. Nevertheless, we can affirm that the metal centres are mostly in the LS state.

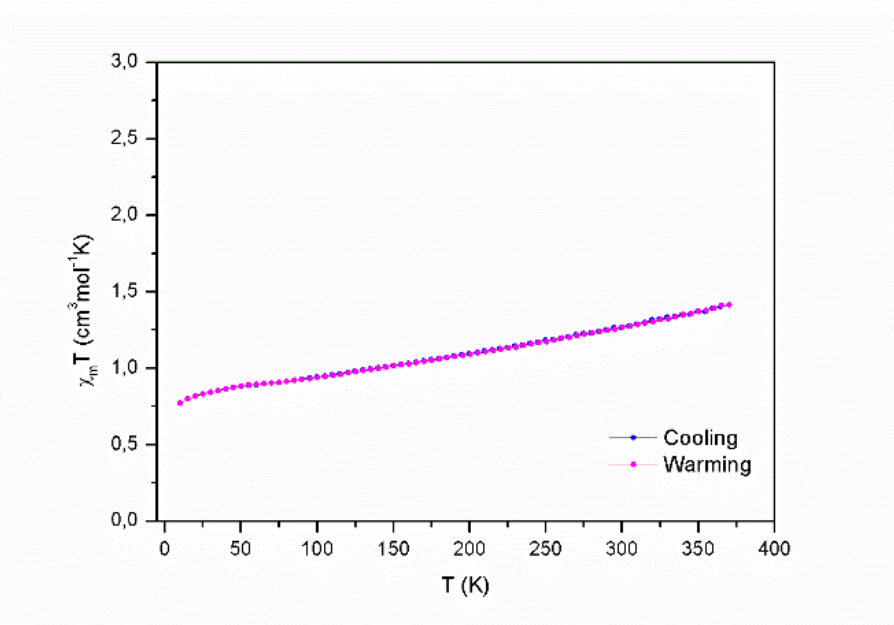


Figure 2.18. Magnetic profile of **P2** when inserting pyridine.

Even though the magnetic profile of **P2** did change with pyridine, the guest molecule insertion test failed in promoting SCO in the compound. This could have happened because the metal centres stabilise mainly in the LS state throughout the temperature range. This way, the energy gap between the $e_g$ and $t_{2g}$ orbitals is higher making it harder to break through this very stabilised state and to promote SCO as opposed to **P1** that stabilised at HS state making it easier to switch on the SCO.

## 2.5 Summary

Two 3D coordination polymers were successfully synthesised. Thee magnetic measurements initially showed that the metal centres were all in the HS state for **P1** and in the LS state for **P2**.

Insertion of guest molecules in the cavities of **P1**, by vapour pressure diffusion, showed, that the magnetic profile changed when inserting pyridine. This guest promoted the spin transition of the metal centres. Also, the tests performed with the L-alanine and the D-alanine amino acids showed a high spin state profile but the values of the magnetic susceptibility were not correspondent to iron(II) being more suitable for iron(III). This suggests a change in the oxidation state of the metal probably caused by the formation of a different structure.

As for **P2,** the guest molecule insertion tests did not reflect in any change of the magnetic profile. It showed that the metal centres stayed mostly in the LS state just as the initial structure with no guest molecule. Even though the profile did change slightly when inserting pyridine, and a small increase of $\chi_M T$ value was observed, it was not possible to observe a complete spin transition.

Luminescence studies performed on **L1** showed four different emissions at 77 K and one emission band at room temperature. However, **P1** showed no emission at both temperatures

.

# 3 1D Iron(II) Coordination Polymers

Herein is presented the synthesis of four 1D coordination polymers. For the assembly of these structures were used four different ligands, **L3** to **L6**, represented in **figure 3.1**.The magnetic behaviour of the 1D polymers was also studied.

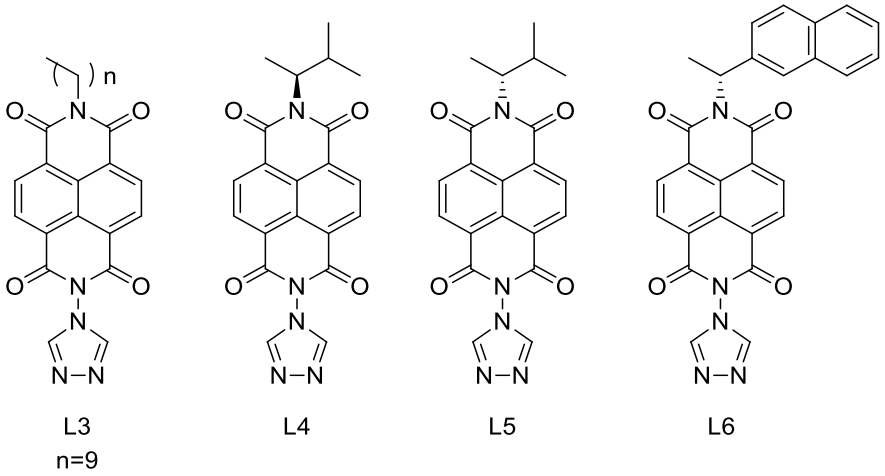


Figure 3.1. Ligands used in the synthesis of 1D polymers.

Four other ligands with a perylene diimide derivative were synthesized (**L7**-**L10**) **(figure 3.2)**. Unfortunately, it was not possible to assemble a 1D polymer with these ligands due to their high insolubility.

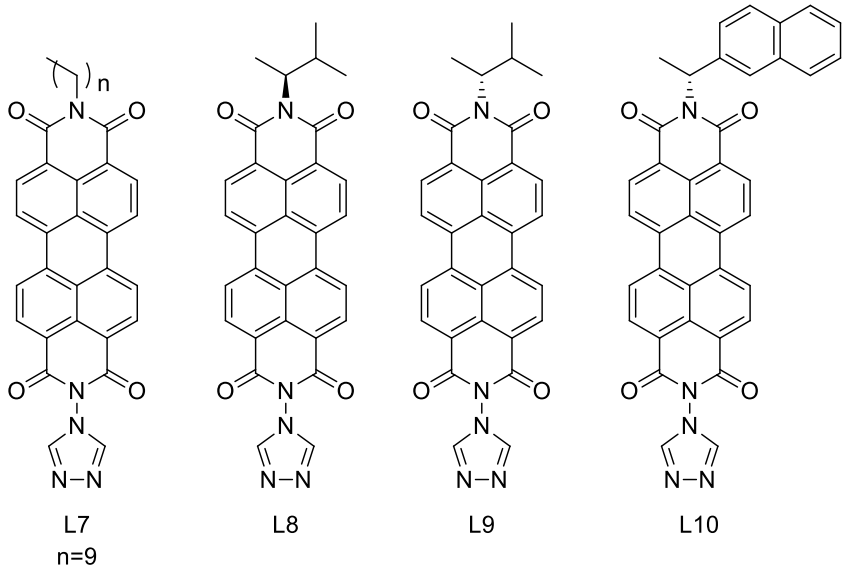


Figure 3.2. Synthesised ligands based on perylene diimides.

## 3.1 Ligands Synthesis

The ligands chosen to assemble this coordination polymers contain three essential parts: a) the triazole that coordinates to the iron centres, b) the bulky dianhydride central part with known fluorescent and conductivity properties, and c) an apolar amine, with or without chirality, that lowers the polarity of the ligand. The amines selected to synthesise the ligands are represented in **figure 3.3**.

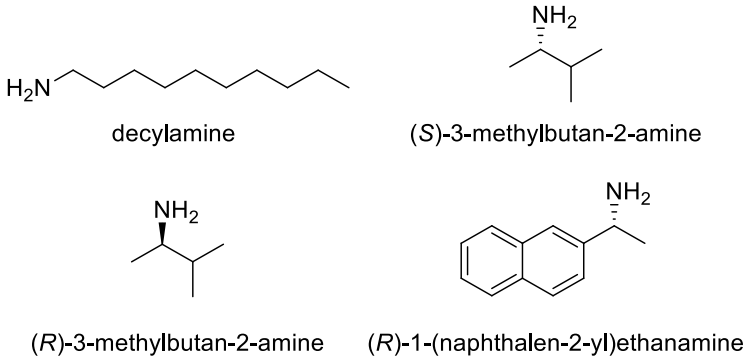


Figure 3.3. Chiral and achiral amines used in the ligand's synthesis.

The properties of the diimines as ligands (luminescence, conductivity) have already been mentioned and for the ligands' syntheses were used two different anhydrides to form the diimide compounds **(figure 3.4)**. Were synthesised two groups of four ligands each, by the same synthetic method as described below.

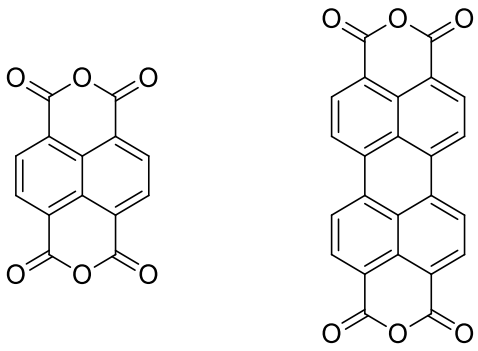

Figure 3.4. Structure of naphthalene-1,4,5,8-tetracarboxylic acid dianhydride and 3,4,9,10-perylenetetracarboxiylic dianhydride.

Ligands from **L3** to **L6** were obtained by a di-substitution in both anhydride positions of naphthalene-1,4,5,8-tetracarboxylic acid dianhydride as represented in **scheme 3.1.** The isolation of the products was fairly simple since they precipitate from solution upon abrupt cooling or by adding water**.** All solids were obtained as a brown solid and the yields were all above 40%.

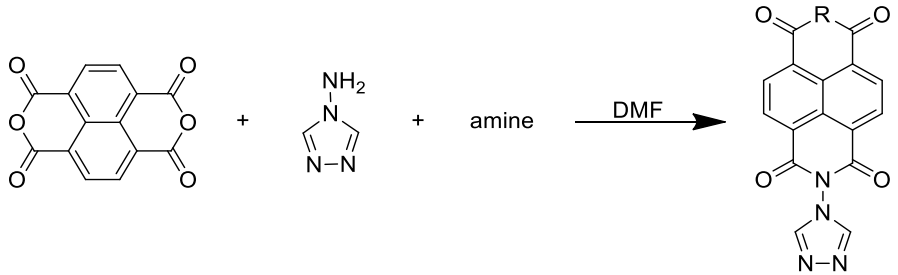


R= decylamine (**L3**), η=65%
R= (*S*)-3-methylbutan-2-amine (**L4**), η=50%
R= (*R*)-3-methylbutan-2-amine (**L5**), η=56%
R= (*R*)-1-(naphtalen-2-yl)ethanamine (**L6**), η=70%

Scheme 3.1. Synthesis of the ligands from **L3** to **L6**.

Ligands from **L7** to **L10** were obtained using the exact same strategy but instead of naphthalene-1,4,5,8-tetracarboxylic acid dianhydride was used 3,4,9,10-perylenetetracarboxiylic dianhydride. The general reaction scheme for the synthesis of **L7** to **L10** is shown in **scheme 3.2.**

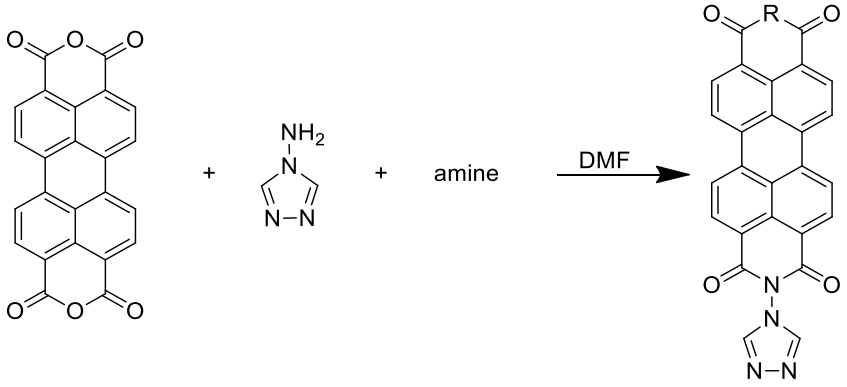


R= decylamine (**L7**), η=56%
R= (*S*)-3-methylbutan-2-amine (**L8**), η=49%
R= (*R*)-3-methylbutan-2-amine (**L9**), η=40%
R= (*R*)-1-(naphtalen-2-yl)ethanamine (**L10**), η=52%

Scheme 3.2. Synthesis of the ligands from **L7** to **L10**.

These last four ligands were obtained as dark red powders. The strong colour is probably due to the perylene dianhydride derivative since it also possesses a strong dark colour. However, the most different observable characteristic of these ligands relatively to the first four (**L3** to **L6**) is their strong luminescence in solution. Upon dissolution of **L7** to **L10** in $CHCl_3$ it was visible their emission properties using the 366 nm wavelength light **(figure 3.5)**.

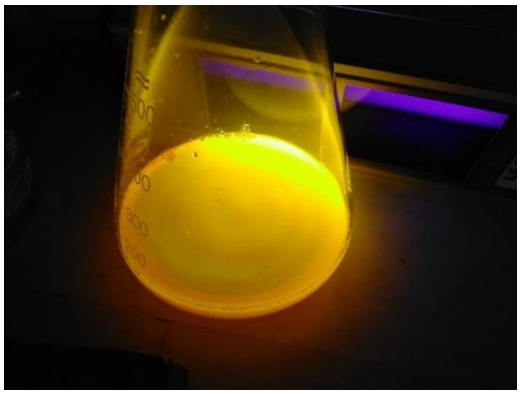

Figure 3.5. Image of **L7** in a $CHCl_3$ solution when exposed to light at 366 nm.

This characteristic may, in the future, lead to the application of this organic ligands in organic light emitting devices (OLEDs) or other alike devices.[60]

## 3.2 Ligands Characterisation

The eight new ligands represented in this chapter were all characterised by NMR spectroscopy. The experiments used were both one dimensional- $^{1}H$ NMR and $^{13}C$ APT- and two dimensional, such as homonuclear experiments (COSY) and heteronuclear experiments (HSQC and HMBC).

As a representative example the characterisation of **L3 (figure 3.6)** will be discussed. The remaining NMR and FTIR characterisation for the other ligands can be found in **figures A9 to A46** in the appendix.

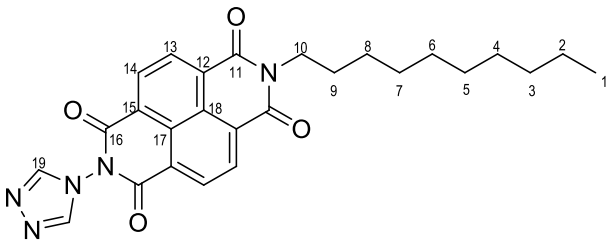

Figure 3.6. **L3** with numeration of the carbons.

These ligands are very bulky and even though they are totally symmetric, the mobility of the aliphatic chain breaks this symmetry. Because of this, in the $^{1}H$ NMR, we can find the chemical shifts corresponding to all the protons of the aliphatic chain of the ligand but only half of the chemical shifts from the naphthalene and from the triazole **(figure 3.7)**. It can be seen, as expected, the signal correspondent to H1 as the most shielded triplet. As for the signals of H2 to H8, they appear all in the same area as a misshapen multiplet. The signals corresponding to H9 and H10 are seen isolated with a better-defined multiplicity than the rest of the protons from the chain. As for the signals corresponding to the protons in the naphthalene derivative and the triazole, they appear as the less shielded and shapeless. It would be expected to observe four doublets and two singlets but instead we observe what looks like two singlets overlapped with a lump. This behaviour was observed in every single $^{1}H$ NMR spectra of all eight ligands and the NMR data for the ligands from **L4** to **L10** can be found in figures **A9** to **A39**.

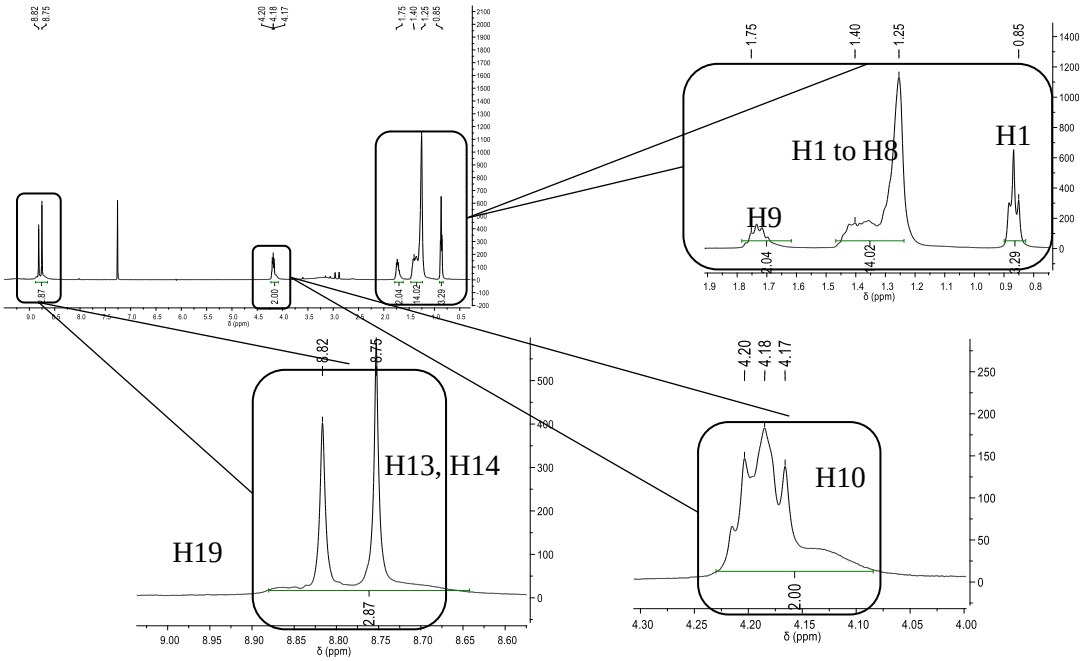


Figure 3.7. $^{1}H$ NMR of **L3** in $CDCl_3$.

By the homonuclear 2D experiment COSY it was possible to observe the interaction up to 1 bond between the protons from the aliphatic chain **(figure 3.8)**. Also, the correlation between H14 and H13 reinforces the presence of two different signals with similar shielding.

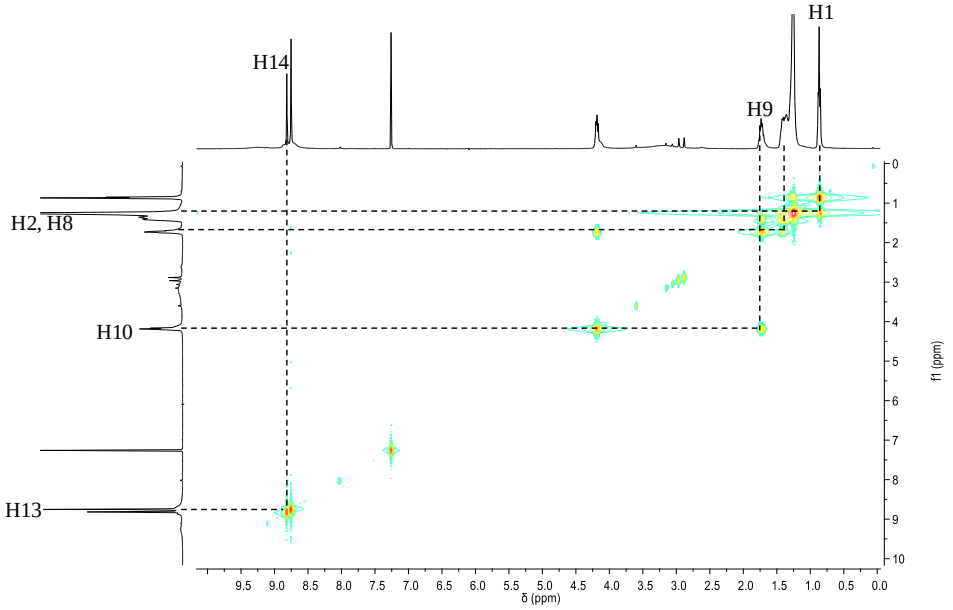


Figure 3.8. 2D homonuclear COSY experiment spectrum of **L3** in $CDCl_3$.

In $^{13}C$ APT experiment it was possible to verify the presence of the carbons following the same idea as for the $^{1}H$ NMR **(figure 3.9)**. This technique allows to differentiate all types of carbons: the quaternary and secondary appear as positive signals (up), the tertiary and primary appear as negative signals (down). In this spectrum we can confirm the presence of the signals from the carbons in the aliphatic chain (even though some presented the same chemical shift), from the naphthalene and from the triazole. By this experiment it was also possible to identify the quaternary carbons.

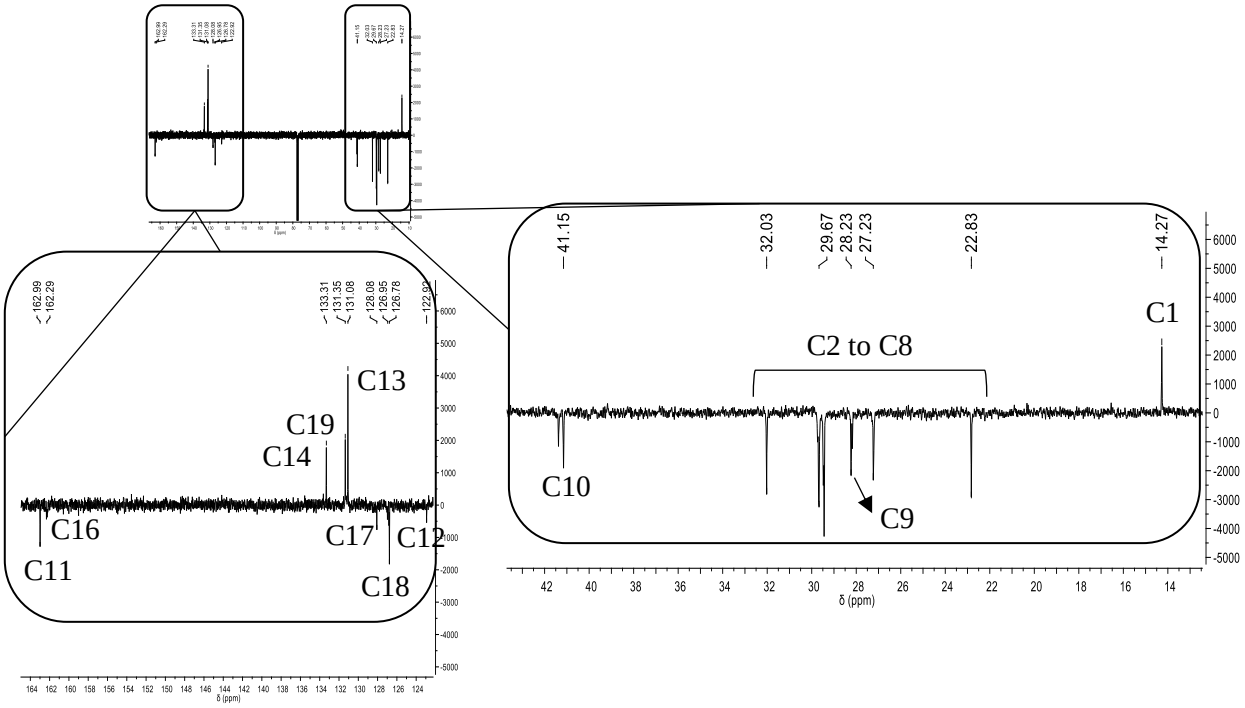


Figure 3.9. $^{13}C$ APT experiment of **L3** in $CDCl_3$.

The assignment of the signals to the carbons in the ligand was possible with the help of the 2D heteronuclear experiments of HSQC (protons from directly linked carbons) and HMBC (protons up to three bonds of distance). The results are presented below. **(figure 3.10)**

Aside from the interactions that were possible to observe with the performed NMR experiments, there were still some signals (from quaternary carbons) left to assign.

As it can be seen in the HSQC spectrum below, the signals from the interactions in the aliphatic chain are at very similar chemical shifts making it harder to distinguish some of the carbons, especially the ones between C2 to C8. Is also important to highlight the fact that the triazole proton signal appears overlapped with the naphthalene ones. Still it is possible to see that there are three carbon signals correlating with the proton signal at 8.75 ppm which reinforces this theory.

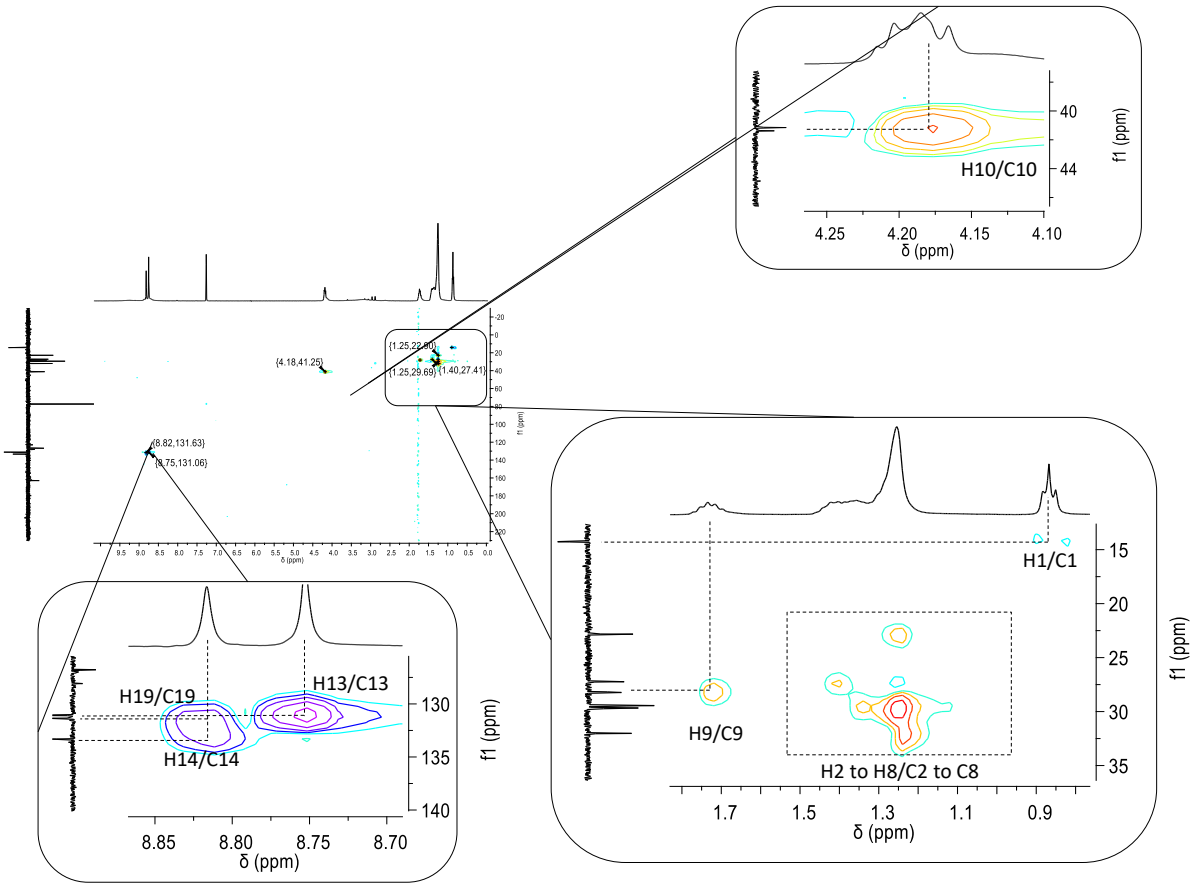


Figure 3.10. 2D heteronuclear HSQC experiment of **L3** in $CDCl_3$.

From the HMBC heteronuclear spectrum it was possible to assign the remaining quaternary carbon signals. **(figure 3.11)**

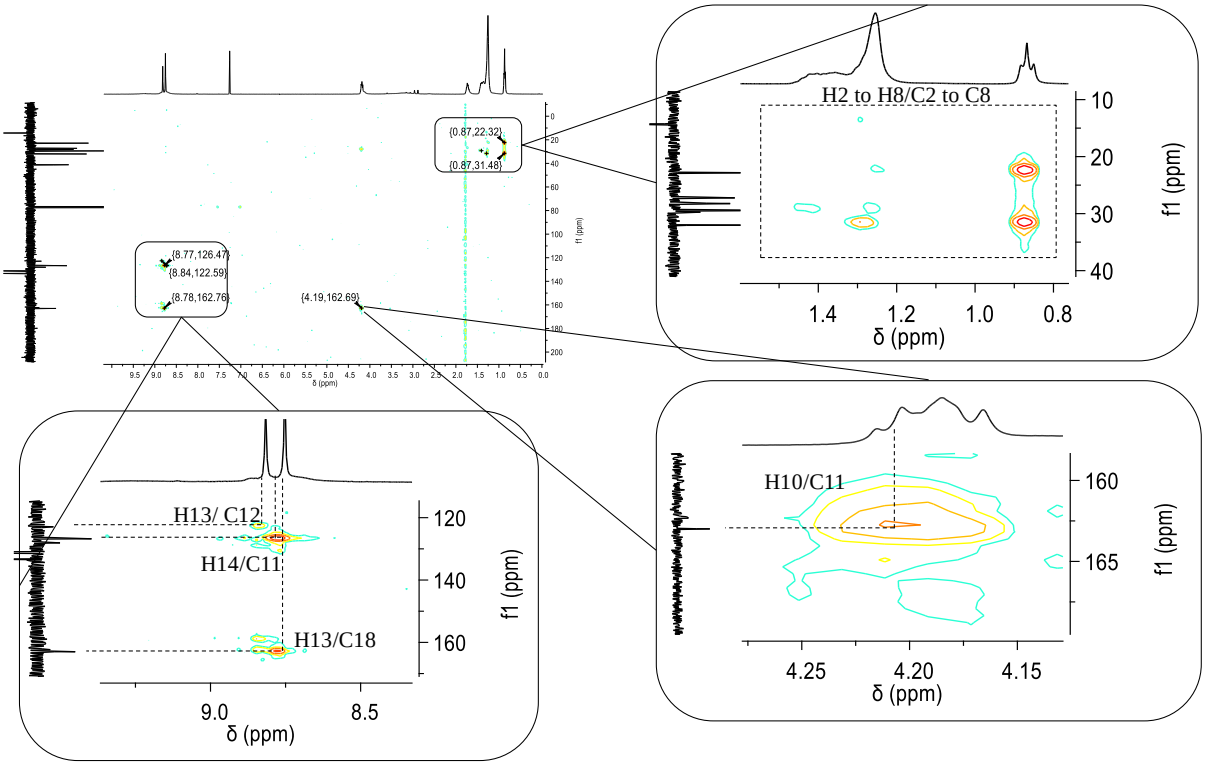


Figure 3.11. 2D heteronuclear HMBC experiment of **L3** in $CDCl_3$.

Above can be seen some of the expected interactions between carbons and protons in the aliphatic chain. It is also shown probably the most important interaction to confirm the presence of the ligand between the quaternary carbon C11 (carbonyl group) and the H10. Also, the correlation between H13 and C18 allows to differentiate between H13 and H14.

The attribution suggested is not unmistakable thus further studies are necessary in order to corroborate this information. The use of different techniques, such as mass spectroscopy, is determinant.

FTIR spectroscopy was used to identify the most characteristic vibrational bands in the ligands. In **figure 3.12** is presented the spectrum of **L3**. The spectra of **L4** to **L10** are similar and presented in **figures A40-A46** in the appendix section.

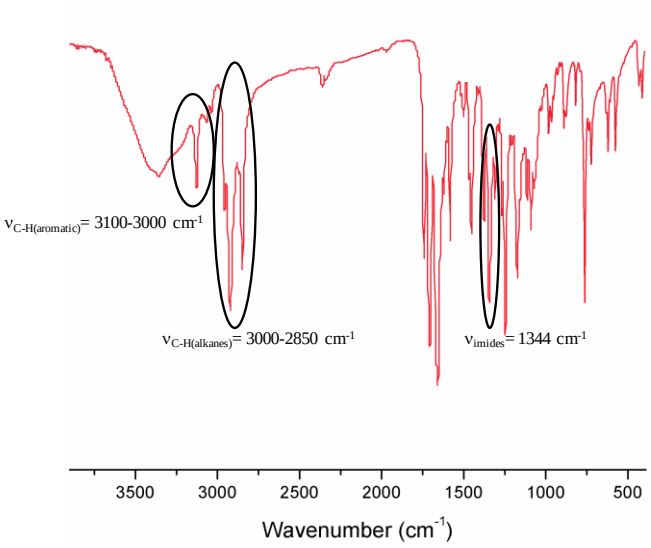


Figure 3.12. FTIR spectrum of **L3**.

The most important bands seen in the spectrum are nominated in **table 3.1**.

Table 3.1. Wavenumber values for the absorption bands observed in the FTIR spectrum of **L3**.

| ν | STRETCHING | BENDING |
|---|---|---|
| C-H (aromatics) | **3100-3000 $cm^{-1}$ (str)** | **690-900 $cm^{-1}$ (str)** |
| C=C (conjugated) | **1500-1600 $cm^{-1}$ (med-wk)** | **-** |
| Diimides (C-N) | **1725-1728 $cm^{-1}$ (str)** | **-** |
| C=O | **1760-1665 $cm^{-1}$ (str)**<br>**1680-1630 $cm^{-1}$ (str)** | **-** |
| C-C (in ring) | **1500-1400 $cm^{-1}$ (wk)**<br>**1600-1585 $cm^{-1}$ (med)** | **-** |
| C-H (alkanes) | **3000-2850 $cm^{-1}$ (med)** | **-** |
| C-H (amines) | **1000-1250 $cm^{-1}$ (med)** | **-** |

## 3.2.1 Luminescence Studies

The only preliminary studies performed for this group of ligands was for **L3** and its spectra are presented in **figure A47** in the appendix section.

The preliminary measures performed at room temperature showed very poor luminescence emission when exciting the species in a range between 250 nm to 525 nm. At a temperature of 77 K the luminescence was more evident even though it was still proven to be very low. This last one was observed when exciting the sample in a range between 275 nm to 375 nm.

## 3.3 1D Polymers Synthesis

Having obtained the eight previously described ligands, the objective was now to obtain the correspondent coordination polymer. Unfortunately, it was not possible to synthesise all the desired polymers in time to be presented in this dissertation. Nevertheless, four 1D coordination polymers were synthesised and the reactional scheme for their synthesis is represented in **scheme 3.3.**

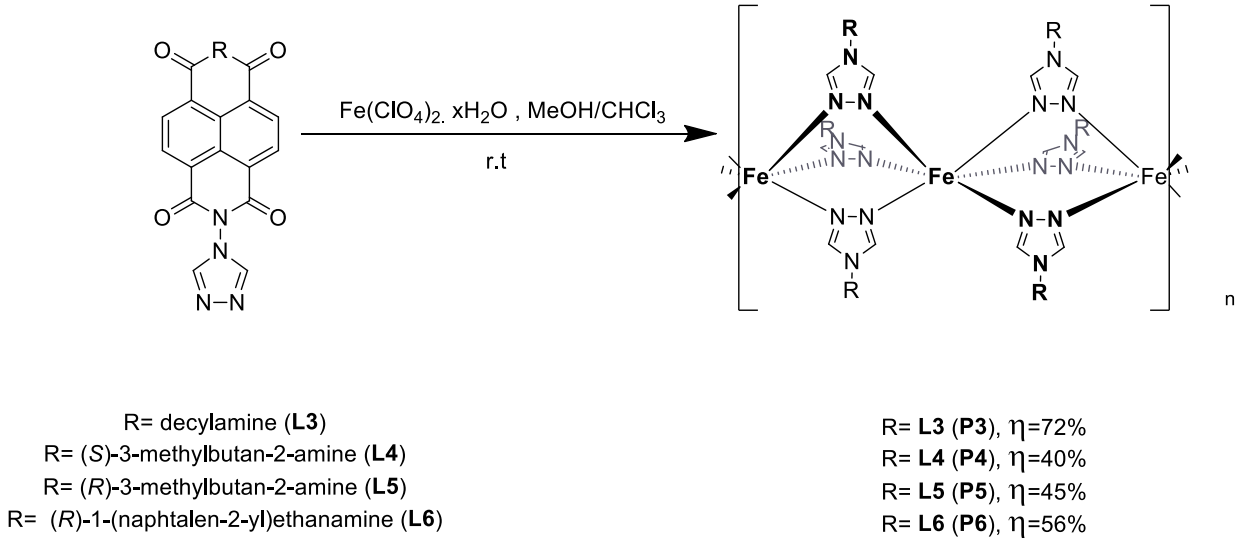


R= decylamine (**L3**)
R= (*S*)-3-methylbutan-2-amine (**L4**)
R= (*R*)-3-methylbutan-2-amine (**L5**)
R= (*R*)-1-(naphtalen-2-yl)ethanamine (**L6**)

R= **L3** (**P3**), η=72%
R= **L4** (**P4**), η=40%
R= **L5** (**P5**), η=45%
R= **L6** (**P6**), η=56%

Scheme 3.3. Synthesis of the polymers **P3** to **P6**

The synthesised structures were characterised by FTIR spectroscopy and its luminescence, magnetic and conductivity properties were also studied. The results are described hereafter.

### 3.3.1 Oligomer Obtention

Ligands from **L7** to **L10** were found to be highly insoluble and the synthesis of the polymers by the precipitation method was not possible. Despite their poor solubility, the compounds were soluble enough to try to obtain crystals by slow diffusion. Since these structures are poorly organised, the obtention of the crystals is not an easy task. So, the idea with the diffusion method in this case was to obtain a crystal from the oligomer or dimmer that would be representative of the structure.

It was used a fair volume of $CHCl_3$ to dissolve the ligands and a small volume of MeOH to dissolve the metal and a NCS salt (NaNCS). The $NCS^-$ should work as a “stopper” for polymer formation, facilitating the obtention of a smaller molecule **(figure 3.13)**.

Figure 3.13. Slow diffusion tubes with the ligands from **L7** to **L10**.

The diffusion method is slow, so it can take some time to obtain the crystals. With this method were obtained two crystals but, up to the delivery of this dissertation, the results form X-ray diffraction have not yet been received.

## 3.4 1D Polymers Characterisation

The FTIR characterisation of these polymers was mainly performed as confirmation of the successful synthesis of the polymers since the most characteristic vibrational modes observed are originated from the ligand. Below is presented the overlapped spectra of the **P3** and **L3**. (**Figure 3.14**) The FTIR spectra for **P4** to **P6** are presented in **figures A48-A50** in the appendix section.

Aside from the bands correspondent to the ligand, it is possible to identify the band correspondent to the $ClO_4^-$ anion present in the iron(II) salt. The presence of this band is a good indicator that the desired product was formed.

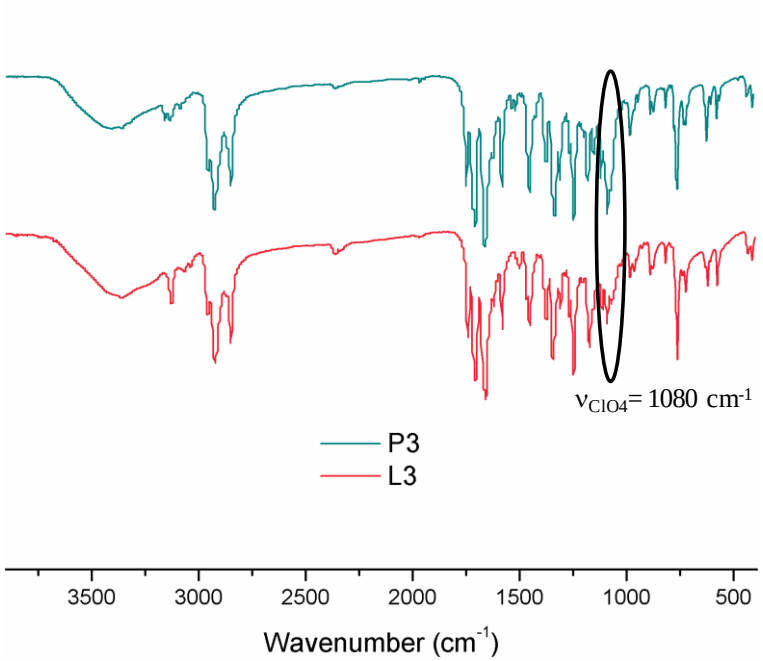


Figure 3.14. Overlapped spectra of **L3** (pink) and **P3** (green).

## Luminescence Studies

Preliminary luminescence studies of **P3** were also performed and below is shown an image of the solid emitting different colours when exposed to a 366 nm light but at different temperatures **(figure 3.15)**.

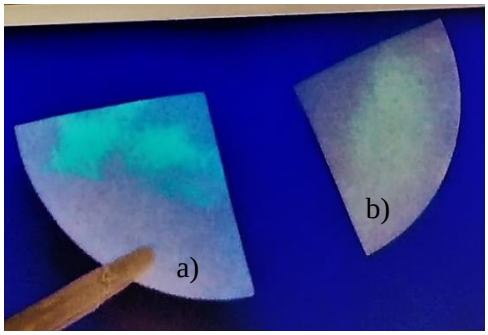


Figure 3.15. Image of the P3 solid when irradiated at 366 nm: a) 77 K and b) room temperature.

The results obtained at both room temperature and 77 K can be seen in **figure A51** in the appendix section. There are two distinct emissions at room temperature. The first one is observed when the sample is excited in a range between 275 nm to 475 nm. The second is observed when exciting at higher wavelength values (over 475 nm). The only emission observed at 77 K is when exciting the sample from 275 nm to 400 nm. At both temperatures the sample showed a strong emission.

This emissive behaviour of the polymer could be promoted upon the coordination of the ligand to the iron(II) since it is known that the luminescent properties are influenced by ligand-metal (LMCT) or metal-ligand (MLCT) charge transfers.[61,62]

## 3.4.2 Magnetic Measurements

Before performing the magnetic analysis using the SQUID, the samples were dipped in liquid nitrogen dropping the temperature from room temperature down to 77 K. When reaching a lower temperature it was verified if there was any alteration in the colour of the sample, which is common for SCO iron(II) compounds as explained before. **(figure 3.16)**. Only for **P3** was observed a colour change. As it is seen it changes from a very light pink colour to a dark blue.

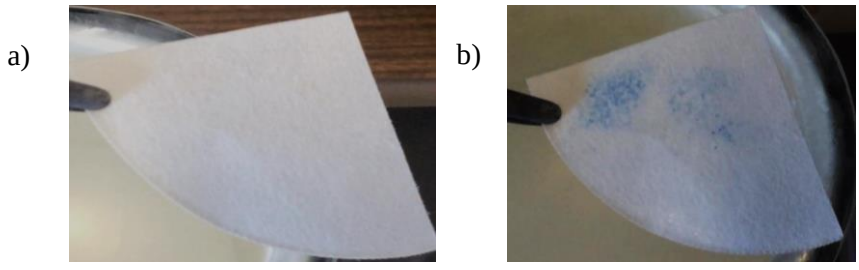


Figure 3.16. Photographic representation of **P3** at different temperatures: a) room temperature; b) 77K.

This was a preliminary indicator that the compound could present SCO. The confirmation was attained with the magnetic profile shown in **figure 3.17**.

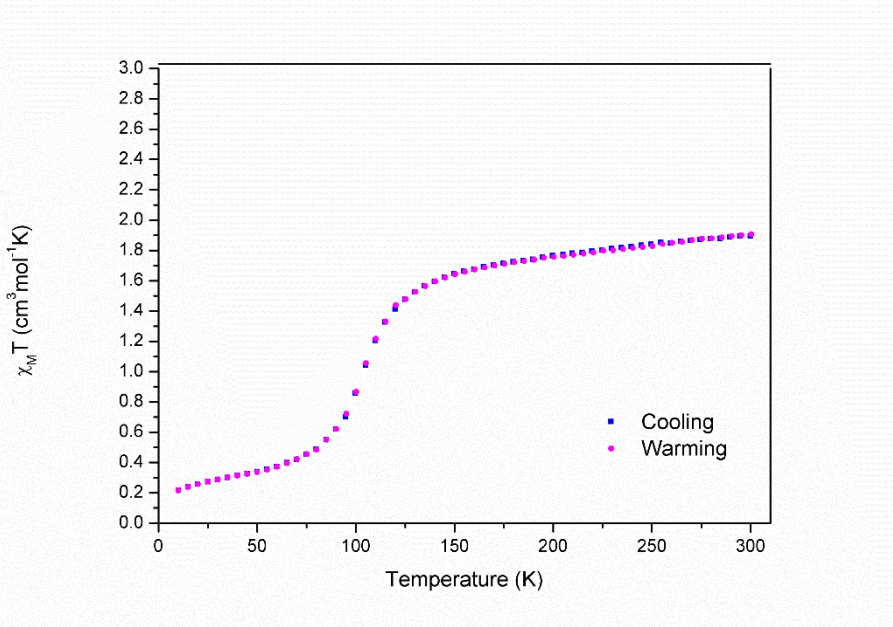


Figure 3.17. Magnetic profile of **P3**.

The magnetic profile displayed indicates a fast-gradual spin transition, even though it is incomplete. The $\chi_M T$ value goes from a minimum of 0.2 $cm^3mol^{-1}K$ at 2 K to a maximum of 2 $cm^3mol^{-1}K$ at 300 K and shows a value of $T_{1/2}$=115 K. The fact that it stabilises at a lower value than what was expected could mean that there is a mixture from iron centres in both spin states. Thus, not all the iron centres undergo spin transition.

The magnetic properties of the remaining 1D polymers were also studied. **P4** and **P5** showed a behaviour characteristic of a mainly HS state compound **(figure 3.18)** with a very slow and incomplete conversion between spin states.

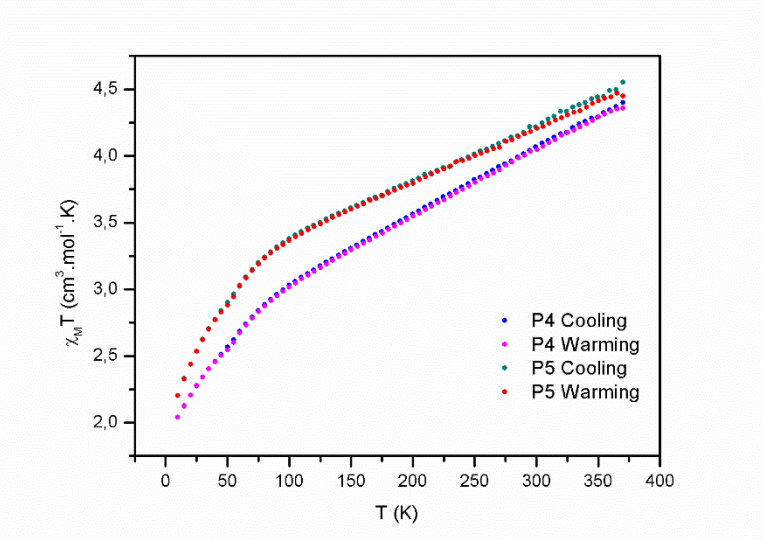


Figure 3.18. Overlapped magnetic profiles of **P4** and **P5**.

In both profiles the values of $\chi_M T$ go from 2 $cm^3mol^{-1}K$ at 2 K to close to 4.5 $cm^3mol^{-1}K$ at 370 K. These values are very high for iron(II) compounds and suggest that we might be in the presence of an iron(III) compound. As for polymer **P6** the values of $\chi_M T$ also go from 2 $cm^3mol^{-1}K$ at 2 K up to a maximum of 5.25 $cm^3mol^{-1}K$ **(figure 3.19)**. This magnetic profile also suggests that the metal centres

are iron(III) and not iron(II), once again because of the high value of $\chi_M T$. If indeed the metal centres are iron(II), this value could be justified by errors associated with molecular mass or by the high contribution of the spin-orbit coupling component (not considered in the values presented previously) that consequently contributes to the increase of the effective magnetic moment ($\mu_{eff}$), thus increasing the calculated magnetic susceptibility. Additional studies by spectroscopic techniques such as $^{57}$Fe Mössbauer and EPR would clarify and distinct between Fe(II) and Fe(III).

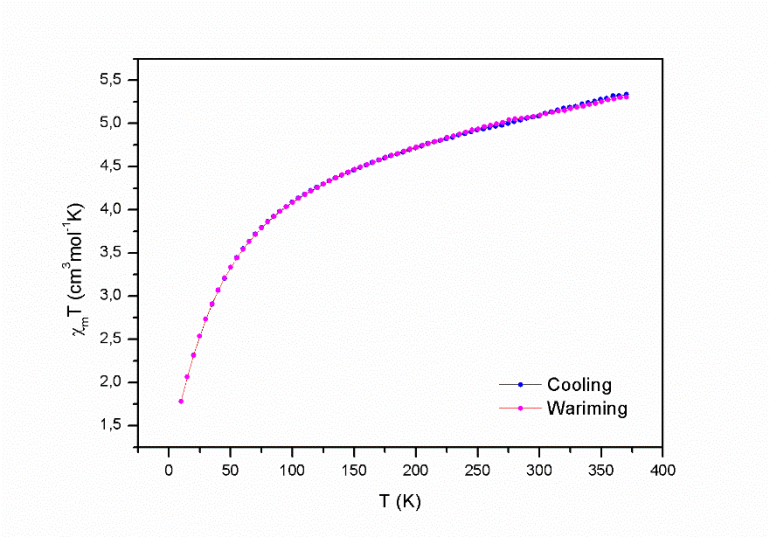


Figure 3.19. Magnetic profile of **P6**.

If this is not the case, the structure could indeed contain iron(III) indicating that the reaction for the polymer formation was not complete and/or were promoted the formation of other species.

## 3.4.3 Conductivity Studies

Since the naphthalene is known for its conductivity properties, **P3** was submitted to conductivity studies.[33]

The study was performed in collaboration with Doctor Jorge Morgado, from IST, by the four contacts technique. Four gold stripes were deposited on the surface of the polymer and then four contacts were linked to the gold using a silver glue. After this, a fixed current was applied to the sample and the potential difference was measured. **(figure 3.20)**

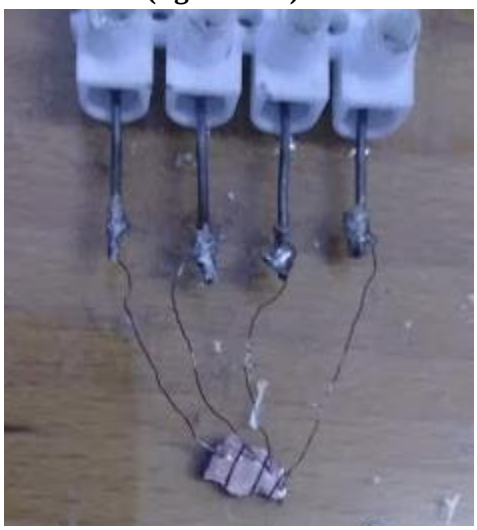

Figure 3.20. Preparation of the sample for the conductivity measurements.

After measuring the potential difference at the different values of current, a function was obtained and adjusted **(figure 3.21)**. The data of linear function adjusted to the results is represented in **table 3.2**.

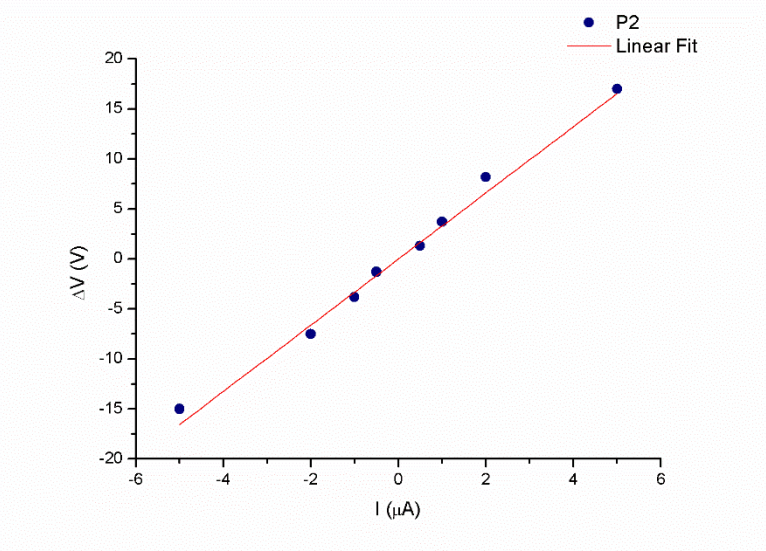


Figure 3.21. Variation of the potential with the current value for **P3**.

Table 3.2. Data of the linear function used to adjust the obtained results.

| | ***P3*** |
|---|---|
| Slope | 3.31 x $10^6$ |
| Intercept | (0,0) |
| $R^2$ | 0.989 |

Since the value of the resistance is given by **expression (2.3)**, the slope of the function was used as the resistance value. The conductivity derives from the resistance as showed in **expressions (2.4)** and **(2.5)**.

(2.3) $$R = \frac{\Delta V}{I}$$

(2.4) $$\rho = \frac{R \times sec}{l}; \quad \text{where } sec = d \times thickness$$

(2.5) $$\sigma = \frac{1}{\rho}$$

This way it was possible to obtain a value for the conductivity of the sample. The calculations are demonstrated below **(expressions 2.6-2.10)**.

(2.6) $$R = 3.309 \times 10^{6}\ \Omega$$

(2.7) $$sec = 6.35 \times 10^{-7}\ \mathrm{m}^2$$

(2.8) $$l = 3.5 \times 10^{-4}\ \mathrm{m}$$

(2.9) $$\rho = \frac{3.309 \times 10^{6} \times 6.35 \times 10^{-7}}{3.5 \times 10^{-4}} \Leftrightarrow \rho = 6003.47\ \ \Omega.\mathrm{m}$$

(2.10) $$\sigma = \frac{1}{\rho} = \frac{1}{6003.47} = 1.7 \times 10^{-4}\ \mathrm{S.m^{-1}}$$

This conductivity value of $1.7x10^{-4}$ $S.m^{-1}$ indicates that the compound behaves as a semiconductor. That is, it has a conducting capacity that stands between a conductor, such as silver or copper ($\sigma = 10^{7}$ $S.m^{-1}$) and a non-conductor, such as wood ($\sigma = 10^{-16}$ $S.m^{-1}$).[33,63]

## 3.5 Summary

Eight R-trz based ligands were synthesised and divided into two groups: naphthalene diimides (**L3** to **L6**) and perylene diimides (**L7** to **L10**). Using the first group of ligands, four coordination polymers (**P3** to **P6**) were synthesised.

The luminescence properties of **L3** and **P3** were evaluated and it was verified that the ligand did not show a strong emission but the polymer, on the other hand, not only showed a very strong emission but showed two different emission profiles at room temperature and a different emission profile at 77 K.

Also, the SQUID measurements performed showed that **P3** has a fast-gradual spin transition when decreasing from room temperature to 2 K. **P4** to **P6** magnetic profiles showed no SCO, and one of them showed typical iron(III) values of magnetic susceptibility. To confirm the oxidation state of the metal in the structure EPR studies should be performed in the future.

The conductivity studies performed for **P3** demonstrated that this polymer behaves as a semi-conductor

.

# 4 Experimental Section

## 4.1 Reagents and Materials

All materials were used as received. 1-Decylamine 95% and Iron(II) tetrafluoroborate hexahydrate were purchased from Sigma Aldrich, 4-amino-4H-1,2,4-triazole 99%, 1,4-dibromo-2,5-dimethylbenzene 98 %, *N*BS 99 %, and 3,4,9,10-perylenetetracarboxiylic dianhydride 98 % were purchased from Acros Organics. Naphthalene-1,4,5,8-tetracarboxylic acid dianhydride 97%, Iron(II) perchlorate hydrate, (*R*)-3-methylbutan-2-amine 99 %, (*S*)-3-methylbutan-2-amine 99 %, (*R*)-1-(naphthalen-2-yl)ethanamine 99 %, potassium tetracyanoniquelate (II) hydrate, tetrakis(triphenylphosphine) palladium (0), potassium carbonate anhydrous 99 % and pyridinyl boronic acid hydrate were purchased from Alfa Aesar. 1,2- dimethoxyethane was purchased from TCI and AIBN was purchased from Fluka.

The silica used in column chromatography was Geduram ® (0.040-0.063 mm) from Merk.

The solvents were used as received: methanol ($CH_3OH$, Chem-lab, 99.87%),carbon tetrachloride ($CCl_4$, Honeywell Research Chemicals, 99%), dimethylformamide (DMF, Acros Organics, 99.8%), tetrahydrofuran (THF, VWR Chemicals, 99.9%), chloroform-d ($CDCl_3$, Cambridge Isotope Laboratories, 99.5%) dimethyl sulfoxide-$d_6$ (DMSO-$d_6$, Sigma Aldrich, 96.9%) and ethanol (EtOH, Honeywell Research Chemicals, 98%).

## 4.2 Instrumentation

NMR experiments carried out on a Bruker Advance 400 MHz instrument and all the signals calibrated in contrast to TMS.

FTIR spectra were obtained on a Nicolet Nexus 6700 spectrophotometer with between 400-4000 $cm^{-1}$ with KBr.

The magnetic profiles of the powdered samples were obtained using a Quantum design MPMS SQUID in a temperature range from 2 to 370 K at.1000 Oe.

The gold deposition for the conductivity studies was performed using a Edwards Coating System E306A. The current and potential difference of the sample were measured using an Agilent 344O1A Digit Multimeter.

The luminescence steady-state emission and excitation spectra were performed with a Horiba Jobin Yvon Fluorolog FL3-11 spectrometer equipped with a JY TBX picosecond detection module.

The elemental analysis (C, N and H) was performed in the University of Vigo at the C.A.C.T.I. analysis centre using a Fisons Carlo Erba EA1108 elemental microanalyser.

# Synthesis

## 4.3.1 Ligands Synthesis

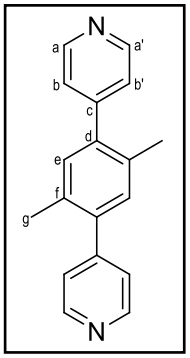

**L1** To a round bottom reaction flask, in inert atmosphere, were added 1,4-dibromo-2,5-dimethylbenzene (0.600 g, 2.3 mmol), pyridinyl boronic acid (0.838 g, 6.9 mmol) and 18 mL of a $K_2CO_3$ aqueous solution (1M) in diethoxyethane (10 mL). The mixture was kept stirring and degassing for 30 minutes. After this time tetrakis(triphenylphosphine)palladium (0) was added (15%, 0.398 g) and the mixture was kept stirring under $N_2$ atmosphere at 100ºC for 24 hours. After this time the mixture was allowed to cool to room temperature and was then extracted with $CH_2Cl_2$. The product was then isolated by column chromatography in $SiO_2$ with petroleum ether/acetone 6:1 (v/v) as eluent and 0.423 g of a white solid was obtained (yield 71%) **$^1$H NMR** (400 MHz, $CDCl_3$, 298 K): δ (ppm) 2.29 (s, 3H, Hg), 7.16 (s, 1H, He), 7.30 (d, 2H, Hb/Hb'), 8.68 (d, 2H, Ha/Ha').

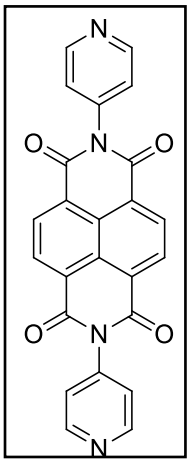

**L2** The ligand was synthesised by a laboratory colleague, Priscila Ramji. To a solution of 4-amino-4H-1,2,4-triazole (0.99 g, 8.2 mmol) in 25 mL of DMF was added a solution of naphthalene-1,4,5,8-tetracarboxilyc acid dianhydride (0.772 g, 4.6 mmol) in 5 mL of DMF. The mixture was kept stirring, for four days in reflux under $N_2$ atmosphere. After cooling to room temperature, the mixture was filtrated and precipitated with MeOH. The precipitated solid was washed with dichloromethane having obtained a black solid. This solid was recrystalised with DMF and 1.93 g of a brown solid was obtained (yield 54 %) **$^1$H RMN** (400 MHz, DMSO-$d_6$, 298 K): δ (ppm) 8.81 (d, 4H), 8.75 (s, 4H), 7.58 (d, 4H).

.

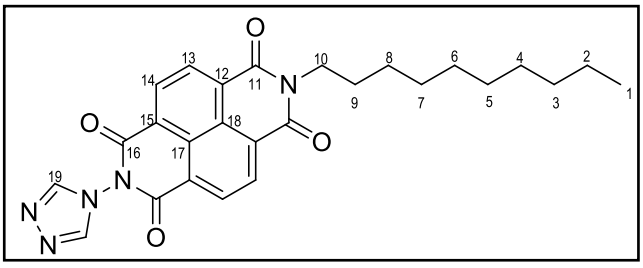

**L3** To a round bottom reaction flask, in inert atmosphere, were added naphthalene-1,4,5,8-tetracarboxilyc acid dianhydride (0.268 g, 1 mmol), decylamine (200 µL, 1 mmol) and 4-amino-1,2,4-triazole (0.084 g, 1 mmol) in dry DMF (10 mL) and the mixture was kept stirring for 18 hours at 140ºC. After this time the mixture was allowed to cool to room temperature and immediately a precipitate started to form. Crushed ice was added and some more precipitate was formed. The solid was filtered and washed with cold water and 0.308 g of a brown solid were obtained (yield 65 %) **$^1$H NMR** (400 MHz, $CDCl_3$, 298 K): δ (ppm) 0.85 (t, 2H, H1), 1.25-1.45 (m, 14H, H2 to H8), 1.75 (m, 2H, H9), 4.18 (t, 2H, H10), 8.75 (s, 1H, H13), 8.82 (m, 2H, H14 and H19). **$^{13}$C NMR** (100 MHz, $CDCl_3$, 298 K): δ (ppm) 14.27 (C1), 22.83/ 27.23/ 29.67/ 32.03(C2 to C8), 28.23 (C9), 41.15 (C10), 122.92 (C12), 126.78 (C15), 126.95 (C18), 128.08 (C17), 131.08 (C13), 131.35 (C14), 133.31 (C19), 162.29 (C16), 162.99 (C11).

**L4** To a round bottom reaction flask, in inert atmosphere, were added naphthalene-1,4,5,8-tetracarboxilyc acid dianhydride (0.268 g, 1 mmol), (*S*)-3-methylbutan-2-amine (12 µL, 1 mmol) and 4-amino-1,2,4-triazole (0,084 g, 1 mmol) in dry DMF (10 mL) and the mixture was kept stirring for 18 hours at 140ºC. After this time the mixture was allowed to cool to room temperature and immediately a precipitate started to form. Crushed ice was added and some more precipitate was formed. The solid was filtered and washed with cold water and 0.203 g of a brown solid were obtained (yield 50 %) **$^{1}$H NMR** (400 MHz, $CDCl_3$, 298 K): δ (ppm) 0.81 (d, 3H, H1), 1.09 (d, 3H, H3), 1.58 (d, 3H, H5), 2.66 (m, 1H, H2), 4.86 (m, 1H, H4), 8.75 (m, 3H, H8, H9 and H14). **$^{13}$C NMR** (100 MHz, $CDCl_3$, 298 K): δ (ppm) 16.98 (C5), 20.18 (C1), 20.90 (C3), 30.42 (C2), 56.74 (C4), 126.85 (C7, C10), 131.32 (C8), 132.08 (C9), 133.31 (C14), 163.08 (C6), 163.48 (C11).

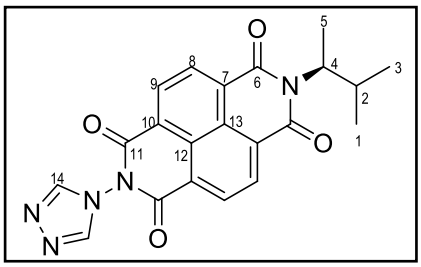

**L5** To a round bottom reaction flask, in inert atmosphere, were added naphthalene-1,4,5,8-tetracarboxilyc acid dianhydride (0.268 g, 1 mmol), (*R*)-3-methylbutan-2-amine (12 µL, 1 mmol) and 4-amino-1,2,4-triazole (0.084 g, 1 mmol) in dry DMF (10 mL) and the mixture was kept stirring for 18 hours at 140ºC. After this time the mixture was allowed to cool to room temperature and immediately a precipitate started to form. Crushed ice was added and some more precipitate was formed. The solid was filtered and washed with cold water and 0.225 g of a brown solid were obtained (yield 56 %) **$^{1}$H NMR** (400 MHz, $CDCl_3$, 298 K): δ (ppm) 0.81 (d, 3H, H1), 1.08 (d, 3H, H3), 1.59 (d, 3H, H5), 2.67 (m, 1H, H2), 4.86 (m, 1H, H4), 8.76 (m, 3H, H8, H9 and H14). **$^{13}$C NMR** (100 MHz, $CDCl_3$, 298 K): δ (ppm) 16.98 (C5), 20.18 (C1), 20.91 (C3), 30.42 (C2), 56.74 (C4), 124.76 (C7), 126.85 (C10), 131.10 (C8), 132.84 (C9), 140.09 (C14), 160.20 (C6), 162.86 (C11).

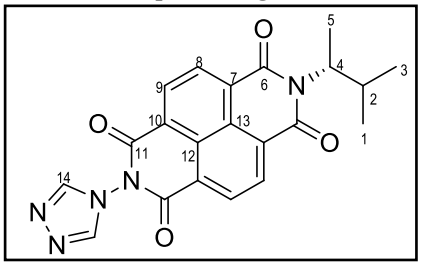

**L6** To a round bottom reaction flask, in inert atmosphere, were added naphthalene-1,4,5,8-tetracarboxilyc acid dianhydride (0.268 g, 1 mmol), (*R*)-1-(naphthalen-2-yl)ethanamine (0.171 g, 1 mmol) and 4-amino-1,2,4-triazole (0.084 g, 1 mmol) in dry DMF (10 mL) and the mixture was kept stirring for 18 hours at 140ºC. After this time the mixture was allowed to cool to room temperature and immediately a precipitate started to form. Crushed ice was added and some more precipitate was formed. The solid was filtered and washed with cold water and 0.340 g of a brown solid were obtained (yield 70 %) **$^{1}$H NMR** (400 MHz, $CDCl_3$, 298 K): δ (ppm) 2.11 (d, 3H, H12), 6.68 (q, 1H, H11), 7.44 (m, 2H, H5 and H6), 7.57 (d, 1H, H10), 7,82 (m, 3H, H4, H7 and H9), 7.97 (s, 1H, H2), 8.70 (m, 3H, H15,H16 and H21). **$^{13}$C NMR** (100 MHz, $CDCl_3$, 298 K): δ (ppm) 16.47 (C12), 51.13 (C11), 125.45 (C10), 126.87 (C14 and C17), 126.95 (C2), 137.53 (C21), 137.74 (C1), 127.70-133.27 (C3 to C9, C15, C16, C19 and C20) 162.68 (C18), 162.82 (C13).

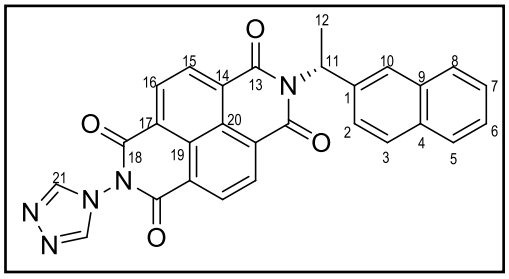

**L7** To a round bottom reaction flask, in inert atmosphere, were added 3,4,9,10-perylenetetracarboxiylic dianhydride (0.392 g, 1 mmol), decylamine (200 µ, L1 mmol) and 4-amino-1,2,4-triazole (0.084 g, 1 mmol) in dry DMF (10 mL) and the mixture was kept stirring for 18 hours at 140ºC. After this time the mixture was allowed to cool to room temperature and immediately a precipitate started to form. Crushed ice was added and some more precipitate was formed. The solid was filtered and washed with cold water and 0.336 g of a dark red solid were obtained (yield 56 %) **$^{1}$H NMR** (400 MHz, $CDCl_3$, 298 K): δ (ppm) 0.86 (t, 2H, H1), 1.25-1.45 (m, 14H, H2 to H8), 1.76 (m, 2H, H9), 4.21 (t, 2H, H10), 8.80 (dd, 4H, H13, H14, H17 and H18).

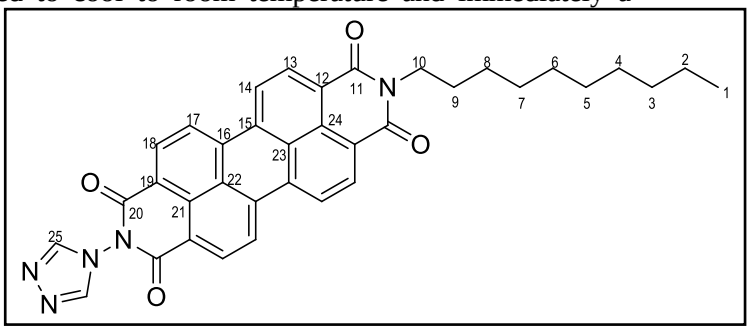

**L8** To a round bottom reaction flask, in inert atmosphere, were added 3,4,9,10-perylenetetracarboxiylic dianhydride (0.392 g, 1 mmol), (*S*)-3-methylbutan-2-amine (12 µL, 1 mmol) and 4-amino-1,2,4-triazole (0.084 g, 1 mmol) in dry DMF (10 mL) and the mixture was kept stirring for 18 hours at 140ºC. After this time the mixture was allowed to cool to room temperature and immediately a precipitate started to form. Crushed ice was added and some more precipitate was formed. The solid was filtered and washed with cold water and 0.259 g of a dark red solid were obtained (yield 49 %) **$^{1}$H NMR** (400 MHz, $CDCl_3$, 298 K): δ (ppm) 0.85 (d, 3H, H1), 1.11 (d, 3H, H3), 1.61 (d, 3H, H5), 2.72 (m, 1H, H2), 4.90 (m, 1H, H4), 8.65 (dd, 4H, H8, H9, H12 and H13). **$^{13}$C NMR** (100 MHz, $CDCl_3$, 298 K): δ (ppm) 17.01 (C5), 20.28 (C1), 20.98 (C3), 30.50 (C2), 56.34 (C4), 123.21 (C9, C12), 124.59 (C7), 129.69 (C16 to C19), 131.10 (C8, C13), 134.67 (C10, C11), 163.96 (C6), 164.10 (C15).

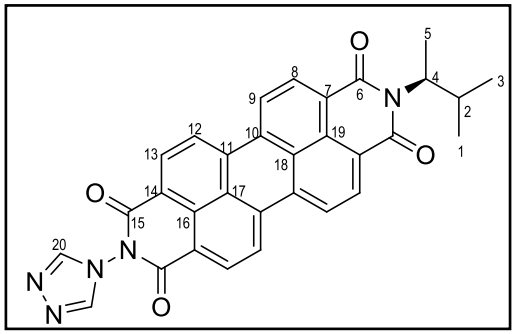

**L9** To a round bottom reaction flask, in inert atmosphere, were added 3,4,9,10-perylenetetracarboxiylic dianhydride (0.392 g, 1 mmol), (*R*)-3-methylbutan-2-amine (12 µL, 1 mmol) and 4-amino-1,2,4-triazole (0.084 g, 1 mmol) in dry DMF (10 mL) and the mixture was kept stirring for 18 hours at 140ºC. After this time the mixture was allowed to cool to room temperature and immediately a precipitate started to form. Crushed ice was added and some more precipitate was formed. The solid was filtered and washed with cold water and 0.211 g of a dark red solid were obtained (yield 40 %) **$^{1}$H NMR** (400 MHz, $CDCl_3$, 298 K): δ (ppm) 0.85 (d, 3H, H1), 1.11 (d, 3H, H3), 1.62 (d, 3H, H5), 2.72 (m, 1H, H2), 4.90 (m, 1H, H4), 8.63 (dd, 4H, H8, H9, H12 and H13). **$^{13}$C NMR** (100 MHz, $CDCl_3$, 298 K): δ (ppm) 16.87 (C5), 20.14 (C1), 20.84 (C3), 30.36 (C2), 56.20 (C4), 123.05 (C9, C12), 126.42 (C7), 129.53 (C16 to C19), 131.44 (C8, C13), 134.50 (C10, C11), 164.04 (C6), 164.34 (C15).

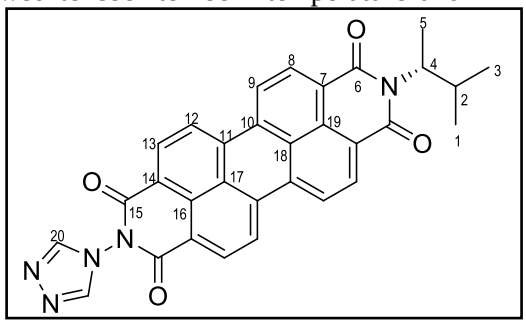

**L10** To a round bottom reaction flask, in inert atmosphere, were added 3,4,9,10-perylenetetracarboxiylic dianhydride (0.392 g, 1 mmol), (R)-1-(naphthalen-2-yl)ethanamine (0.171 g, 1 mmol) and 4-amino-1,2,4-triazole (0.084 g, 1 mmol) in dry DMF (10 mL) and the mixture was kept stirring for 18 hours at 140ºC. After this time the mixture was allowed to cool to room temperature and immediately a precipitate started to form. Crushed ice was added and some more precipitate was formed. The solid was filtered and washed with cold water and 0.320 g of a dark red solid were obtained (yield 52 %) **$^{1}$H NMR** (400 MHz, $CDCl_3$, 298 K): δ (ppm) 2.14 (d, 3H, H12), 6.72 (q, 1H, H11), 7.39-7.91 (m, 6H, H4 to H7, H9 and H10), 8.04 (s, 1H, H2), 8.54 (m, 5H, H15,H16, H19, H20 and H27). **$^{13}$C NMR** (100 MHz, $CDCl_3$, 298 K): δ (ppm) 16.45 (C12), 50.68 (C11), 123.15 (C16, C19), 125.68 (C2), 130.35 (C27), 131.63 (C15, C20), 138.07 (C1), 123.61-135.06 (C3 to C9, C17, C18, C21, C23 to C26) 163.01 (C13), 163.52 (C22).

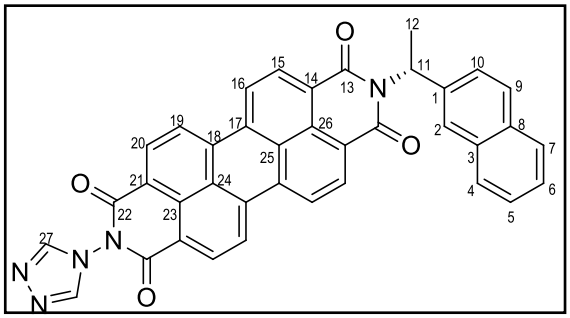

## 4.3.2 Coordination Polymer Synthesis

**P1. 3D Hofmann type Iron(II) coordination polymer** To 10 mL of a solution containing **L1** (0.058 g, 0.222 mmol) in dichloromethane were added 10 mL of a methanolic solution of $Fe(BF_4)_2$. (0.075 g, 0.222 mmol). To this mixture was added dropwise an aqueous solution of $K_2[Ni(CN)_4]$ (0.053 g, 0.222 mmol) and a yellow solid precipitated immediately. The solid was washed with water and methanol. Yield: 0.135 g, 70%. **Elemental Analysis (%)** ($C_{22}H_{16}B_2F_8FeK_2N_6Ni$. 2.3 $H_2O$) e**xp. C** 34.30 **H** 2.67 **N** 10.91; **calc. C** 34.51 **H** 2.20 **N** 10.56.

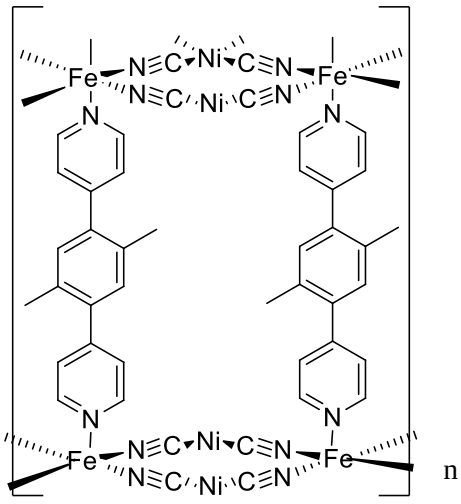

**P2. 3D Hofmann type Iron(II) coordination polymer** To 10 mL of a solution containing **L2** (0.093 g, 0.222 mmol) in dichloromethane were added 10 mL of a methanolic solution of $Fe(BF_4)_2$ (0.075 g, 0.222 mmol). To this mixture was added dropwise an aqueous solution of $K_2[Ni(CN)_4]$ (0.053 g, 0.222 mmol) and a yellow solid precipitated immediately. The solid was washed with water and methanol. Yield: 0.180 g, 91%.

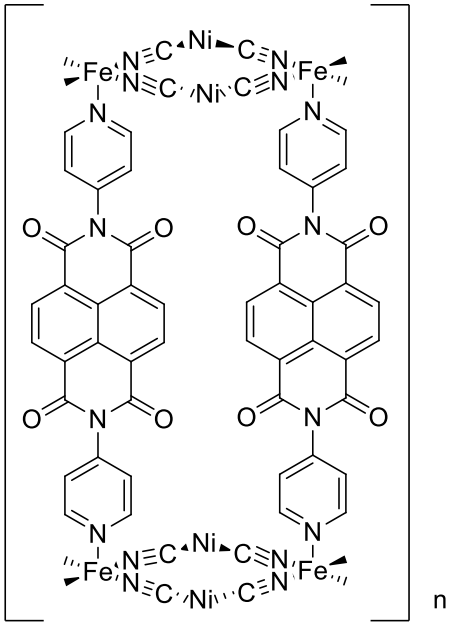

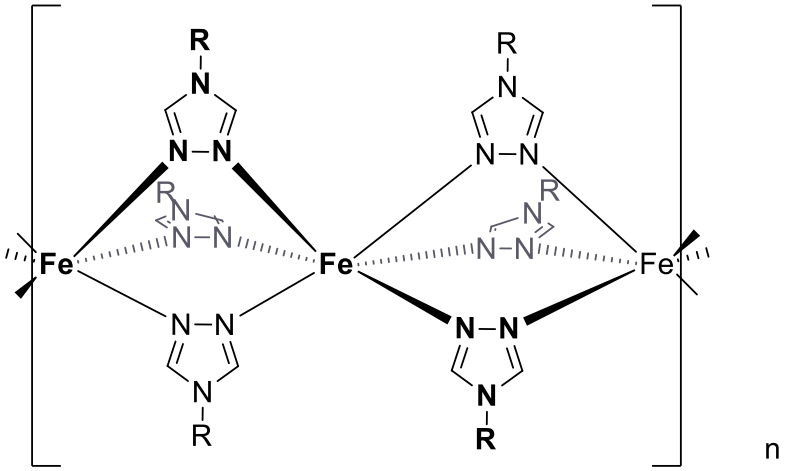

**P3. 1D Iron(II) coordination polymers (R=L3)** A methanolic solution (10 mL) containing $Fe(ClO_4)_2$ (0.497 g, 1.95 mmol) and ascorbic acid was added dropwise to a solution containing **L3** (0.308 g, 0.65 mmol) in chloroform and methanol (10 mL, 1:1) and a light pink precipitate was formed instantly. This solid was filtered and washed with methanol (3 x 10 mL) and dried in vacuo. Yield: 0.272 g (72 %)

**P4. 1D Iron(II) coordination polymers (R=L4)** A methanolic solution (10 mL) containing $Fe(ClO_4)_2$ (0.382 g, 1.5 mmol) and ascorbic acid was added dropwise to a solution containing **L4** (0.203 g, 0.50 mmol) in chloroform and methanol (10 mL, 1:1) and a light brown precipitate was formed instantly. This solid was filtered and washed with methanol (3 x 10 mL) and dried in vacuo. Yield: 0.130 g (40 %)

**P5. 1D Iron(II) coordination polymers (R=L5)** A methanolic solution (10 mL) containing $Fe(ClO_4)_2$ (0.428 g, 1.68 mmol) and ascorbic acid was added dropwise to a solution containing **L5** (0.225 g, 0.56 mmol) in chloroform and methanol (10 mL, 1:1) and a light pink precipitate was formed instantly. This solid was filtered and washed with methanol (3 x 10 mL) and dried in vacuo. Yield: 0.146 g (45 %)

**P6. 1D Iron(II) coordination polymers (R=L6)** A methanolic solution (10 mL) containing $Fe(ClO_4)_2$ (0.535 g, 2.10 mmol) and ascorbic acid was added dropwise to a solution containing **L6** (0.340 g, 0.70 mmol) in chloroform and methanol (10 mL, 1:1) and a light pink precipitate was formed instantly. This solid was filtered and washed with methanol (3 x 10 mL) and dried in vacuo. Yield: 0.243 g (56 %)

## 4.3.3 Other Intermediate Compounds

**1.** To a round bottom reaction flask were added 1,4-dibromo-2,5-dimethylbenzene (1.9 mmol, 0.5 g) and benzoyl peroxide (0.171 mmol, 0.044 g) in solution with $CCl_4$ (11.5 mL) as solvent. *N*BS (11.97 mmol, 2.13 g) was slowly added as the reaction mixture stirred. After all the *N*BS was added the mixture refluxed at 77ºC for 72 hours. Once the reaction stopped the product was filtered and washed with hexane and the solvent was evaporated. Recrystallisation with hexane failed so the product was isolated by column chromatography in $SiO_2$ with petroleum ether as eluent and 0.739 g of a white solid was obtained (yield 68%) **$^1$H NMR** (400 MHz, $CDCl_3$, 298 K): δ 6.95 (s, 1H, H4), 8.15 (s, 1H, H2).

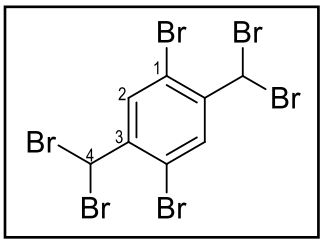


**2.** To a round bottom reaction flask was added compound **2** (1.27 mmol, 0.739 g) in ethanol and the solution was kept stirring. Simultaneously $AgNO_3$ (5.32 mmol, 0.904 g) was dissolved in water (6 mL) and added to the previous solution. The mixture was refluxed and stirred for 1 hour. After cooling to room temperature, the precipitate AgBr was washed with ethanol and removed. The obtained solution was evaporated neutralized with water and finally vacuum dried giving 0.368 g of an off-white solid (yield 99%) **$^1$H NMR** (400 MHz, $CDCl_3$, 298 K): δ 8.18 (s, 1H, H2), 10.37 (s, 1H, H4).

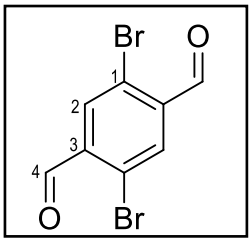


**3.** To a round bottom reaction flask were added 1,4-dibromo-2,5-dimethylbenzene (1.9 mmol, 0.5 g) and benzoyl peroxide (0.18 mmol, 0.046 g) in solution with $CCl_4$ (20 mL). The mixture was kept stirring and the *N*BS (4.20 mmol, 0.75 g) was slowly added. The mixture was left stirring in reflux for 121 hours and followed by TLC. After this time the reaction was stopped, the mixture filtered and washed with hexane and the desired product was isolated by column chromatography in $SiO_2$ with petroleum ether as eluent giving 0.216 g of a white solid (yield 27%) **$^1$H NMR** (400 MHz, $CDCl_3$, 298 K): δ 4.51 (s, 2H, H4), 7.66 (s, 1H, H2).

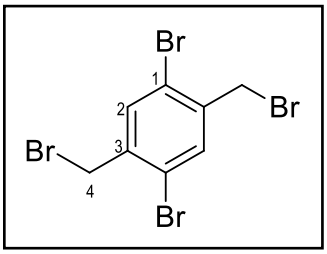

**4.** To a round bottom reaction flask, in inert atmosphere, were added (*S*)-3-methylbutan-2-amine (0.711 mmol, 0.083 g) and $K_2CO_3$ (0.924 mmol, 0.128 g) in dry THF (3 mL) and mixture was kept stirring for 20 minutes. After this time compound **3** was added and the mixture refluxed for 49 hours and followed by TLC. After this time the mixture was filtered and washed with THF. The desired compound was purified by column chromatography in $Al_2O_3$ with acetone/petroleum ether 1:20 (v/v) as eluent giving 0.073 g of an orange oil (yield 71%) **$^1$H NMR** (400 MHz, $CDCl_3$, 298 K): δ 0.90 (t, 7H, H9 and 10), 1 (s, 3H, H7), 1.46 (s, 1H, H5), 1.72 (m, 1H, H8), 2.47 (q, 1H, H6), 7.59 (s, 1H, H2), 3.73/3.82 (dd, 2H, H4).

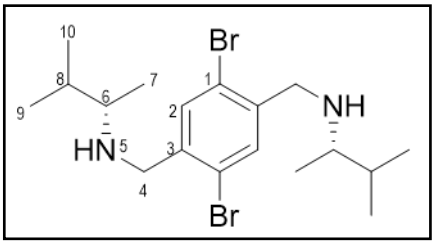


**5.** To a round bottom reaction flask, in inert atmosphere, were added *(R)*-1-(naphtalen-2-yl)ethanamine (0.474 mmol, 0.200 g) and $K_2CO_3$ (1.617 mmol, 0.223 g) in dry THF (7 mL) and the mixture was kept stirring for 20 min. After this time compound **3** was added and the mixture refluxed for 72 hours and was followed by TLC. The desired compound was purified by column chromatography in $Al_2O_3$ with acetone/ petroleum ether 1:20 (v/v) as eluent giving 0.197 g of an yellow solid (yield 64 %) **$^1$H NMR** (400 MHz, $CDCl_3$, 298 K): δ 3.74 (s, 2H, H7), 3.94 (q, 1H, H-8), 7.47 (m, 3H, H9, H16 and H17), 7.76 (s, 1H, H2), 7.84 (m, 4H, H11, H12, H13 and H14).

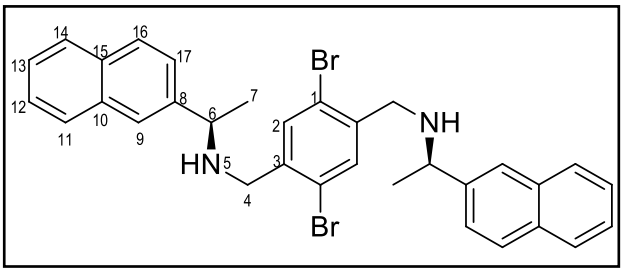

# 5 Perspectives

The work developed in this thesis was divided in the synthesis of new ligands for 3D Hofmann clathrate formation and for the fabrication of new 1D coordination polymers.

A bipyridine based ligand (**L1**) was successfully synthesised in good yields and the ligand characterised by NMR and FTIR spectroscopy. The luminescent properties were also studied. Two ligands (**L1** and **L2**) were successfully used in the fabrication of two new 3D Hofmann structures (**P1** and **P2**) in reasonably good yields (> 50%) for both cases. The ordered structures were characterised by FTIR spectroscopy, elemental analysis, luminescence and their magnetic profile determined by SQUID magnetometry. After performing guest-molecule insertion tests by vapour diffusion with several molecules (using **P1** and **P2** as hosts), it was verified that only pyridine promoted a SCO behaviour in **P1**. In opposition **P2** remained in the LS state for all vapour diffused molecules. Chiral guest molecules (D-phenylalanine, L-phenylalanine, D-alanine and L-alanine) were used with **P1**. The first two did not promote a change in the magnetic behaviour that remained in the HS state but the samples after the insertion test with the last two ( D-phenylalanine and L-phenylalanine) showed a magnetic profile with $\chi$MT values typical for iron(III) suggesting an oxidation of the metal centres or the formation of new compounds. The luminescence studies performed suggest the occurrence of a quenching effect upon coordination of the ligand **L1** to the metal since **L1** showed a very strong emissive profile and **P1** was not emissive. Further studies of guest molecule insertion should be performed using, for instance, other guest molecules or changing the test conditions (temperature, vials, etc.). Circular dichroism, TGA and Raman spectroscopy allied with theoretical calculations will be important to further understand the systems used.

Eight new triazole based ligands (**L3** to **L10**) were successfully synthesised in in reasonably good yields (above 40%). The ligands were characterised by NMR and FTIR spectroscopy and for **L3** luminescent properties were determined. Starting from **L3** to **L6** were synthesised four new 1D coordination polymers (**P3** to **P6**) in yields above 40%. The polymers were characterised by FTIR spectroscopy and their magnetic profiles analysed by SQUID. **P3** demonstrated a SCO behaviour with a fast-gradual incomplete transition. The conductivity and luminescent properties of **P3** were studied. The results suggest that the polymer behaves as a semiconductor and the profiles obtained for the luminescence studies demonstrated that the polymer is more emissive than the ligand **L3**. They also showed that the emission profiles at room temperature are different from the emission profiles at 77 K which indicates a change in the luminescent behaviour of the sample with the temperature. Its luminescence emission and semiconductor behaviour allied with the SCO behaviour, makes it a promising polymer to be applied as a multifunctional material. Ligands **L7** to **L10** appeared to be emissive in chloroform solutions, at room temperature, but the luminescence studies for these ligands were not yet performed.

Future work would include additional characterisation techniques. Mössbauer spectroscopy and EPR for confirmation on the oxidation state of the metal centres and also for information on the ratio between the metal centres in the HS and LS state. Single crystal X-ray diffraction is essential to the confirmation of structure details, such as the spatial arrangement of the atoms, bond length, angles measures and, ultimately, to observe the interactions with other species. In the case of 3D structures, it will also help to confirm the presence of the cavities, their size and ability to host other molecules. Elemental analysis will also be performed for polymers **P2** to **P6**.

# 6 References

[1] G. R. Whittell, I. Manners, *Adv. Mater.* **2007**, *19*, 3439–3468.

[2] E. Chelebaeva, J. Larionova, Y. Guari, R. A. S. Ferreira, L. D. Carlos, F. A. A. Paz, A. Trifonov, C. Guérin, *Inorg. Chem.* **2009**, *48*, 5983–5995.

[3] R. J. Kuppler, D. J. Timmons, Q. R. Fang, J. R. Li, T. A. Makal, M. D. Young, D. Yuan, D. Zhao, W. Zhuang, H. C. Zhou, *Coord. Chem. Rev.* **2009**, *253*, 3042–3066.

[4] F. Ke, Y.-P. Yuan, L.-G. Qiu, Y.-H. Shen, A.-J. Xie, J.-F. Zhu, X.-Y. Tian, L.-D. Zhang, *J. Mater. Chem.* **2011**, *21*, 3843.

[5] M. Kurmoo, *Chem. Soc. Rev.* **2009**, *38*, 1353–1379.

[6] D. Maspoch, D. Ruiz-Molina, J. Veciana, *J. Mater. Chem.* **2004**, *14*, 2713–2723.

[7] C. Janiak, J. K. Vieth, *New J. Chem.* **2010**, *34*, 2366–2388.

[8] P. W. Atkins, T. Overton, J. Rourke, M. Weller, F. Armstrong, M. Hangerman, *Inorganic Chemistry*, Oxford University Press, New York, **2010**.

[9] C. E. Housecroft, A. G. Sharpe, *Inorganic Chemistry*, Pearson Education Limited, Essex, **2001**.

[10] P. Gütlich, Y. Garcia, H. A. Goodwin, *Chem. Soc. Rev.* **2000**, *29*, 419–427.

[11] O. Kahn, *Molecular Magnetism (Kahn, Olivier)*, **1995**.

[12] D. Gatteschi, *Adv. Mater.* **1994**, *6*, 635–645.

[13] J.-F. Létard, P. Guionneau, L. Goux-Capes, in *Spin Crossover Transit. Met. Compd. III*, **2004**, pp. 221–249.

[14] A. Bousseksou, G. Molnár, L. Salmon, W. Nicolazzi, *Chem. Soc. Rev.* **2011**, 3313–3335.

[15] P. Gamez, J. S. Costa, M. Quesada, G. Aromí, *J. Chem. Soc. Dalt. Trans.* **2009**, 7845–7853.

[16] X. Bao, H. J. Shepherd, L. Salmon, G. Molnμr, M. Tong, A. Bousseksou, *Angew. Chemie - Int. Ed.* **2013**, 1198–1202.

[17] P. D. Southon, L. Liu, E. A. Fellows, D. J. Price, G. J. Halder, K. W. Chapman, B. Moubaraki, K. S. Murray, *J. Am. Chem. Soc.* **2009**, *131*, 10998–11009.

[18] B. Weber, J. Obel, D. Henner-vásquez, W. Bauer, *Eur. J. Inorg. Chem.* **2009**, 5527–5534.

[19] Y. Garcia, O. Kahn, L. Rabardel, B. Chansou, L. Salmon, J. P. Tuchagues, *Inorg. Chem.* **1999**, *38*, 4663–4670.

[20] C. Lochenie, K. Schötz, F. Panzer, H. Kurz, B. Maier, F. Puchtler, S. Agarwal, A. Köhler, B. Weber, *J. Am. Chem. Soc.* **2018**, *140*, 700–709.

[21] A. B. Gaspar, M. C. Muñoz, J. A. Real, *J. Mater. Chem.* **2006**, *16*, 2522–2533.

[22] B. Weber, W. Bauer, J. Obel, *Angew. Chemie - Int. Ed.* **2008**, *47*, 10098–10101.

[23] G. Agustí, M. C. Muñoz, A. B. Gaspar, J. A. Real, *Inorg. Chem.* **2008**, *47*, 2552–2561.

[24] O. Roubeau, *Chem. - A Eur. J.* **2012**, *18*, 15230–15244.

[25] C. Bartual-Murgui, L. Salmon, A. Akou, N. A. Ortega-Villar, H. J. Shepherd, M. C. Muñoz, G. Molnár, J. A. Real, A. Bousseksou, *Chem. - A Eur. J.* **2012**, *18*, 507–516.

[26] X. Zhu, X. Y. Wang, B. L. Li, J. Wang, S. Gao, *Polyhedron* **2012**, *31*, 77–81.

[27] P. J. Van Koningsbruggen, Y. Garcia, O. Kahn, L. Fournès, H. Kooijman, A. L. Spek, J. G. Haasnoot, J. Moscovici, K. Provost, A. Michalowicz, et al., *Inorg. Chem.* **2000**, *39*, 1891–1900.

[28] M. Hasegawa, F. Renz, T. Hara, Y. Kikuchi, Y. Fukuda, J. Okubo, T. Hoshi, W. Linert, *Chem. Phys.* **2002**, *277*, 21–30.

[29] J. Linares, E. Codjovi, Y. Garcia, *Sensors* **2012**, *12*, 4479–4492.

[30] O. Kahn, C. J. Martinez, *Science (80-. ).* **1998**, *279*, 44–48.

[31] C.-M. Jureschi, J. Linares, A. Boulmaali, P. Dahoo, A. Rotaru, Y. Garcia, *Sensors* **2016**, *16*, 187.

[32] S. V. Bhosale, C. H. Jani, S. J. Langford, *Chem. Soc. Rev.* **2008**, *37*, 331–342.

[33] G. Ghosh, M. Paul, T. Sakurai, W. Matsuda, S. Seki, *Chem. - A Eur. J.* **2018**, *24*, 1938–1946.

[34] S. Mukherjee, D. Samanta, P. S. Mukherjee, *Cryst. Growth Des.* **2013**, *13*, 5335–5343.

[35] Z. G. Gu, Y. F. Xu, X. H. Zhou, J. L. Zuo, X. Z. You, *Cryst. Growth Des.* **2008**, *8*, 1306–1312.

[36] Y. Garcia, G. Bravic, C. Gieck, D. Chasseau, W. Tremel, P. Gütlich, *Inorg. Chem.* **2005**, *44*, 9723–9730.

[37] G. Aromí, L. A. Barrios, O. Roubeau, P. Gamez, *Coord. Chem. Rev.* **2011**, *255*, 485–546.

[38] Y. Garcia, V. Niel, M. C. Muñoz, J. A. Real, in *Spin Crossover Transit. Met. Compd. I*, **2004**, pp. 229–257.

[39] M. Giménez-Marqués, M. L. García-Sanz De Larrea, E. Coronado, *J. Mater. Chem. C* **2015**, *3*, 7946–7953.

[40] W. Bauer, S. Schlamp, B. Weber, *Chem. Commun.* **2012**, *48*, 10222–10224.
[41] J. Y. Li, Z. P. Ni, Z. Yan, Z. M. Zhang, Y. C. Chen, W. Liu, M. L. Tong, *CrystEngComm* **2014**, *16*, 6444–6449.
[42] I. A. Gural'Skiy, O. I. Kucheriv, S. I. Shylin, V. Ksenofontov, R. A. Polunin, I. O. Fritsky, *Chem. - A Eur. J.* **2015**, *21*, 18076–18079.
[43] H. J. Shepherd, C. Bartual-Murgui, G. Molnár, J. A. Real, M. C. Muñoz, L. Salmon, A. Bousseksou, *New J. Chem.* **2011**, *35*, 1205.
[44] G. Massasso, M. Rodríguez-Castillo, J. Long, J. Haines, S. Devautour-Vinot, G. Maurin, A. Grandjean, B. Onida, B. Donnadieu, J. Larionova, et al., *Dalt. Trans.* **2015**, *44*, 19357–19369.
[45] J. Suárez-Varela, H. Sakiyama, J. Cano, E. Colacio, *Dalt. Trans.* **2007**, 249–256.
[46] G. Agustí, S. Cobo, A. B. Gaspar, G. Molnár, N. O. Moussa, P. Á. Szilágyi, C. Vieu, M. C. Muñoz, J. A. Real, A. Bousseksou, *Chem. Mater.* **2008**, *20*, 6721–6732.
[47] J. A. Real, E. Andrés, M. C. Muñoz, M. Julve, T. Granier, A. Bousseksou, F. Varret, *Science (80-. ).* **1995**, *268*, 265–7.
[48] T. Kitazawa, T. Enokib, *J. Mater. Chem. A* **1996**, *6*, 119–121.
[49] V. Niel, J. M. Martinez-Agudo, M. C. Muñoz, A. B. Gaspar, J. A. Real, *Inorg. Chem.* **2001**, *40*, 3838–3839.
[50] J. Jin, X. Zhao, P. Feng, X. Bu, *Angew. Chemie - Int. Ed.* **2018**, *57*, 1–6.
[51] Y. Uek, J. Okabayash, T. Kitazawa, *Chem. Lett.* **2017**, *46*, 747–749.
[52] P. Sixou, P. Dansas, *Berichte der Bunsen-Gesellschaft* **1976**, *80*, 364–389.
[53] D. W. Davidson, *Can. J. Chem.* **1970**, 1224–1242.
[54] G. J. Halder, C. J. Kepert, B. Moubaraki, K. S. Murray, J. D. Cashion, *Science (80-. ).* **2002**, *298*, 1762–1765.
[55] B. Valeur, *Molecular Fluorescence: Principles and Applications*, Wiley-VCH, Grunstadt, **2001**.
[56] J. W. Lichtman, J. A. Conchello, *Nat. Methods* **2005**, *2*, 910–919.
[57] C. Wang, R. Li, X. Chen, R. Wei, L. Zheng, J. Tao, *Angew. Chemie Int. Ed.* **2014**, *53*, 1–5.
[58] H. S. Scott, M. Shivanna, A. Bajpai, K. J. Chen, D. G. Madden, J. J. Perry, M. J. Zaworotko, *Cryst. Growth Des.* **2017**, *17*, 1933–1937.
[59] U. Resch-Genger, K. Rurack, *Pure Appl. Chem.* **2013**, *85*, 2005–2026.
[60] H. Sasabe, J. Kido, *Chem. Mater.* **2011**, *23*, 621–630.
[61] G. V. Loukova, W. Huhn, V. P. Vasiliev, V. A. Smirnov, *J. Phys. Chem. A* **2007**, *111*, 4117–4121.
[62] P. Chábera, Y. Liu, O. Prakash, E. Thyrhaug, A. El Nahhas, A. Honarfar, S. Essén, L. A. Fredin, T. C. B. Harlang, K. S. Kjær, et al., *Nature* **2017**, *543*, 695–699.
[63] D. J. Griffiths, R. College, *Introduction to Electrodynamics*, Prentice Hall, New Jersey, **1999**.

# Appendix

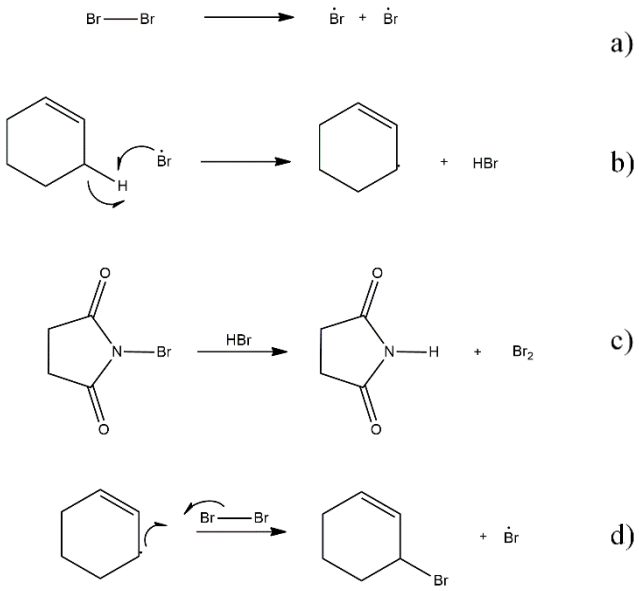


Scheme A 1.Whol-Ziegler reaction scheme: a) homolytic fission using an initiator; b) radical formation in the alkene group; c) bromine regeneration; d) bromination of the alkene.

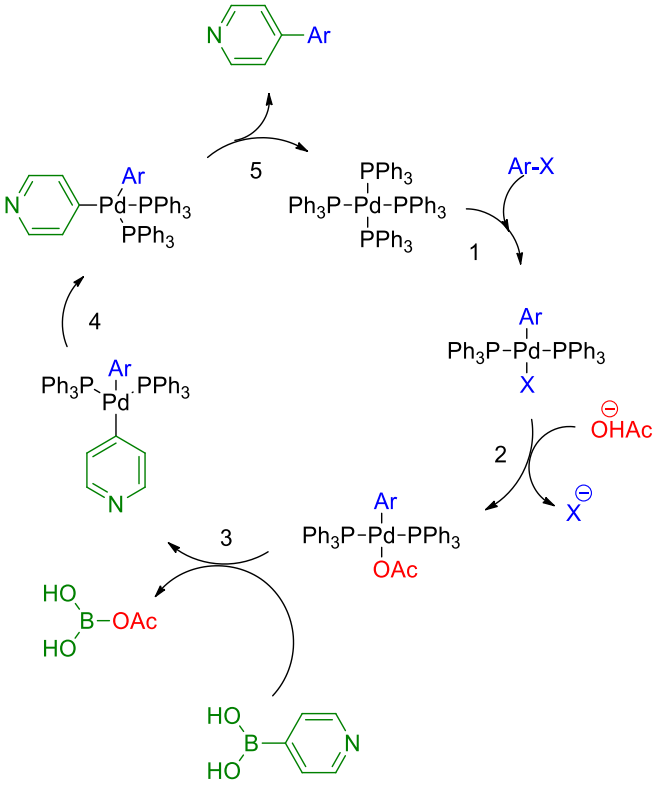


Scheme A 2: Catalytic cycle of a general Suzuki coupling reaction: 1-oxidative addition; 2-ligands substitution; 3-transmetalation; 4- trans/cis isomerisation; 5- reductive elimination.

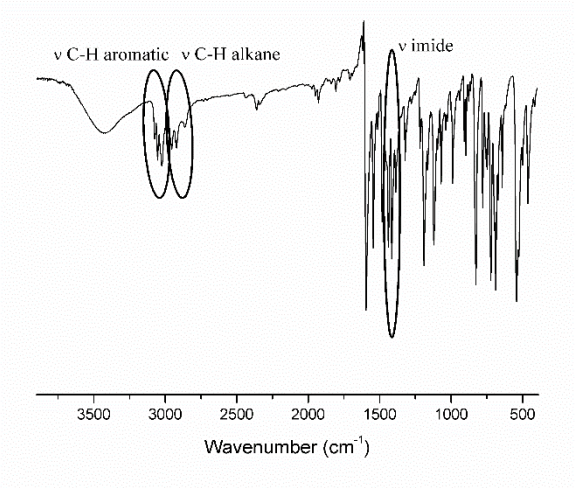


Figure A 1. FTIR spectrum of **L1**.

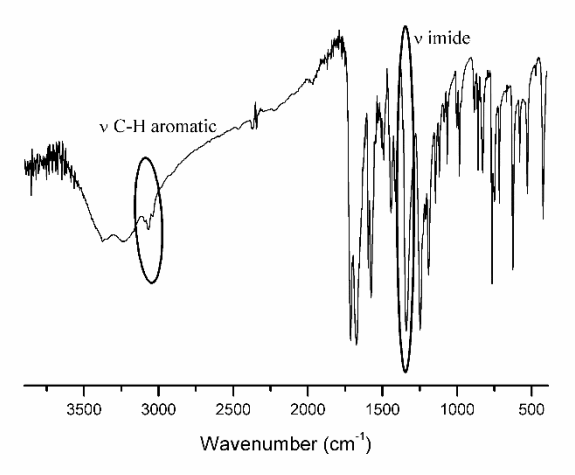


Figure A 2. FTIR spectrum of **L2**.

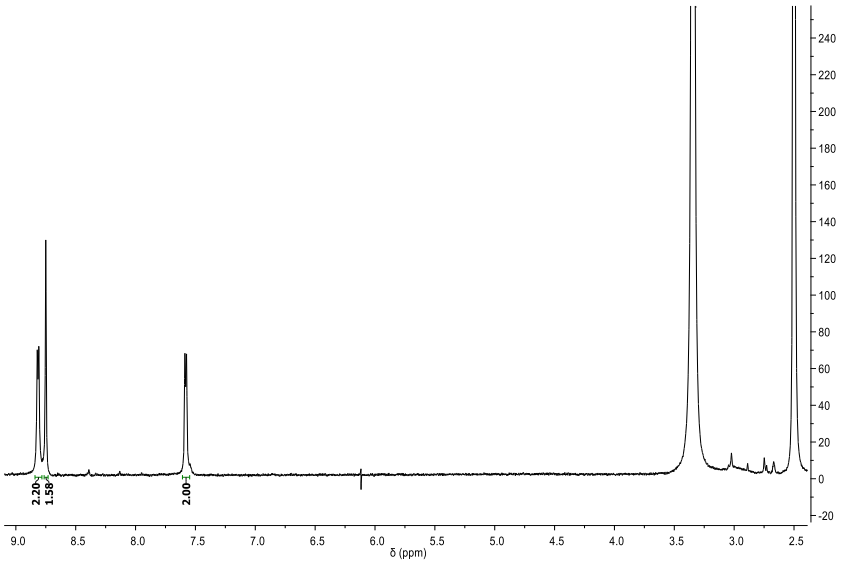


Figure A 3. $^{1}H$ NMR for **L2** in DMSO-$d_6$.

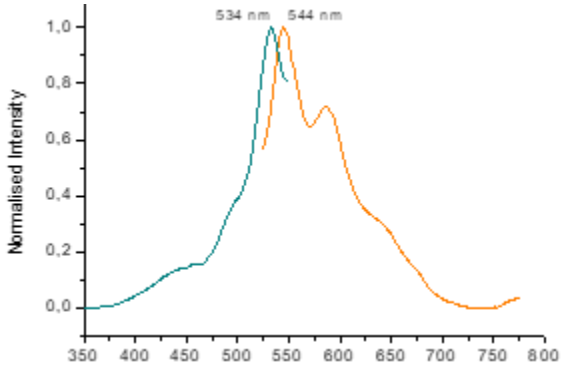


Figure A 4. Excitation spectrum (blue) and emission spectrum (orange) of **L1** at room temperature.

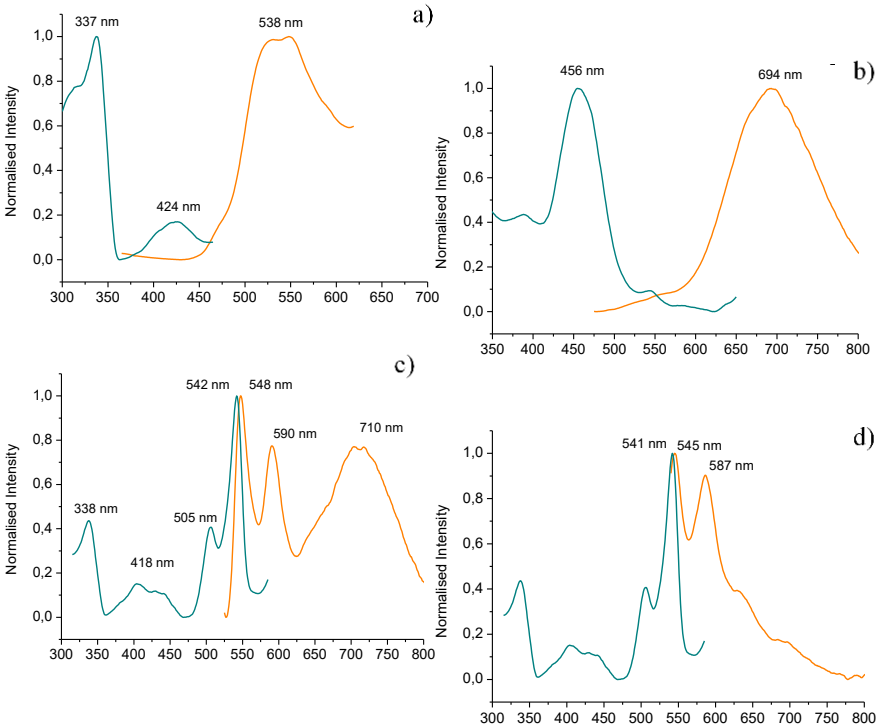


Figure A 5. Excitation spectra (blue) and emission spectra (orange) of **L1** at 77 K: a) excitation 275-325 nm; b) excitation 375-475 nm; c) excitation 500 nm; d) excitation 525 nm.

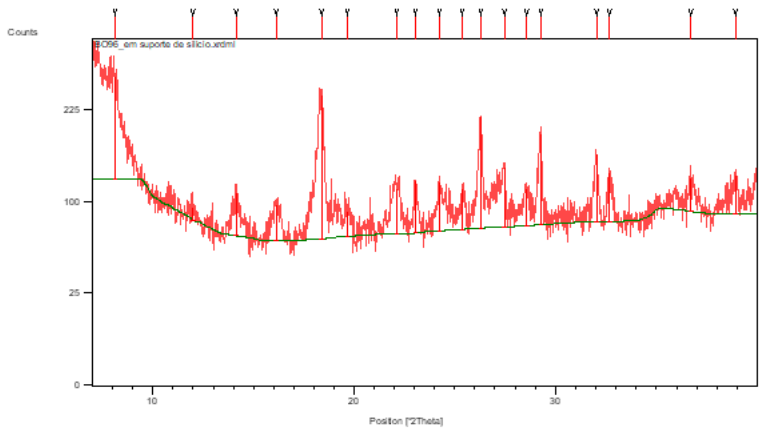


Figure A 6. X-ray powder diffractogram for **P1**.

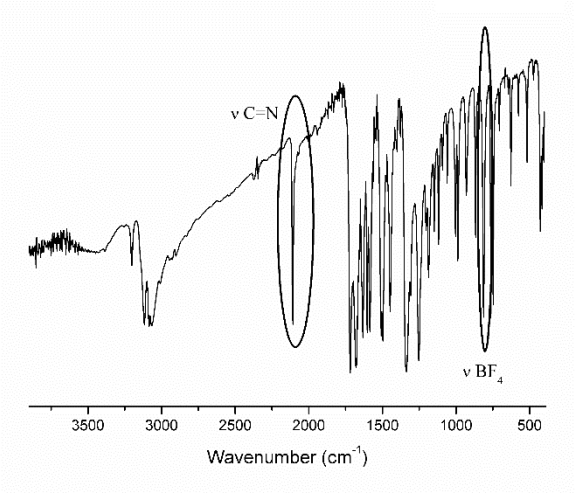


Figure A 7. FTIR spectrum for **P2**.

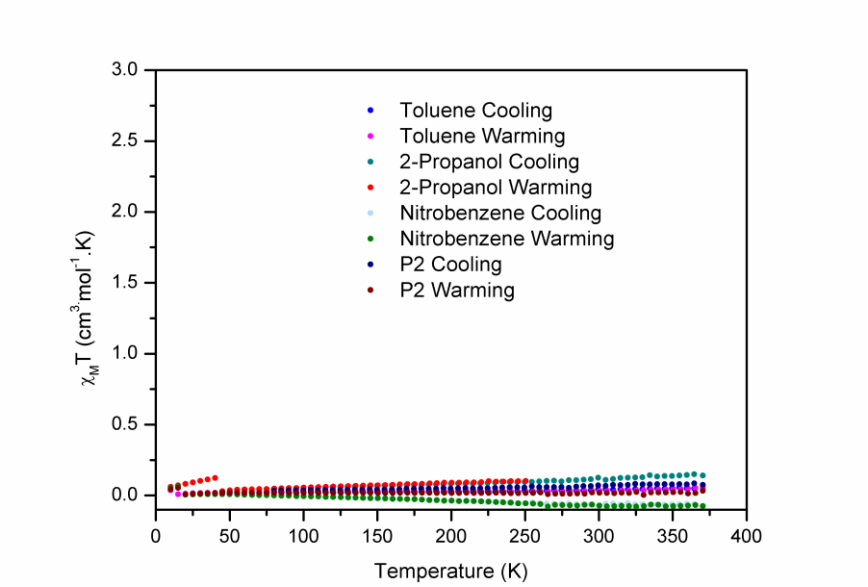


Figure A 8. Magnetic profile of **P2** after insertion of toluene 2-propanol, nitrobenzene.

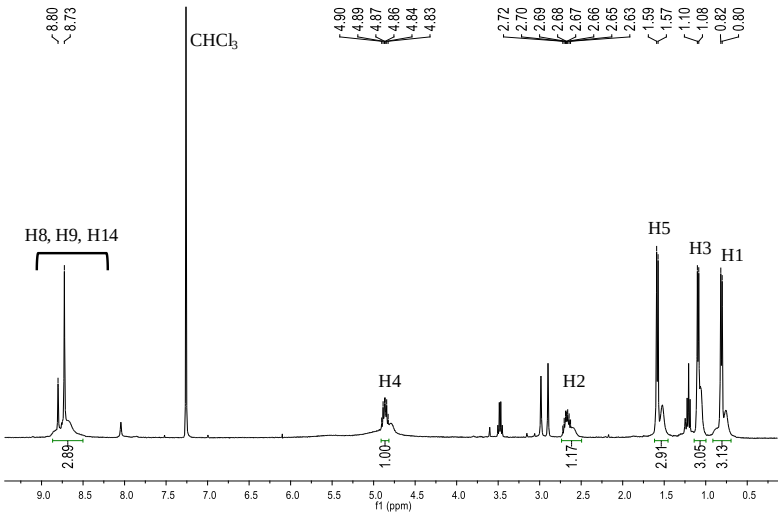


Figure A 9. $^{1}$H NMR for **L4** in $CDCl_3$.

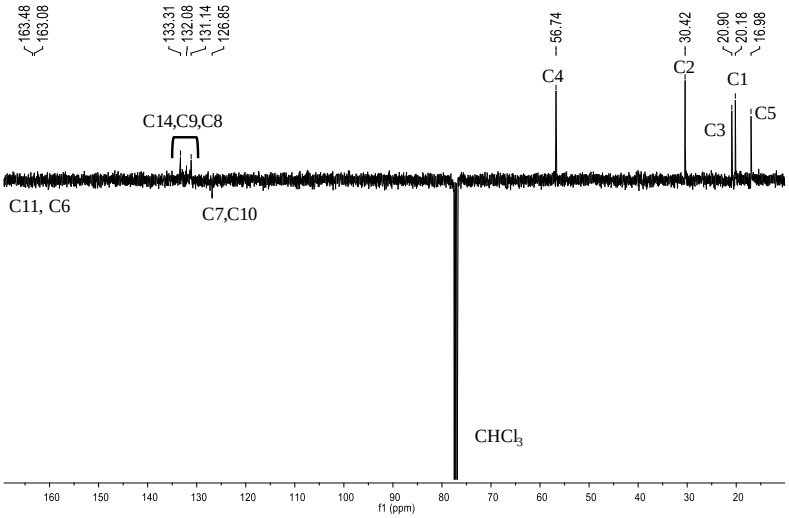


Figure A 10. $^{13}C$ APT for **L4** in $CDCl_3$.

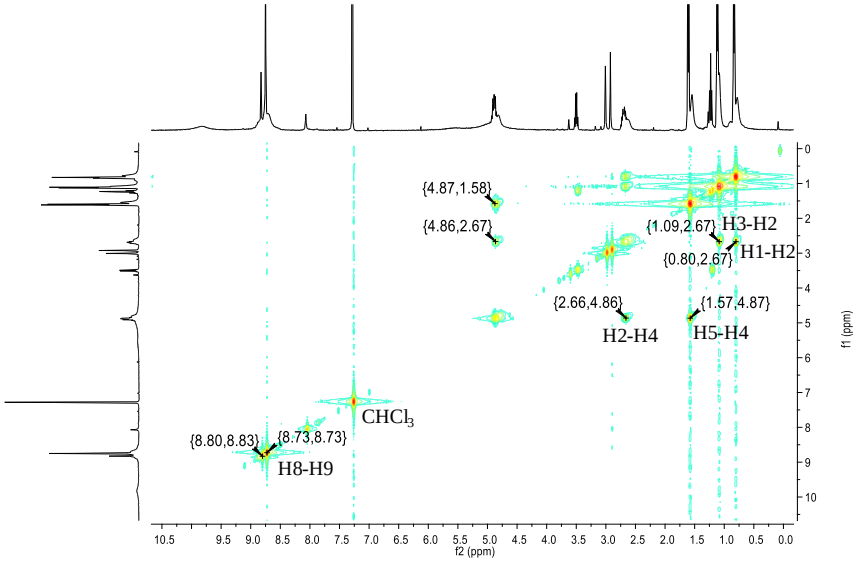


Figure A 11. 2D homonuclear COSY for **L4** in $CDCl_3$.

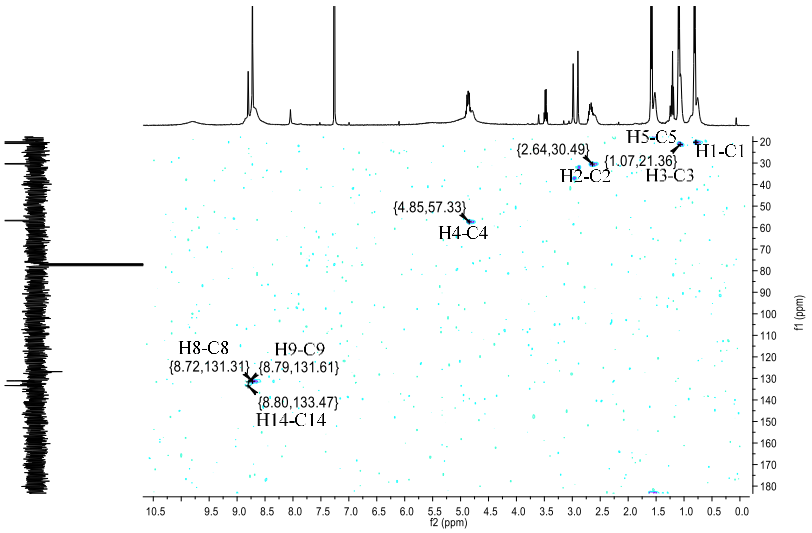


Figure A 12. 2D heteronuclear HSQC for **L4** in$CDCl_3$.

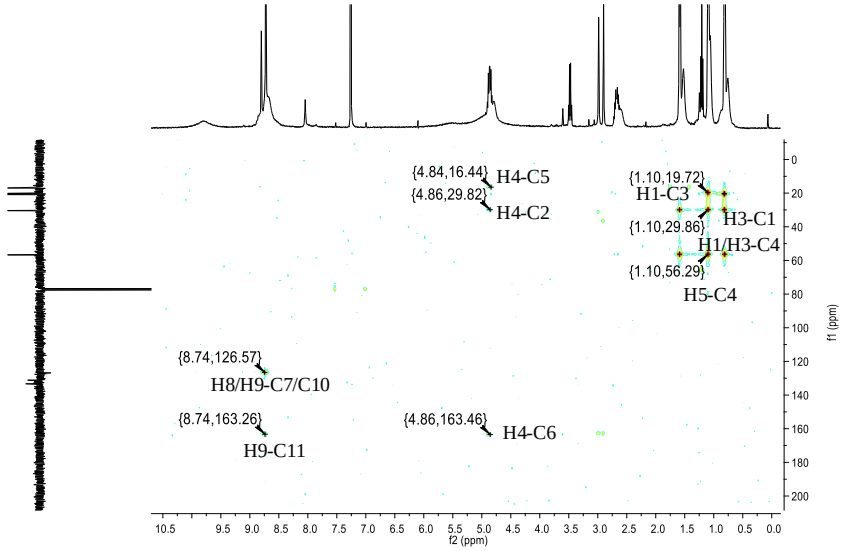


Figure A 13. 2D heteronuclear HMBC for **L4** in $CDCl_3$.

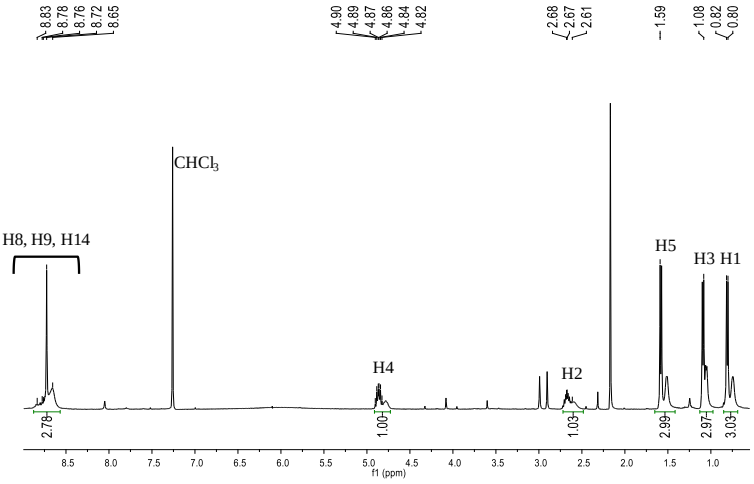


Figure A 14. $^{1}H$ NMR for **L5** in $CDCl_3$.

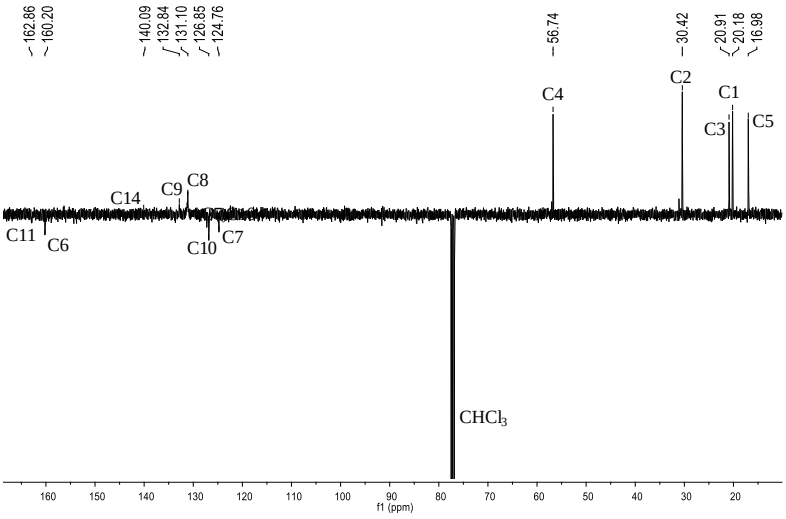


Figure A 15. $^{13}C$ APT for **L5** in $CDCl_3$.

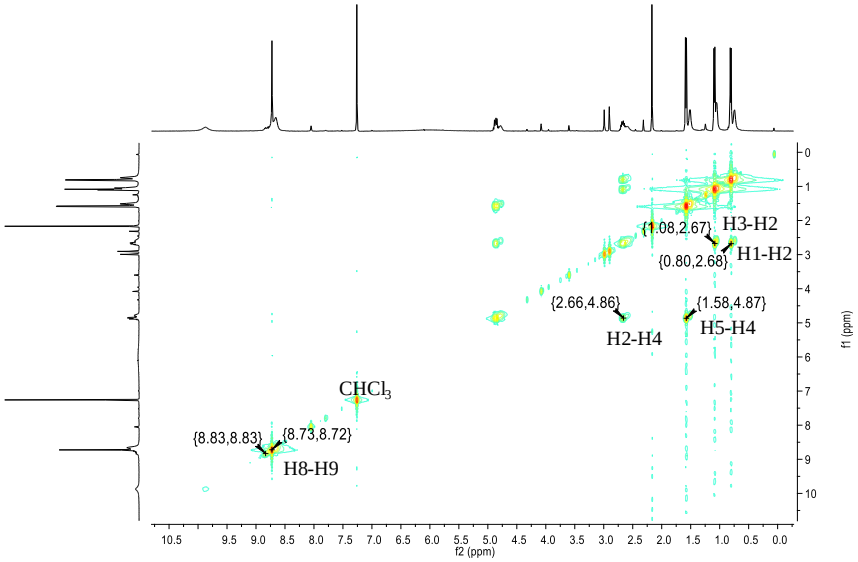


Figure A 16. 2D heteronuclear COSY for **L5** in $CDCl_3$.

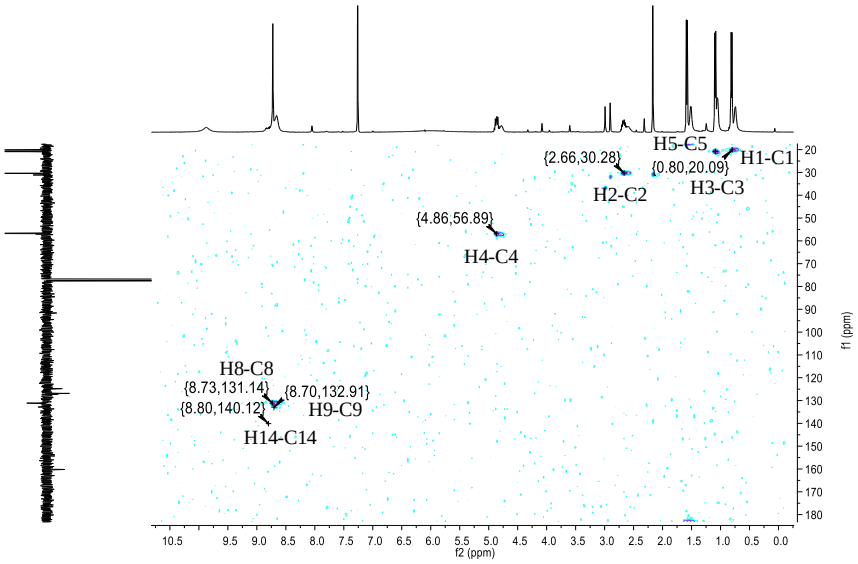


Figure A 17. 2D heteronuclear HSQC for **L5** in $CDCl_3$.

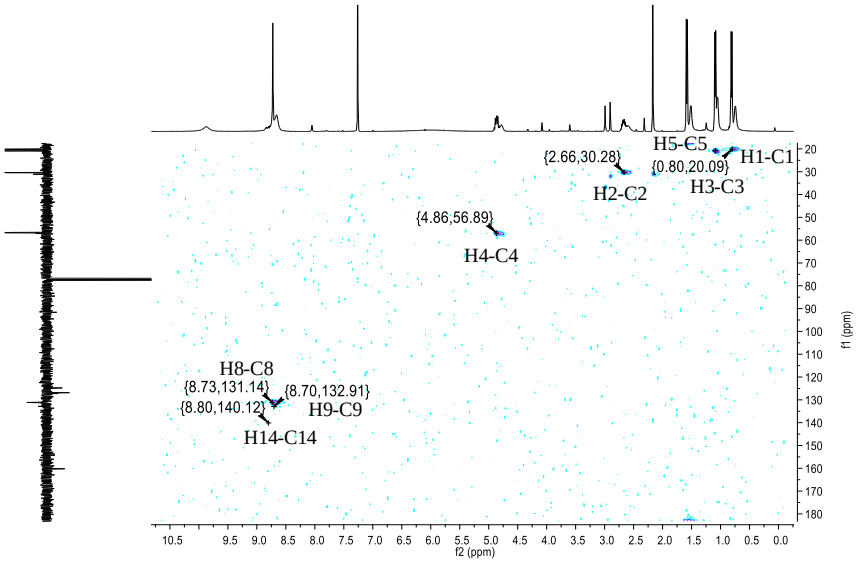


Figure A 18. 2D heteronuclear HMBC for **L5** in $CDCl_3$.

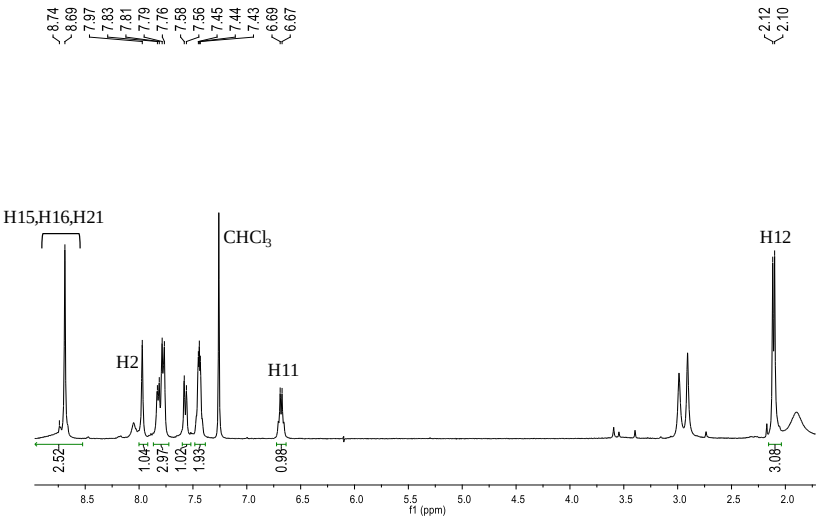


Figure A 19. $^{1}$H NMR for **L6** in $CDCl_3$.

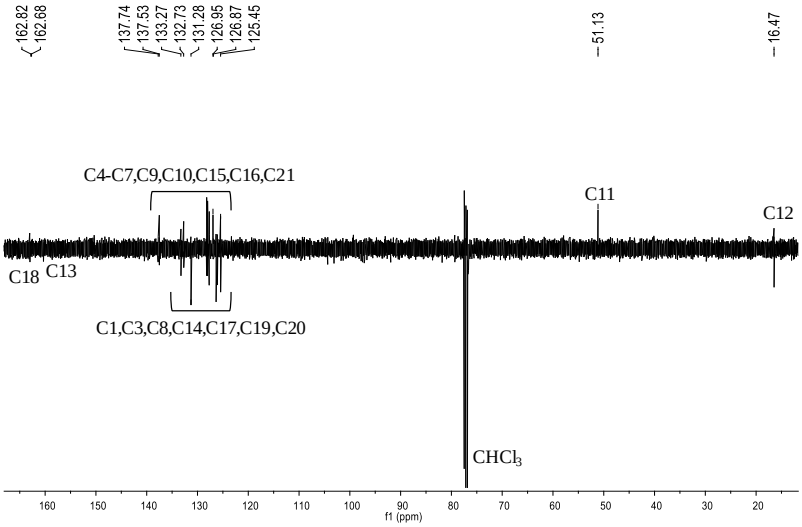


Figure A 20. $^{13}$C APT for **L6** in $CDCl_3$.

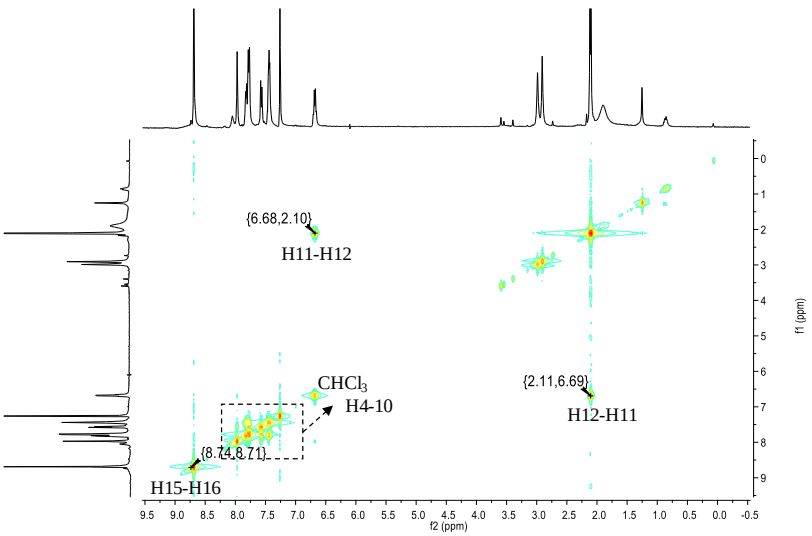


Figure A 21. 2D heteronuclear COSY for **L6** in $CDCl_3$.

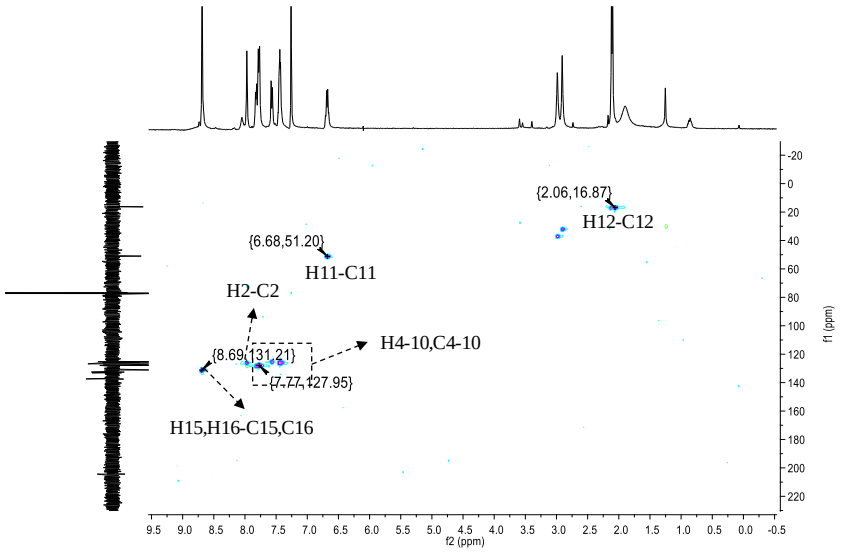


Figure A 22. 2D heteronuclear HSQC for **L6** in $CDCl_3$.

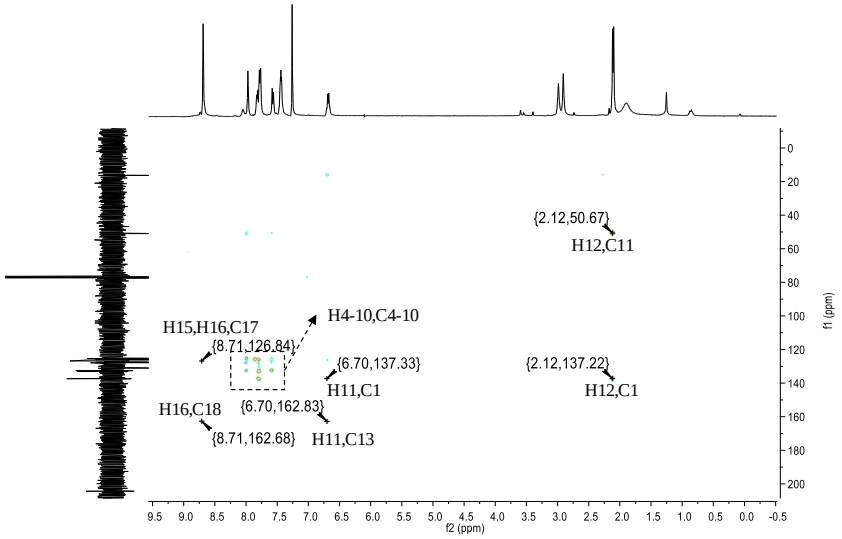


Figure A 23. 2D heteronuclear HMBC for **L6** in $CDCl_3$.

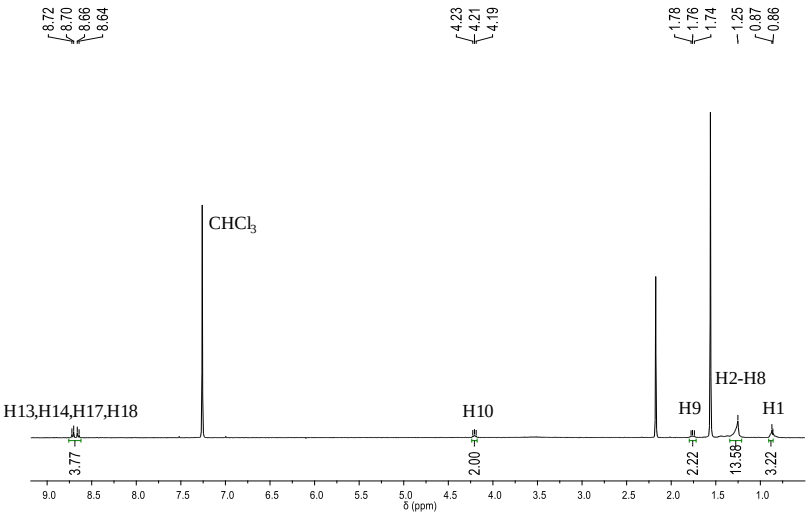


Figure A 24. $^1$H NMR for **L7** in $CDCl_3$.

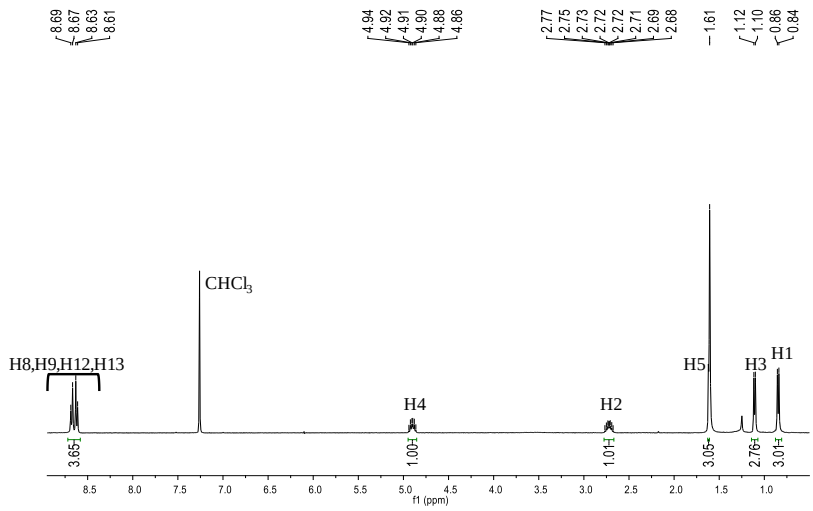


Figure A 25. $^{1}$H NMR for **L8** in $CDCl_3$.

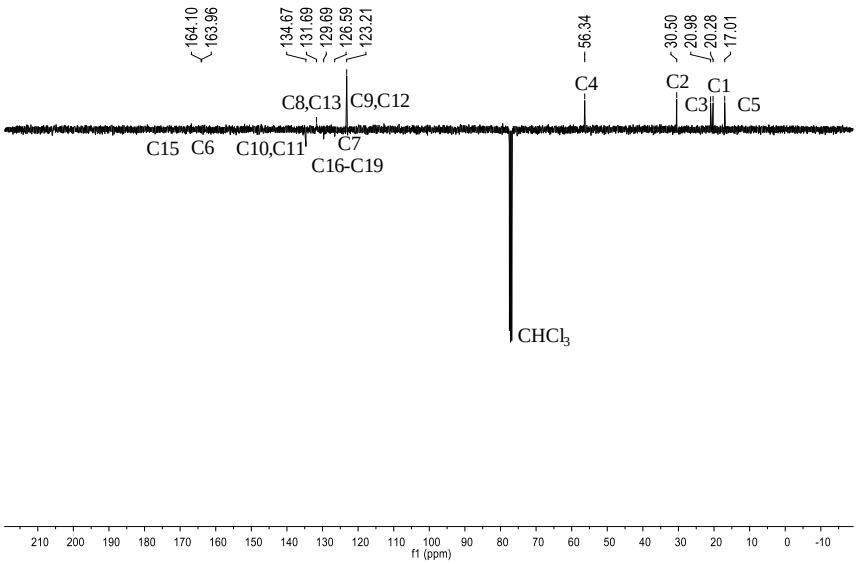


Figure A 26. $^{13}$C APT for **L8** in $CDCl_3$.

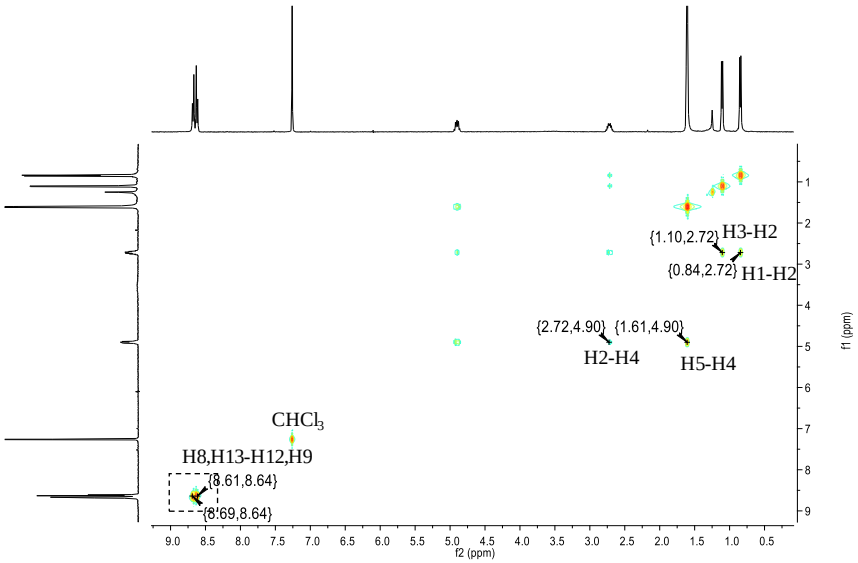


Figure A 27. 2D heteronuclear COSY for **L8** in $CDCl_3$.

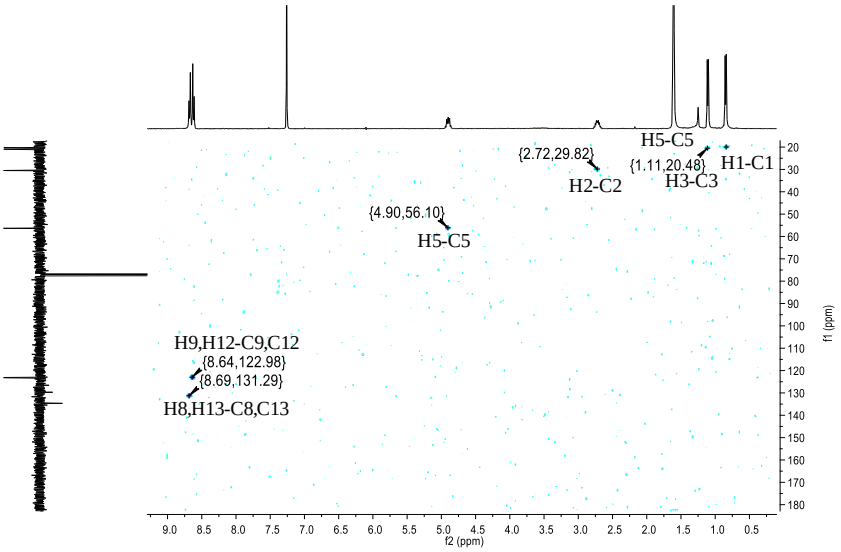


Figure A 28. 2D heteronuclear HSQC for **L8** in $CDCl_3$.

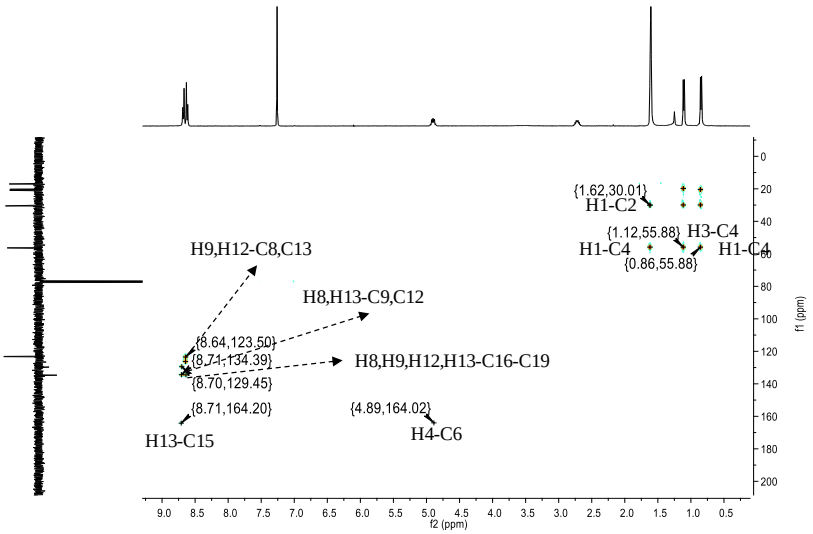


Figure A 29. 2D heteronuclear HMBC for **L8** in $CDCl_3$.

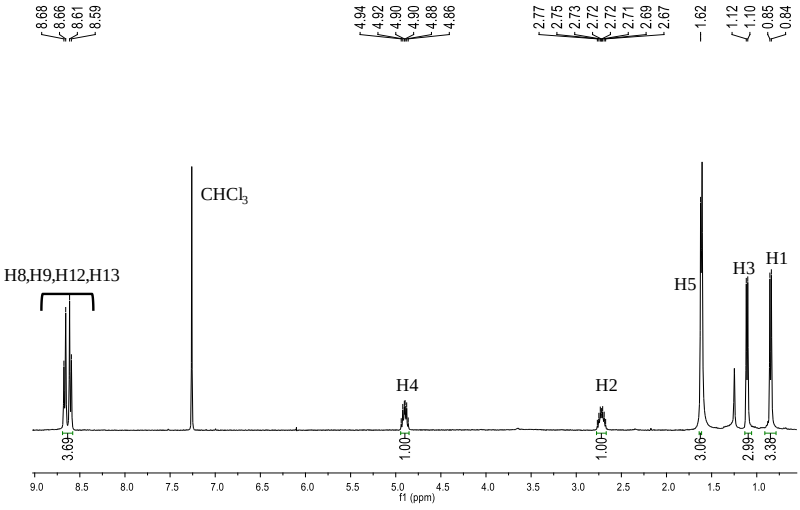


Figure A 30. $^1$H NMR for **L9** in $CDCl_3$.

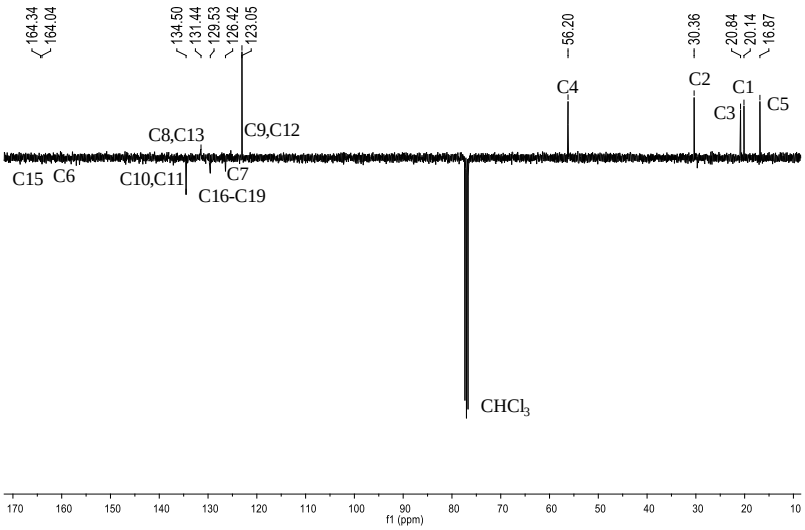


Figure A 31. $^{13}C$ APT for **L9** in $CDCl_3$.

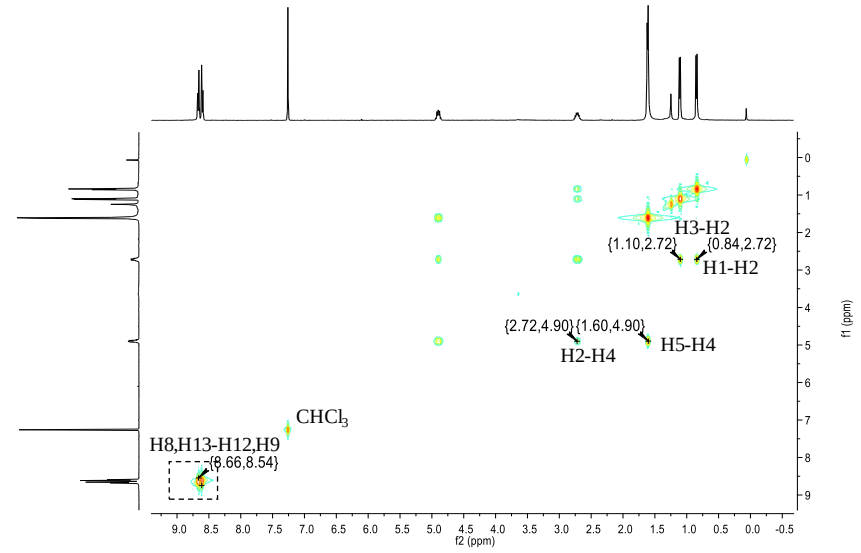


Figure A 32. 2D heteronuclear COSY for **L9** in $CDCl_3$.

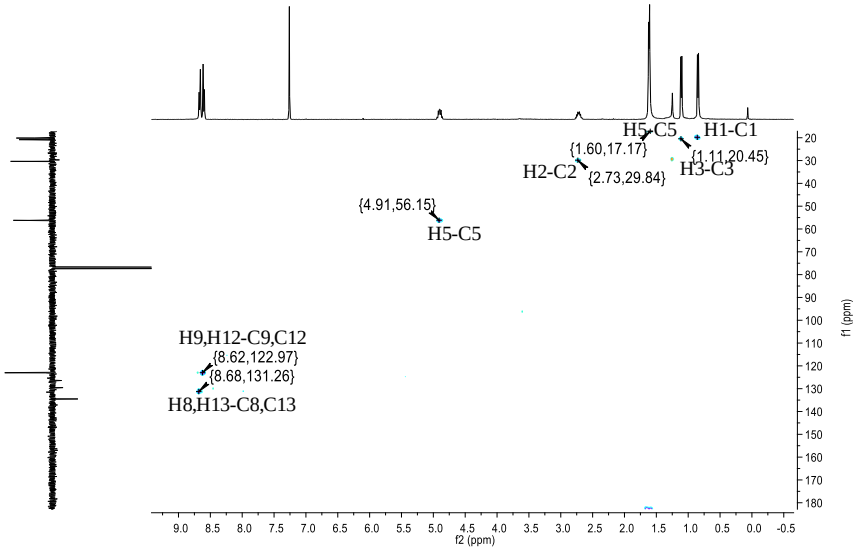


Figure A 33. 2D heteronuclear HSQC for **L9** in $CDCl_3$.

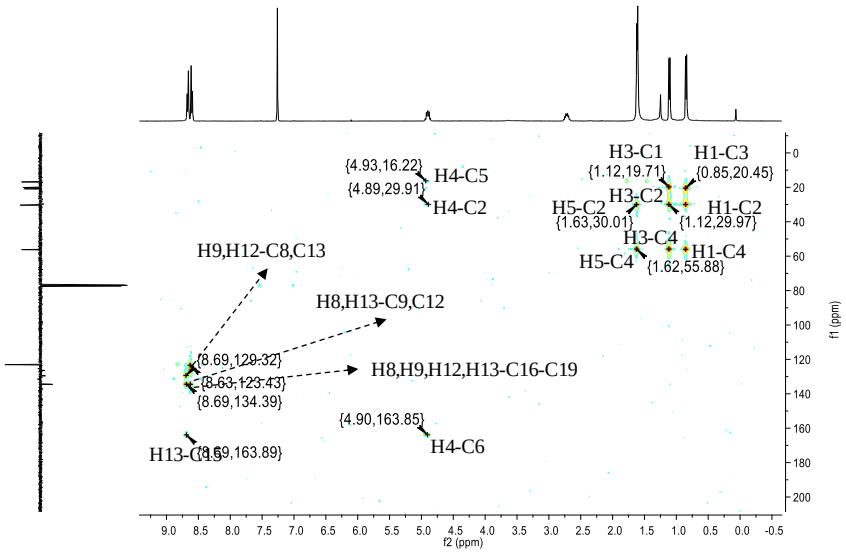


Figure A 34. 2D heteronuclear HMBC for **L9** in $CDCl_3$.

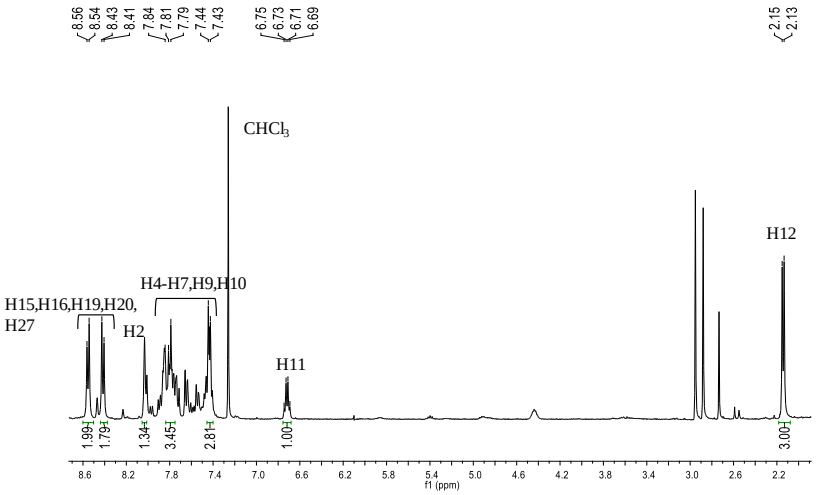


Figure A 35. $^{1}H$ NMR for **L10** in $CDCl_3$.

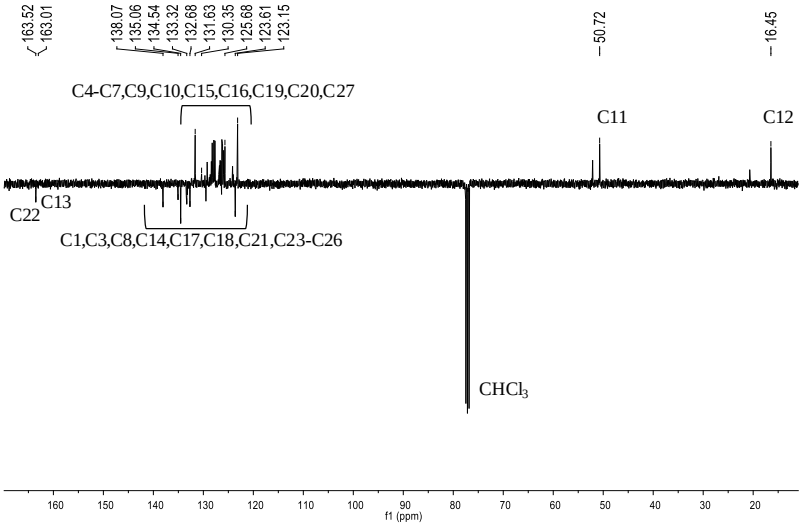


Figure A 36. $^{13}C$ APT for **L10** in $CDCl_3$.

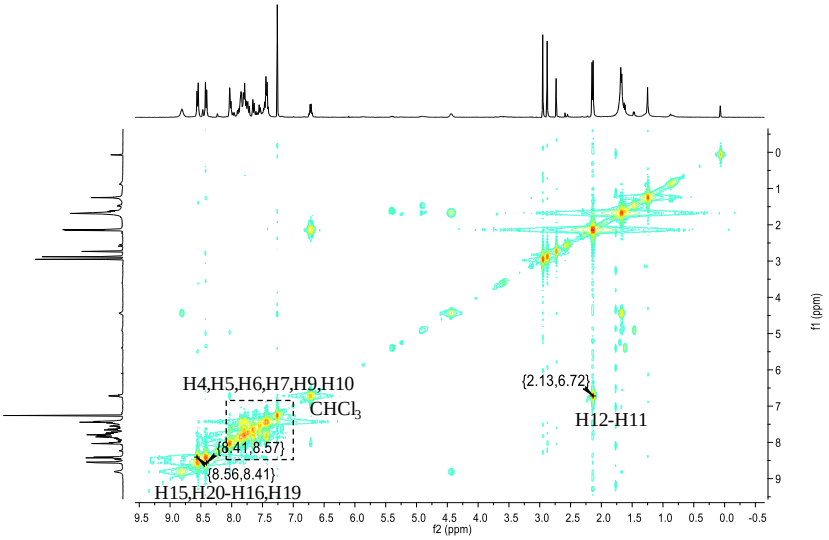


Figure A 37. 2D heteronuclear COSY for **L10** in $CDCl_3$.

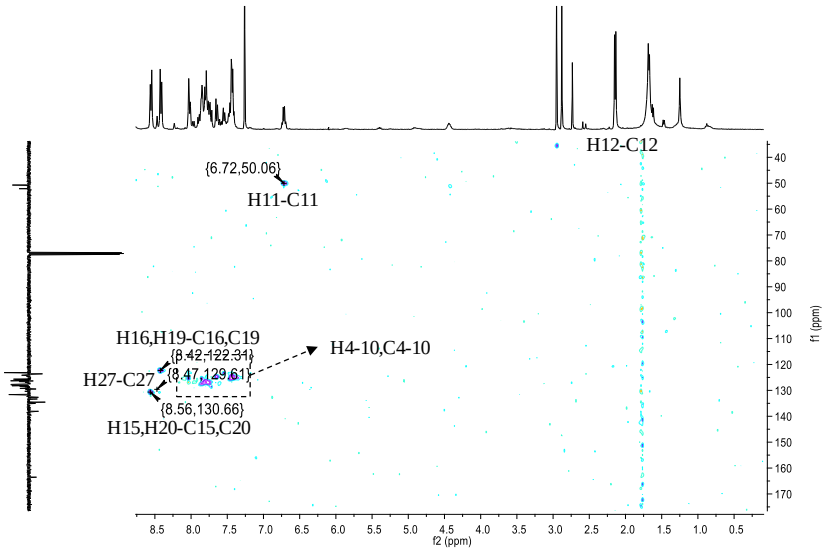


Figure A 38. 2D heteronuclear HSQC for **L10** in $CDCl_3$.

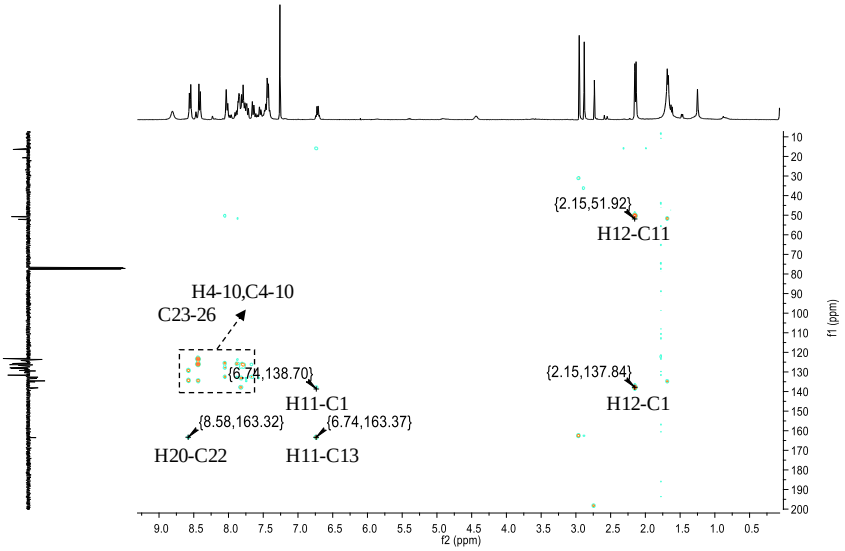


Figure A 39. 2D heteronuclear HMBC for **L10** in $CDCl_3$.

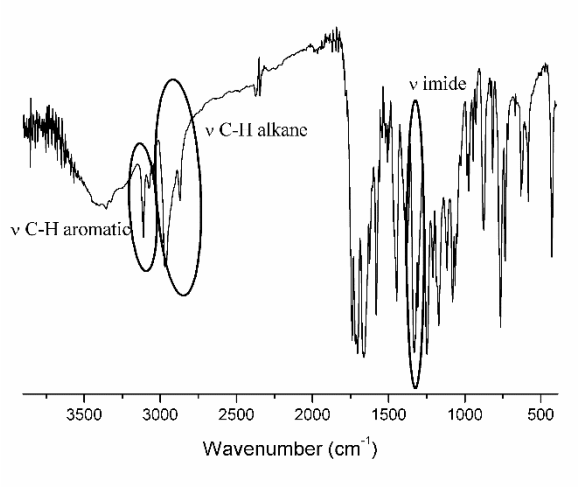


Figure A 40. FTIR spectrum for **L4**.

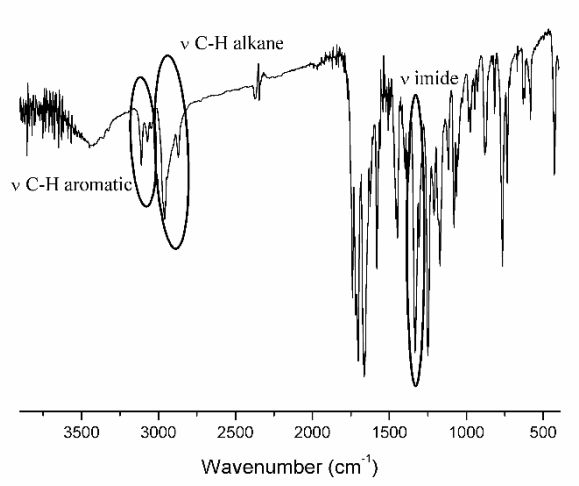


Figure A 41. FTIR spectrum for **L5**.

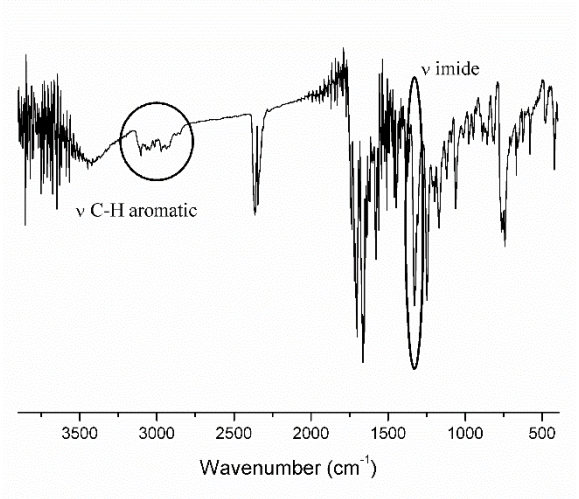


Figure A 42. FTIR spectrum for **L6**.

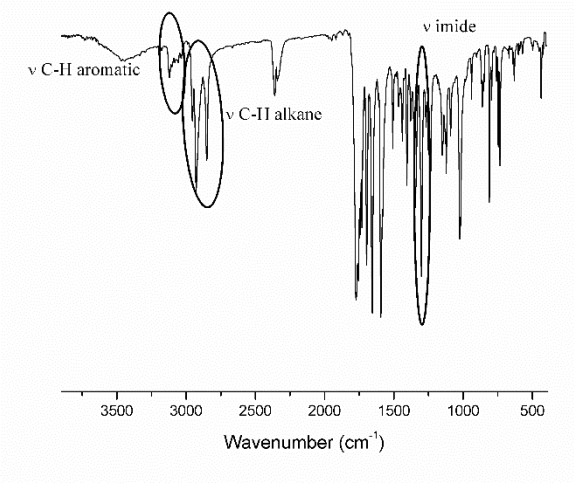


Figure A 43. FTIR spectrum for **L7**.

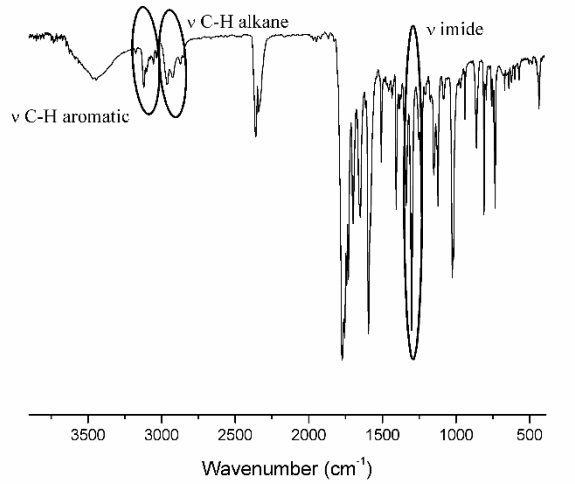


Figure A 44. FTIR spectrum for **L8**.

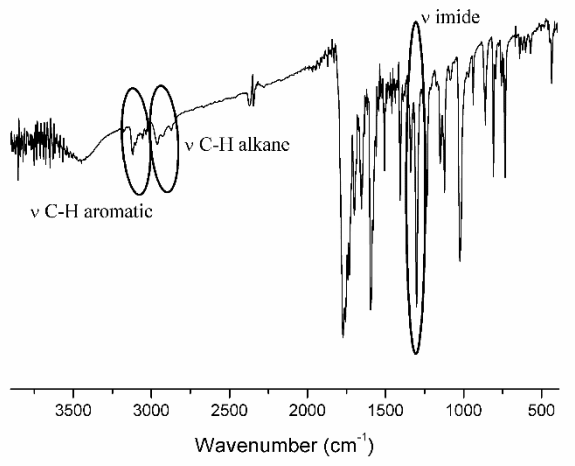


Figure A 45. FTIR spectrum for **L9**.

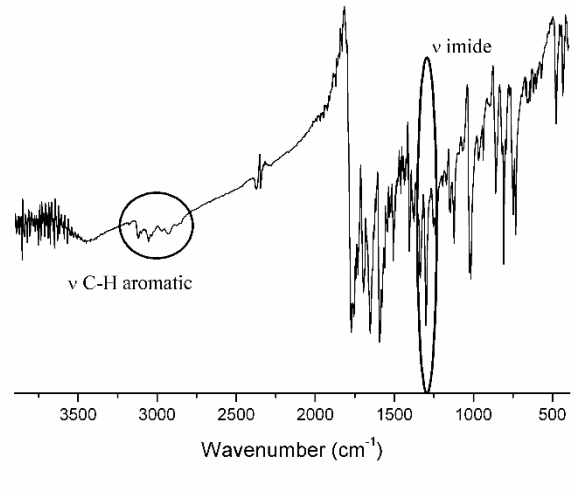


Figure A 46. FTIR spectrum for **L10**.

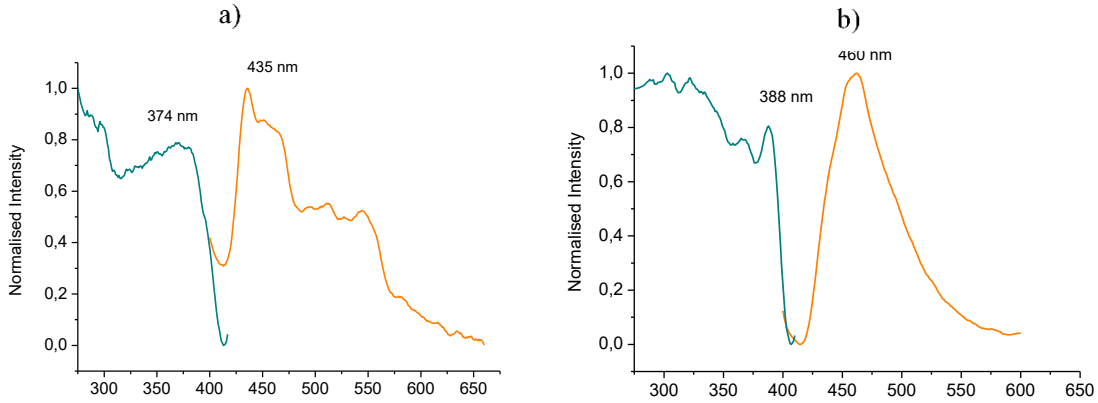


Figure A 47. Emission spectra (orange) of **L3**: a) room temperature; b) 77K.

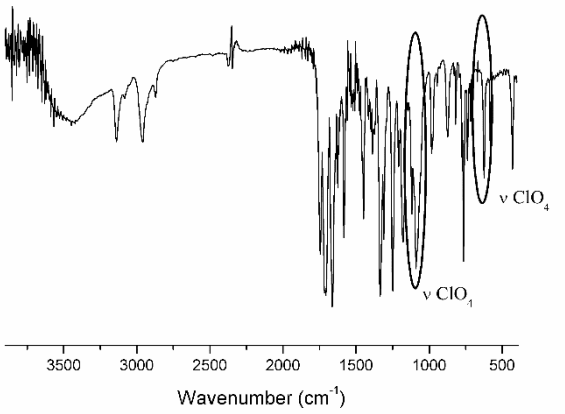


Figure A 48. FTIR spectrum for **P4**.

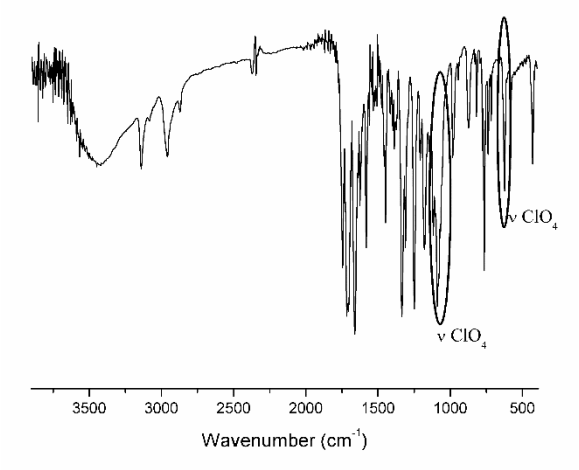


Figure A 49. FTIR spectrum for **P5**.

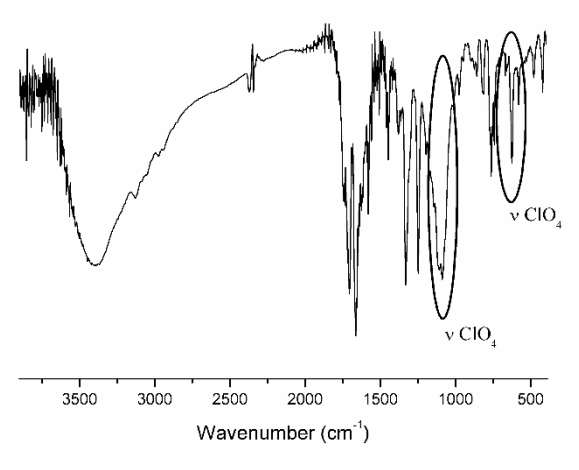


Figure A 50. FTIR spectrum for **P6**.

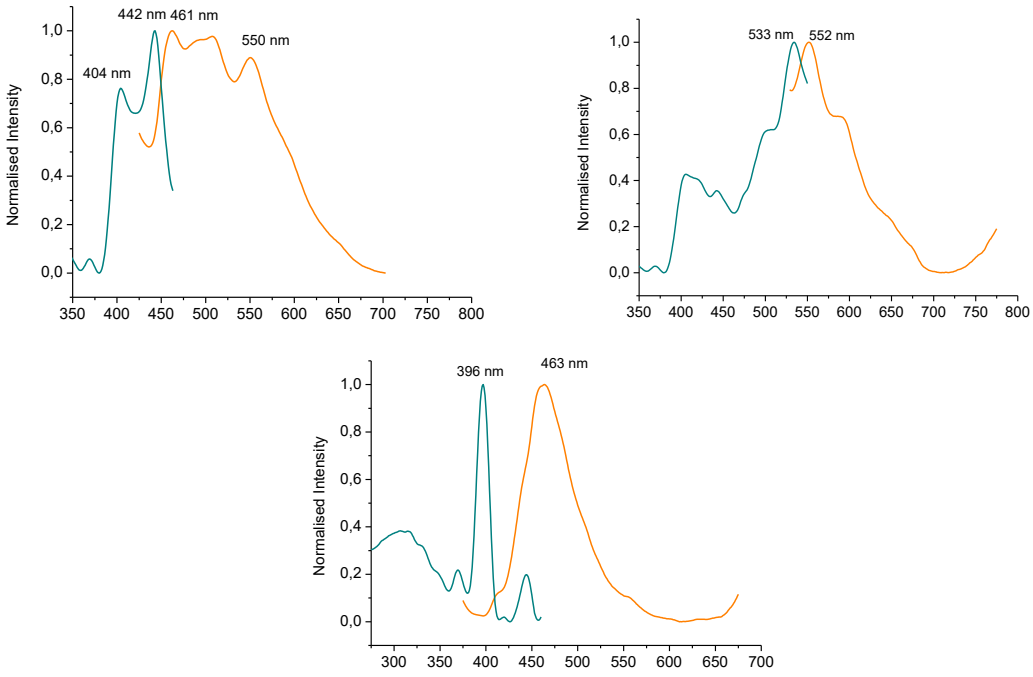


Figure A 51. Emission spectra (orange) of **P3**: up) room temperature; bottom) 77K